## General Disclaimer

## One or more of the Following Statements may affect this Document

- This document has been reproduced from the best copy furnished by the organizational source. It is being released in the interest of making available as much information as possible.

- This document may contain data, which exceeds the sheet parameters. It was furnished in this condition by the organizational source and is the best copy available.

- This document may contain tone-on-tone or color graphs, charts and/or pictures, which have been reproduced in black and white.

- This document is paginated as submitted by the original source.

- Portions of this document are not fully legible due to the historical nature of some of the material. However, it is the best reproduction available from the original submission.

A COMCOM COMPANY

DCC-1837-881-UM-1258
WP #1121A



# DEVELOPMENT, IMPLEMENTATION, AND TEST RESULTS ON INTEGRATED OPTICS SWITCHING MATRIX

October 1980

Goddard Space Flight Center
Greenbelt, Maryland 20771

Contract NAS5-25827


**DIGITAL COMMUNICATIONS CORPORATION**
**11717 EXPLORATION LANE**
**GERMANTOWN, MARYLAND 20874**

**TELEPHONE: (301) 428-5500**
**TWX: 710-828-0541**
**DIGICOMM GTWN**

TECHNICAL REPORT STANDARD TITLE PAGE

| 1. Report No. | 2. Government Accession No. | 3. Recipient's Catalog No. |
|---|---|---|
| DCC-1837-881-UM-1258 | | |

| 4. Title and Subtitle | 5. Report Date |
|---|---|
| DEVELOPMENT, IMPLEMENTATION, AND TEST RESULTS ON INTEGRATED OPTICS SWITCHING MATRIX | OCTOBER, 1980 |
| | 6. Performing Organization Code |
| 7. Author(s) DR. E. RUTZ | 8. Performing Organization Report No. |
| 9. Performing Organization Name and Address<br>DIGITAL COMMUNICATIONS CORPORATION<br>11717 EXPLORATION LANE<br>GERMANTOWN, MARYLAND 20874 | 10. Work Unit No. |
| | 11. Contract or Grant No.<br>NAS5-25827 |
| 12. Sponsoring Agency Name and Address<br>N.A.S.A. GODDARD SPACE FLIGHT CENTER<br>GREENBELT, MARYLAND<br>THOMAS MCDONALD | 13. Type of Report and Period Covered<br>FINAL REPORT<br>8/24/79 TO 10/3/80 |
| | 14. Sponsoring Agency Code |

15. Supplementary Notes

16. Abstract

A small integrated optics switching matrix has been developed, implemented, and tested, and it indicates high performance. The matrix serves as a model for the design of larger switching matrices. The larger integrated optics switching matrix should form the integral part of a switching center with high data rate throughput of up to 300 megabits per second. The switching matrix technique that has been developed under this contract can accomplish the design goals of low crosstalk and low distortion.

This report contains about 50 illustrations to help explain and depict the many phases of the integrated optics switching matrix. Also contained in this report are many equations which are used to explain and calculate the experimental data.

| 17. Key Words (Selected by Author(s)) | 18. Distribution Statement |
|---|---|
| Laser beam propagation<br>Laser beam deflection<br>Switching Matrix<br>Optical switch tuning<br>Optical Switch size | |

| 19. Security Classif. (of this report) | 20. Security Classif. (of this page) | 21. No. of Pages | 22. Price* |
|---|---|---|---|
| UNCLASSIFIED | UNCLASSIFIED | 120 | — |

## PREFACE

The objective of this program is the development of a small integrated optics swtiching matrix, which should be able to serve as a building block for a larger integrated optics switching matrix in an optical switching center. The larger switching matrix should be designed with either four input lines and four output lines, or with eight input and sixteen output lines. High data rate throughput (up to 300 megabits per second), low crosstalk, and low distortion are of major importance. Fiber optic transmission is considered, and injection lasers will be used.

The switching matrix uses electro-optic Bragg diffraction switches in planar optical waveguide, where the light is guided in only one dimension. In the planar waveguide, the optical beams can cross over each other without interaction.

The alignment of the switching matrix requires rotation of the entire matrix in reference to the incident laser beam. Low crosstalk requires that the laser beams not become distorted when propagating through the waveguide and below the switches, and also that the deflected beam not be distorted by nonuniformities in the phase grating of the switches. The requirement for distortionless propagation through the waveguide, which was formed by titanium in-diffusion, could be met only at low optical intensities. At higher intensities, the observed optical damage can be avoided when the waveguide is formed by out-diffusion. In future development of a large switching matrix, the formation of the planar waveguide must be changed to out-diffusion.

The design of the small integrated optics switching matrix developed under this contract indicates high performance. The performance can be accomplished without tuning of the individual switches. The accuracy of the photolithographic processing of the periodic electrodes of the switches indicates that the periodicity of the switches for the larger matrices can be reduced from 8 microns to 4 microns, or less. This capacity will allow for a reduction in the size of the switching matrices by a factor of 2, at least.

The implementation of an optical switching center, using a switching matrix similar in design to the one developed under this contract, will require development of input-output fiber links. In addition, methods need to be developed to speed-up the slow decay of the electric field of the switches, which will decrease the crosstalk. Crosstalk reduction, using a spatial filter in the Fournier plane of a lens, requires development.

TABLE OF CONTENTS


| Section | Title | Page |
|---|---|---|
| 1.0 | INTRODUCTION | 1-1 |
| 2.0 | SUMMARY | 2-1 |
| 3.0 | SWITCHING MATRIX | 3-1 |
| 3.1 | Design | 3-1 |
| 3.2 | Experimental Results | 3-12 |
| 4.0 | ELECTRO-OPTIC BRAGG DIFFRACTION SWITCH | 4-1 |
| 4.1 | Width of Diffraction Grating | 4-1 |
| 4.2 | Overlap Integral | 4-6 |
| 4.3 | Electrical Field Distribution | 4-7 |
| 4.4 | Optical Field Distribution | 4-8 |
| 4.5 | Width of Diffracted Beam | 4-14 |
| 4.6 | Periodic Electrodes | 4-15 |
| 4.7 | Wavelength Dependence | 4-17 |
| 5.0 | ELECTRO-OPTIC BRAGG DIFFRACTION SWITCH | 5-1 |
| 5.1 | Implementation and Test Results | 5-1 |
| 6.0 | EVALUATION OF MINIMUM SEPARATION BETWEEN ADJACENT CHANNELS TO REDUCE COUPLING TO LESS THAN 50 dB | 6-1 |
| 6.1 | Traveling Wave Interaction | 6-1 |
| 6.2 | Effect of Optical Components at the Output Ports on Crosstalk | 6-7 |
| 7.0 | COUPLING PRISM AND SUBSTRATE | 7-1 |
| 7.1 | Design of Prism Coupler | 7-1 |
| 7.2 | Investigation of Availablility of Single Crystal $LiNbO_3$ Substrate as a Function of Size, Surface Finish and Cost | 7-5 |

TABLE OF CONTENTS (Cont.)


| Section | Title | P |
|---|---|---|
| 8.0 | $LiTiNbO_3$ WAVEGUIDE | 8-1 |
| 9.0 | COMPUTATION OF EXTERNAL OPTICS TO YIELD A COLLIMATED LASER BEAM INSIDE THE OPTICAL WAVEGUIDE OVER THE LENGTH OF THE SWITCHING MATRIX (IN THE Y-DIRECTION) | 9-1 |
| 10.0 | OPTICAL DAMAGES | 10-1 |

## LIST OF ILLUSTRATIONS


| Figure | Title | Page |
|---|---|---|
| 1-1 | Integrated Optics 4 x 4 Switching Matrix | 1-2 |
| 1-2 | Integrated Optics Switching Matrix in Operation | 1-3 |
| 3-1 | Design of 2 x 2 Switching Matrix | 3-3 |
| 3-2 | Beam Transforamtion Through 2x2 Switching Matrix in Figure 3-1 | 3-5 |
| 3-3 | Optical Switch Matrix | 3-6 |
| 3-4 | Optical Switch Matrix Pattern | 3-7 |
| 3-5a | Switching Matrix Using Mask SU-MF 002 of 12-10-79 | 3-9 |
| 3-5b | Beam Transformation Through Switching Matrix in Figure 3-5a | 3-10 |
| 3-6a & b | Photographs of Magnified Periodic Electrodes of Switches I and II | 3-13 |
| 3-6c | Photograph of Magnified Periodic Electrodes of Switch III | 3-14 |
| 3-7 | Photograph of the Switching Matrix Shown in Figure 3-5a | 3-14 |
| 3-8 | Test Set-U | 3-15 |
| 3-9 | Optical Design of Crosstalk Reduction | 3-18 |
| 3-10 | Coupling of Radiation From the Two Output Ports to Two Optical Fibers | 3-20 |
| 4-1 | Electro-Optic Bragg Diffraction Switch in $LiTiNbO_3$ Waveguide | 4-2 |
| 4-2 | Phase Relation in Bragg Diffraction Domain | 4-4 |
| 4-3 | Amplitudes of the Five Lowest Space Harmonics as Functions of b | 4-9 |
| 4-4 | The Field Amplitude in Depth for a Planar Diffused Waveguide with V = 3.55 is Shown as a Function of the Normalized Diffusion Depth x/D | 4-11 |
| 4-5 | Relation Between the Beamwidth of the Incident Beam, the Width of the Phase Grating and the Beamwidth (in the near-field of the Diffracted Beam | 4-13 |

## LIST OF ILLUSTRATIONS (Cont.)


| Figure | Title | Page |
|---|---|---|
| 5-1 | Periodic Electrode Structure | 5-2 |
| 5-2 | Intensity Distribution of Laser Beam Deflected by Bragg Diffraction Switch | 5-3 |
| 5-3 | Intensity Distribution of Laser Beam Propagating Through $LiTiNbO_3$ Waveguide | 5-4 |
| 5-4 | Intensity Distribution of Laser Beam Propagating Through $LiTiNbO_3$ | 5-5 |
| 5-5 | Intensity Distribution of Laser Beam Propagating Below Bragg Diffraction Switch | 5-6 |
| 5-6 | Decrease in Intensity of Deflected Beam Displaced From Center of Switch | 5-8 |
| 5-7 | Intensity Distribution of Laser Beam Deflected by Bragg Diffraction Switch Beam Displaced from Center of Switch by 0.09 mm along z-Axis | 5-9 |
| 5-8a | Momentum Scattering for Plane, Monochromatic Optical and Acoustic Waves | 5-10 |
| 5-9b & c | Scattering with Phase Grating and Light Beams of Finite Width | 5-11 |
| 6-1 | (a) Sketch to Two Adjacent Rectangular Waveguides Propagating Modes<br>(b) Definition of the Dielectric Discontinuity $o_1(xyz)$ | 6-2 |
| 6-2 | Mode Profile of a Rectangular Channel Guide | 6-4 |
| 6-3 | Crosstalk Reduction | 6-8 |
| 6-4 | Transformation Through a Lens | 6-10 |
| 6-5 | Transformation of Two Light Beams Through Lens 3 | 6-11 |

## LIST OF ILLUSTRATIONS (Cont.)


| Figure | Title | Page |
|---|---|---|
| 7-1 | Traveling Wave Coupling from Prism to Optical Waveguide | 7-2 |
| 7-2 | Truncated Coupling Prism | 7-6 |
| 7-3 | Truncated Coupling Prism | 7-7 |
| 8-1 | Relative Optical Power Coupled into Planar Optical Waveguide as a Function of Synchronous Angle and of Relative Propagation Constant $\frac{-}{k}$ of Zero-order Mode. | 8-2 |
| 8-2 | Relative Optical Power Coupled into Planar Optical Waveguide as a Function of Synchronous Angle and of Relative Propagation Constant $\frac{-}{k}$ of Zero-order Mode | 8-3 |
| 8-3 | Normalized - Diagram of a Planar Slab Waveguide Showing the Guide Index b as a Function of the Normalized Thickness V of Asymmetry | 8-5 |
| 8-4 | The Functional Relation Between the Refractive Index and the Depth of $LiTiNbO_3$ Waveguide for $\frac{m=o}{k} = 2.3069$ | 8-7 |
| 9-1 | Contour of Gaussian Beam Focused in the Center of the $LiTiNbO_3$ Waveguide | 9-2 |
| 9-2 | Contour of Gaussian Beam | |

## LIST OF ILLUSTRATIONS


| Figure | Title | Page |
|---|---|---|
| 10-1 | Experimental Arrangement for Observation of Coupling and Intermode Scattering | 10-2 |
| 10-2 | In Plane Scattered-Energy Distribution as a Function Scattering Angle | 10-4 |
| 10-3 | Output Intensity Profiles of $LiNbO_3$ Waveguides Along the m line and as a Function of Time | 10-6 |
| 10-4 | Output Intensity Profile of $LiTiNbO_3$, Waveguide Along z-axis | 10-7 |
| 10-5 | Output Intensity Profile of $LiTiNbO_3$, Waveguide Along z-axis | 10-9 |
| 10-6 | Output Intensity Profile of $LiTiNbO_3$, Waveguide Along z-axis | 10-10 |
| 10-7 | Output Intensity Profile of $LiTiNbO_3$, Waveguide Along z-axis | 10-12 |

## LIST OF TABLES


| Table | Title | Page |
|---|---|---|
| 7-1 | Refractive Indices of $TiO_2$ and $SrTiO_3$ | 7-4 |
| 8-1 | Waveguide Properties | 8-4 |

# SECTION 1
# INTRODUCTION

The objective of this program, under the NASA Contract NAS5-25827, is the development of a small integrated optics switching matrix. The small switching matrix should be able to serve as a building block for a larger integrated optics switching matrix in an optical switching center. The larger switching matrix should be designed with either four inputs and four outputs, as shown in Figure 1-1, or with eight input lines and sixteen output lines. A high data rate throughput of up to 300 Mbits/s is required. Low crosstalk and low distortion are of major importance. Fiber optic transmission is considered for interconnections in the switching center. This seems necessary because of the high data rate and considerable transmission distances within the center. The optical transmitters of the future switching center will use injection lasers and will transform the output from RF receivers to optical data streams. Because direct modulation of the injection lasers will be used, a separate optical channel for each RF receiver will be required.

In 1978-79 under NASA Contract NAS5-2449 a comparison was made, as part of the feasibility study, between the integrated optical switching concept and other switching methods, for meeting the design goal outlined above. The integrated optical switching concept was found to be the optimal solution, because of its potentially high efficiency, high reliability, minimal power consumption, wide bandwidth, simple distribution, and ability to connect optical fibers to an optical switching matrix.

The integrated optics switching matrix uses electro-optic Bragg diffraction switches. It also uses terminations inline with the input laser beams. A key feature of the electro-optic Bragg diffraction switches is that the switched "off" position does not adversely affect wave propagation. The feedthrough due to the limited deflection efficiency (76%) of the switch in the "on" position, can be absorbed by the optical terminations. An additional feature, as shown in Figure 1-2, is that only one switch in the matrix needs to be energized for connection of an input port to an output port.

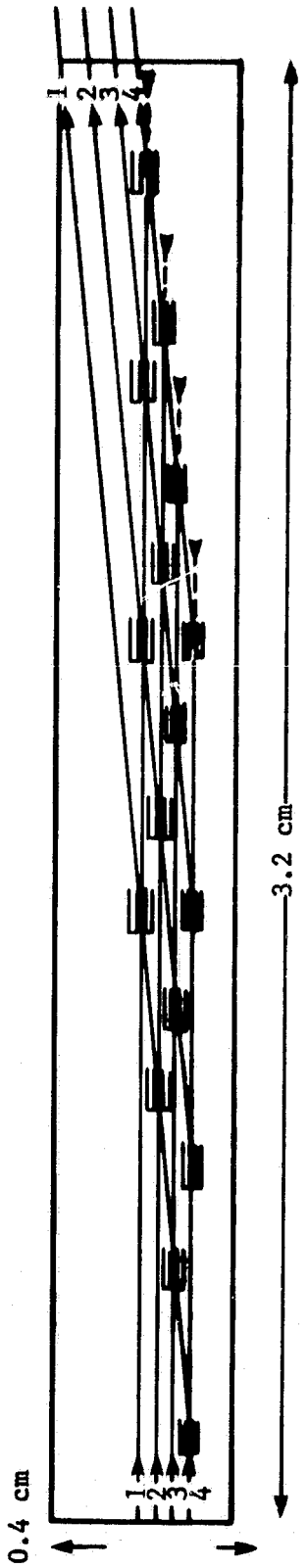


Figure 1-1. Integrated Optics 4x4 Switching Matrix

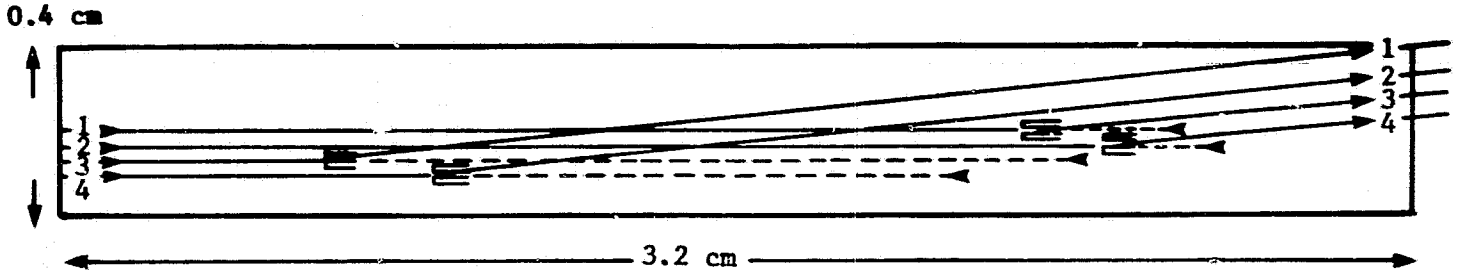


2348
8/81

Figure 1-2. Integrated Optics Switching Matrix in Operation

The electro-optic Bragg diffraction switches in the switching matrix are built in planar waveguide. This one-dimensional confinement property prevents the "off" position of the switch from adversely affecting wave propagation. This design requires that the radiation from the input optical fibers be collimated by external optics. The collimated laser beams forming the input terminals, and the deflected laser beams forming the output terminals, must be parallel to each other.

The design of the electro-optic Bragg diffraction switches for the 4 x 4 and the 8 x 16 switching matrix must be commensurable with the limited size of the single ferroelectric crystal forming the substrate of the switching matrix. Fortuitously, the geometry of a 4 x 4 and a 8 x 16 switching matrix can be well matched to the cross section of a pulled single ferroelectric crystal. To conserve space on the single ferroelectric crystal, coupling of the radiation from the optical fiber input lines to the switching matrix should be performed by endfire couplers.

The small integrated optics switching matrix which was developed in 1979-80, under the NASA Contract NAS5-25827, must be considered a scaled building block of the 4 x 4 and of the 8 x 16 switching matrix. Therefore, the design of the small switching matrix was optimized with regard to the limitation imposed on the larger switching matrices by the size of the single crystal. The design goal of the small switching matrix is low crosstalk and low distortion.

The small switching matrix has been tested using a single HeNe laser source. A careful evaluation of the test results yielded sufficient information of the switching characteristics to proceed with the design of the larger switching matrices.

## SECTION 2
## SUMMARY

Under NASA Contract NAS5-25027, a small integrated optics switching matrix has been developed, implemented, and tested. The matrix serves as a model for the design of larger switching matrices. The larger integrated optics switching matrix should form the integral part of a switching center with high data rate throughput of up to 300 Mbits/s. The design goals for the switching matrix are low crosstalk and low distortion.

The switching matrix implementation technique that has been developed under this contract can accomplish this design goal.

The switching matrix uses electro-optic Bragg diffraction switches in planar optical waveguide. In this waveguide, the light is guided in only one dimension. In the orthogonal dimension, the light is confined by focusing the spatially coherent laser beam into the matrix. The focused laser beamwaist, i.e., beam position where the wave front is plane, extends over the entire matrix. It is fortuitous that the length of the beamwaist in the waveguide is extended by its larger refractive index. In the planar waveguide, the optical beams can cross over each other without interaction.

The electro-optic Bragg diffraction switches, which require linearly-polarized spatially coherent laser light, are implemented with a periodic electrode pattern on top of the planar waveguide. A voltage of 12 volts, when applied to these electrodes, deflects the incident laser beam. When the voltage is removed, so that the switch is turned off, the light passes below the peroidic electrodes without interaction. With the switch activated the beam deflection angle depends on the angle of incidence, the design of the periodic electrodes, the optical wavelength, and the refractive index of the optical waveguide. A change of the electric field changes only the deflection efficiency. Since all of these parameters were known, the switching matrix was designed and proper switching action was observed.

The switching positions in the switching matrix are not between the "off" and "on" positions of the switches. Instead, the connections between

the input and output ports are formed using only the "on" position of the switches. This design approach reduces the crosstalk considerably. Only one switch needs to be energized in the switching matrix to connect an input port to an output port.

The alignment of the switching matrix requires rotation of the entire matrix in reference to the incident laser beams. Tuning of the individual switches is not necessary. However, low crosstalk in the switching matrix requires that the laser beams not become distorted when propagating through the waveguide and below the switches. It also requires that the deflected beam not be distorted by nonuniformities in the phase grating of the switches. The requirement for distortionless propagation through the waveguide, which was formed by titanium in-diffusiuon, could be met only at low optical intensities. At higher intensities, optical damage was observed. However, it has been reported (Section 10) that optical damage at higher optical intensities can be avoided when the waveguide is formed by out-diffusion. In a future development of a larger switching matrix, the formation of the planar waveguide must be changed to out-diffusion.

Credit for the success of the work under this contract must go to Microwave Associates and their excellent photolithographic processing. The great uniformity of the periodic electrodes yielded uniform phase gratings and undistorted deflected beams.

A small switching matrix has been built by Microwave Associates which uses three of these switches. The following switching positions can be attained:

Input port 1 to output port 4 - Switch I
Input port 2 to output port 4 - Switch II
Input port 1 to output port 3 - Switch III

The input beam from port 1 was aligned to propagate through switches I and III; the deflected beams went to output ports 4 and 3, respectively, which are spaced 1.06 mm apart. The input beam from port 2 was deflected by switch II

to output port 4. At output port 4, the beams deflected by the switches I and II coincided within 2 microns. Crosstalk was below 30 dB. No additional optics were used to reduce the crosstalk.

The performance of the small integrated optics switching matrix developed under this contract indicates that the design can yield high performance. This performance can be accomplished without tuning of the individual switches. The accuracy of the photolithographic processing of the periodic electrodes of the switches is such that the periodicity of the switches for the larger matrices can be reduced from 8 microns to 4 microns or less. This capability will allow a reduction in size of the switching matrices by at least a factor of 2.

One problem that has been observed is the slow decay of the electric field of the switches. For low crosstalk, it is essential that the field decays rapidly. Methods to attain faster decay have to be developed.

The implementation of an optical switching center, using a switching matrix similar in design to the one developed under this contract, will require development of input-output fiber links. In addition, crosstalk reduction, using a spatial filter in the Fourier plane of a lens requires development.

# SECTION 3
# SWITCHING MATRIX

## 3.1 DESIGN

The main task under this program is the development and evaluation of a 2 X 2 integrated optics switching matrix as a building block for larger 4 X 4 or 8 X 16 switching matrices.

The major requirement for the switching matrix is low crosstalk and low distortion. To meet these requirements, the switches of the matrix are Bragg diffraction switches built in planar integrated optics waveguide. In the planar waveguide, the waves are confined in one dimension only (x-axis). The guiding of the optical waves in the orthogonal direction (z-axis) takes advantage of the high directivity of spatially coherent laser beams. The confinement of the width of the laser beams along the z-axis is accomplished by focusing the laser beams to the center of the switching matrix. This design approach eliminates waveguide junctions. The optical beams can cross over in the planar waveguide without interaction. When the optical waves were guided in channel waveguides, scattering would occur at the junctions where the optical waves cross over. Also, there is no traveling wave interaction between optical beams in the planar waveguide. (Section 6)

In the 2 X 2 switching matrix, four electro-optic Bragg diffraction switches are required. The switching positions are not between the "off" and "on" positions of each switch. Instead, the connections between input and output ports are formed using only the "on" position of the switches. This type of operation is advantageous in attaining low crosstalk, since the deflection efficiency of the Bragg diffraction switches from the "off" to the "on" position is limited to 75%. The feed-through of the undeflected beams is absorbed by an optical termination. Since the connections are formed using only the "on" position of the switches, the connections can be completely interrupted when the electric field is removed from the switches. In the switching matrix, only one switch needs to be energized to connect an input port to an output port.

To facilitate fabrication, the first model of the 2 X 2 switching matrix was constructed as a scaled model of the future building block. That is, the width and the spacings of the periodic electrodes of the Bragg diffraction switches are scaled to twice the size of those in the larger switching matrices. The use of a scaled model of the 2 X 2 switching matrix could expedite and facilitate the development, reduce the cost for its fabrication, and increase the probability of uniformaity of the periodic electrode structure in the first model to be built. In addition, scaling of the first model of the 2 X 2 switching matrix was required because it was operated with a HeNe laser, rather than an injection laser radiating at longer wavelengths.

The design of a 2 X 2 switching matrix in the $LiTiNbO_3$ planar waveguide using four electro-optic Bragg diffraction switches, and an optical matched termination, is shown in Figure 3-1. The planar waveguide and the Bragg diffraction switches are of the same design as those tested previously (Section 4.8). The switches are placed so that the optical beam from input port 1 propagates through switches I and III; the optical beam from input port 2 propagates through switches II and IV. The deflected beams from switches I and II propagate to output port 4 and the deflected beams from switches III and IV propagate to output port 3.

The switching matrix shown in Figure 3-1 is designed for highest deflection efficiency. This requires that the angle of incidence of the optical beams on the diffraction grating (formed by the Bragg switches), $\Theta_i$, be made equal to the angle of deflection $\Theta_d$. For $\Theta_i = \Theta_d$ the Bragg diffraction condition is given by

$$\sin \Theta_i = \sin \Theta_d = \frac{\lambda_o}{2n\Lambda} \qquad (3\text{-}1a)$$

where $\lambda_0$ is the optical wavelength in free space, $\Lambda$ is the periodicity of the diffraction grating ( $\Lambda$ = 8 microns) and n is the refractive index of the $LiTiNbO_3$ waveguide (n = 2.234). The Bragg angle $\Theta_i$ from Eq. 3-1a is 1.014°. The placement of the switches in the matrix is given by the tangent of the Bragg angle $\Theta_i$.

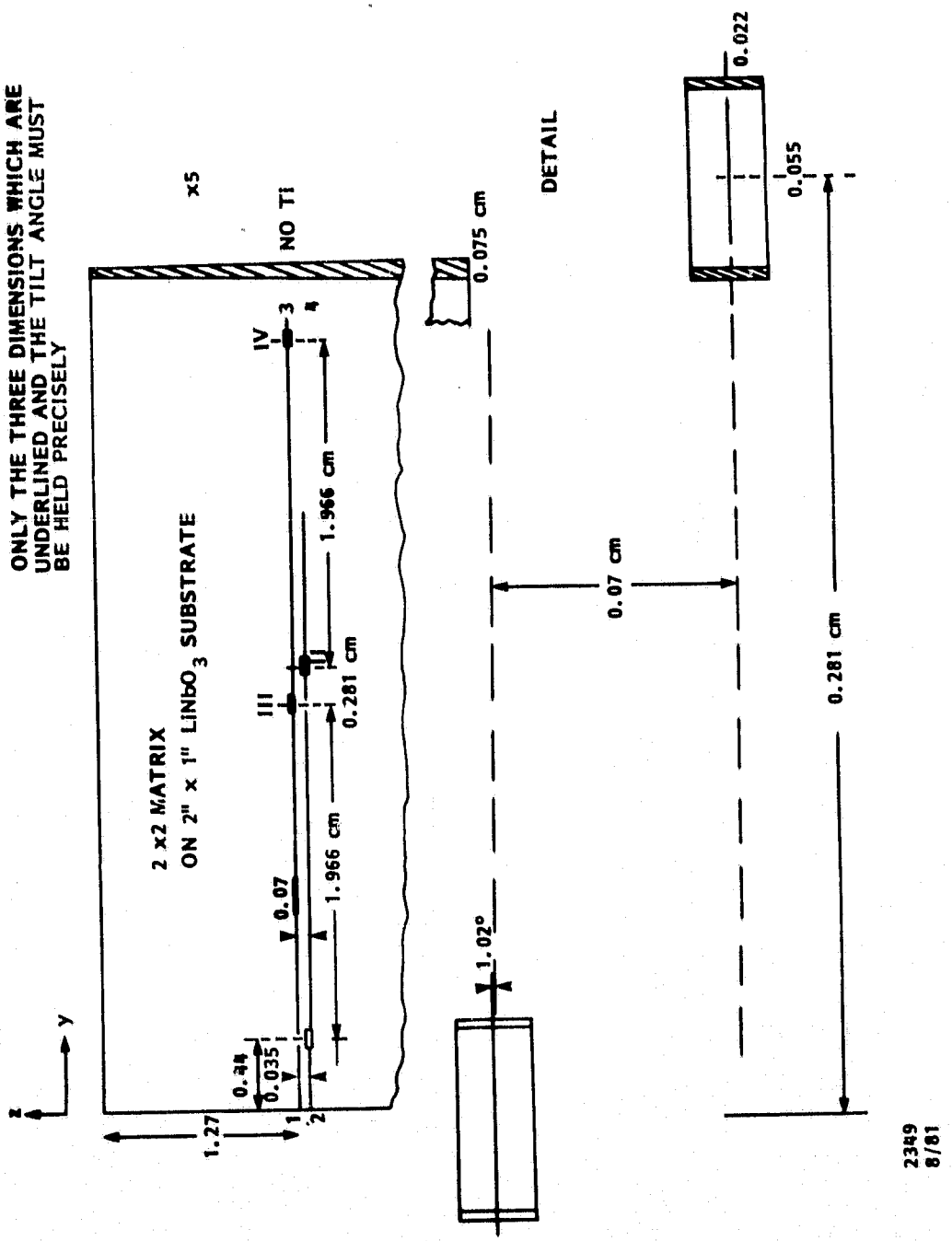


Figure 3-1. Design of 2 x 2 Switching Matrix

The schematic of the switching action is shown in Figure 3-2. The switch positions are:

| | |
|---|---|
| Switch I: | input port 1 to output port 4 |
| Switch II: | input port 2 to output port 4 |
| Switch III: | input port 1 to output port 3 |
| Switch IV: | input port 2 to output port 3 |

The undeflected beams are not directed to an output port. They are terminated by the optically matched termination shown schematically in Figure 3-1. The optically matched termination takes advantage of the phenomena that an unsymmetrical dielectric waveguide has a cut-off for guiding electromagnetic waves. The $LiTiNbO_3$ waveguide, which is sandwiched between the $LiNbO_3$ substrate and air, is unsymmetrical; and a guided optical wave is transformed to a radiating wave when the depth of the in-diffused titanium decreases below the waveguide cut-off. To form the optically matched termination, it is necessary to gradually decrease the amount of titanium which is diffused into the $LiNbO_3$ substrate, as shown in Figure 3-1.

The design of the switching matrix shown in Figure 3-1 was sent to Microwave Associates for fabrication on August 10, 1980. However, Microwave Associates could not fabricate this switching matrix. Because the program was late, there was insufficient time to make a new mask for the lithographic process of forming the periodic electrodes on the $LiTiNbO_3$ waveguide shown in Figure 3-1. Instead, in order to fabricate the switching matrix, a mask had to be used which had been designed and implemented in December 1979. The periodic electrodes on this mask are not tilted as is required for the electro-optic Bragg diffraction switches. Figure 3-3 shows the design of the December 1979 mask that had to be used to form the periodic electrodes of the switching matrix. As shown in Figure 3-4, each block on the mask shown in Figure 3-3 is a complete set of periodic electrodes.

Because of the restrictions imposed by the December 1979 mask design, the switching matrix shown in Figure 3-1 could not be implemented. The design had to be changed and switch IV had to be omitted. To fit the geometry of the switching matrix into the pattern shown in Figure 3-3, the angle of incidence of the optical beams on the diffraction switches could no longer equal the

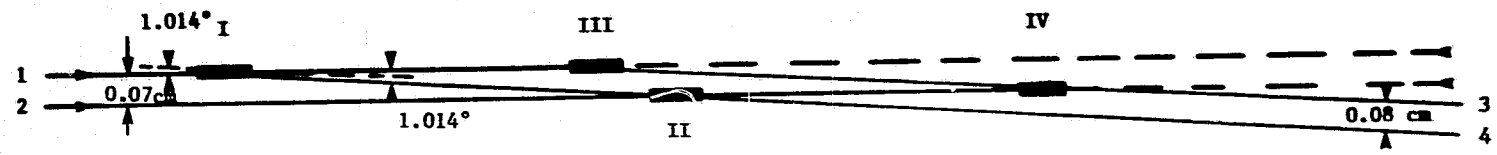


2350
8/81

Figure 3-2. Beam Transformation Through 2 X 2 switching matrix in Figure 3-1

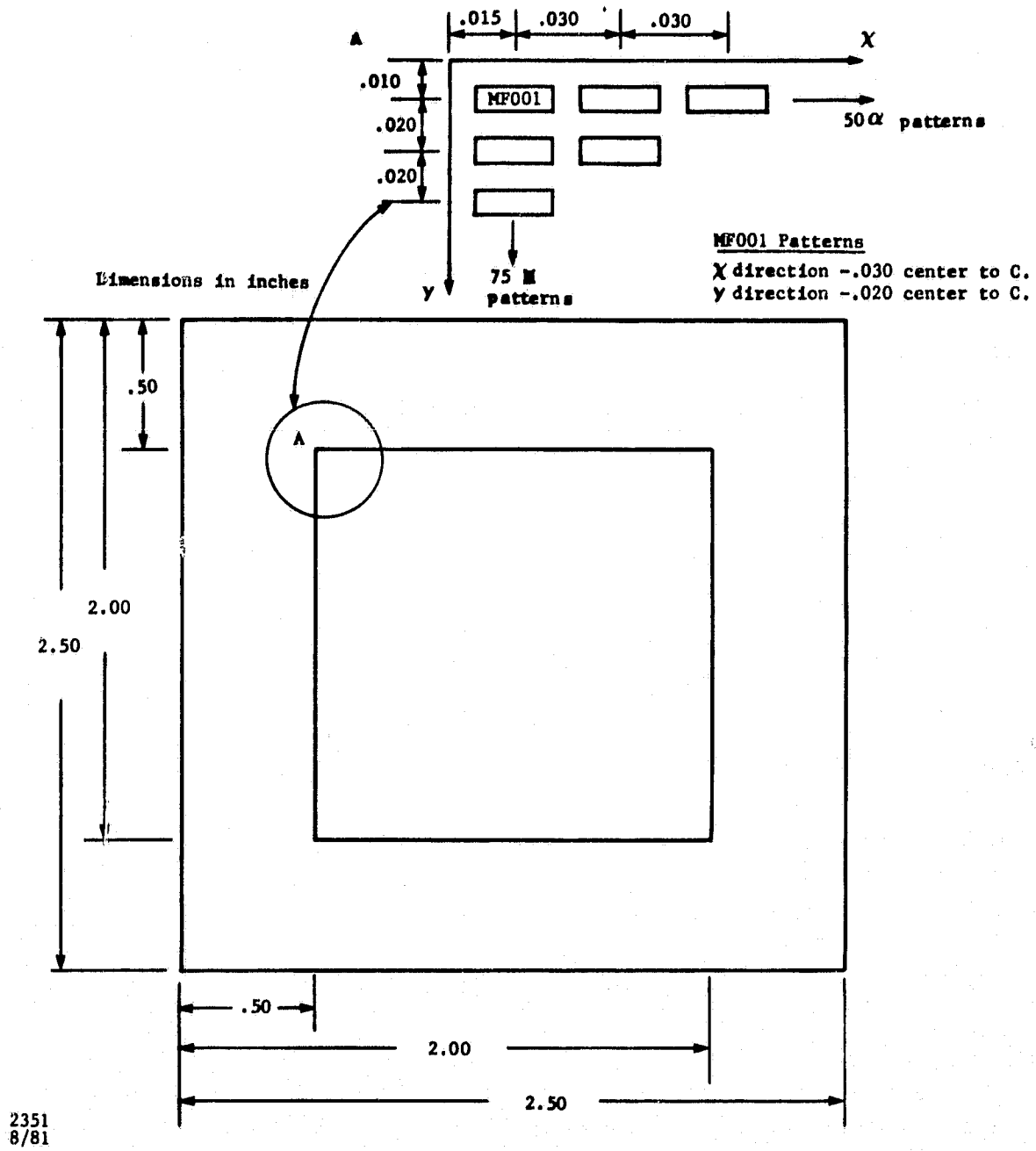


Figure 3-3. Optical Switch Matrix

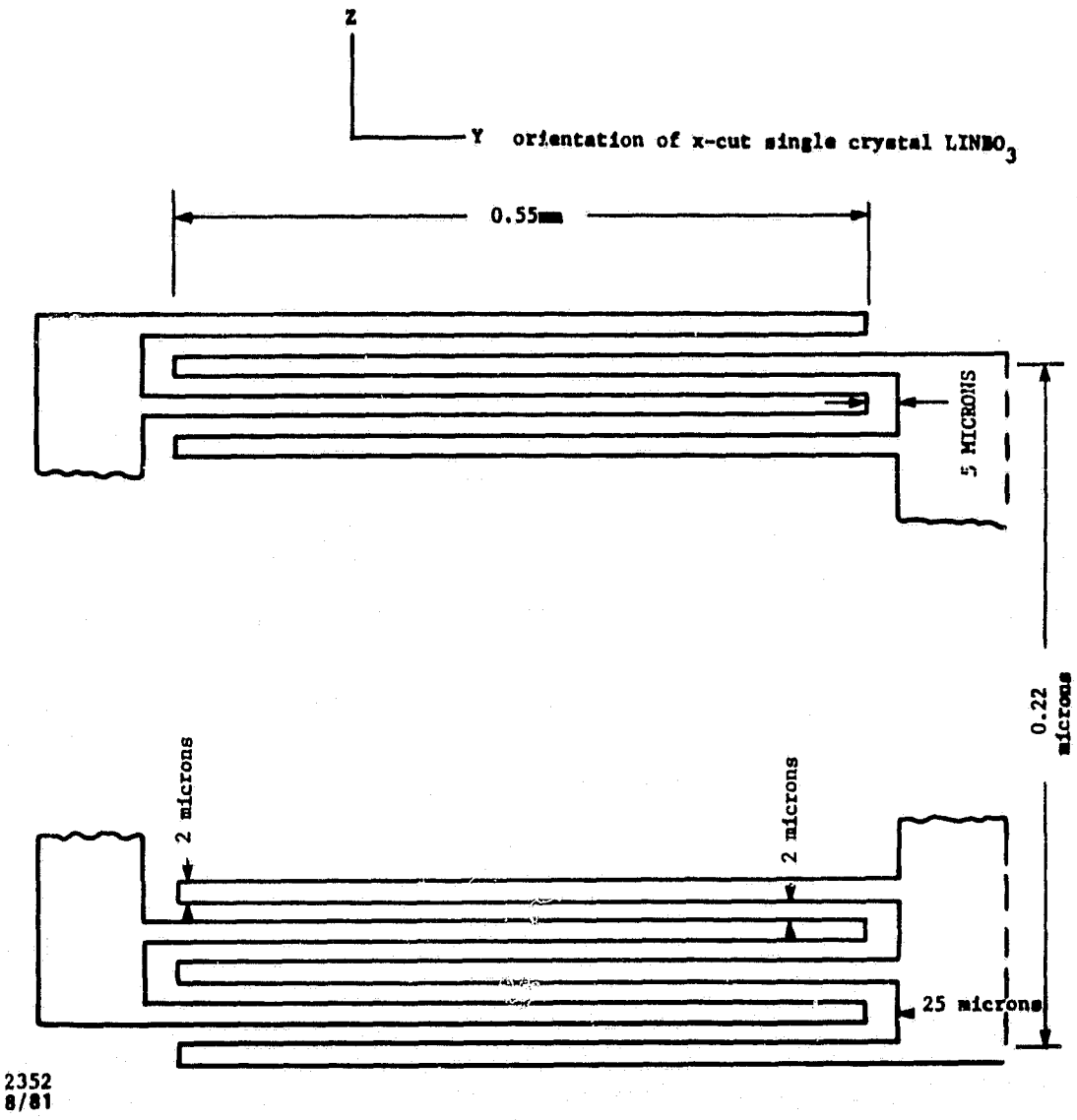


Figure 3-4. Optical Switch Matrix Pattern

angle of the deflected beams. The Bragg diffraction condition for the case that $\theta_i \neq \theta_d$ becomes

$$\sin \theta_i + \sin \theta_d = \frac{\lambda_o}{n \Lambda} \qquad (3\text{-}1b)$$

To fit the geometry of the switching matrix into the pattern shown in Figure 3-3, the angle of incidence $\theta_i$, computed from Eq. 3-1b had to be made $\theta_i = 0.909°$, and the angle of deflection had to be made $\theta_d = 1.12°$, assuming a refractive index of the $LiTiNbO_3$ waveguide of $n = 2.234$. However, the fit could not be made perfect.

The location of the three switches on the mask of December 1979 is shown in Figure 3-5a, and the beam transformation through the switching matrix is shown in Figure 3-5b. The optical beam from input port 1 propagates through switches I and III, and the optical beam from input port 2 propagates through switch II. The deflected beams from switches I and II propagate to output port 4, and the deflected beam from switch III propagates to output port 3.

The design of the switching matrix shown in Figure 3-5 is such that the distance between the output beams is larger than that of the input beams. This design is advantageous so far as crosstalk is concerned, since the output beams from the Bragg diffraction switches are slightly wider than the input beams (Section 5).

The possible switch positions of the matrix in Figure 3-5 are:

| | |
|---|---|
| Switch I | input port 1 to output port 4 |
| Switch II | input port 2 to output port 4 |
| Switch III | input port 1 to output port 3. |

The geometry of the switching matrix could not be fitted perfectly to the pattern shown in Figure 3-3, and the centers of the deflected beams from switches I and II do not coincide exactly. However, the computed difference between beam centers is only 2 microns, which is insignificant.

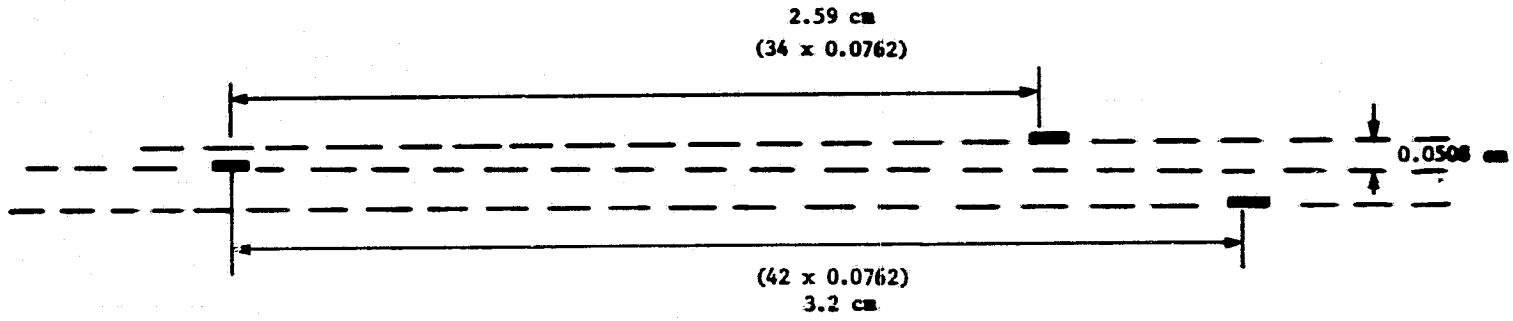


2353
8/81



Figure 3-5a. Switching Matrix Using Mask SU-MF 002 of 12-10-79

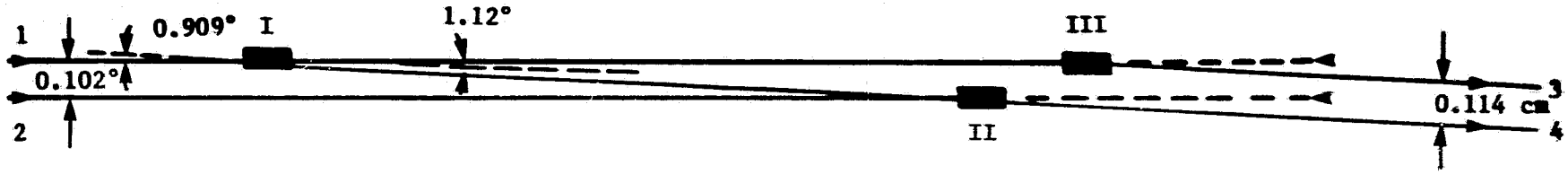


2354
8/81





Figure 3-5b. Beam Transformation Through Switching Matrix in Figure 3-5a

The design of the switching matrix shown in Figure 3-5 uses a refractive index of the $LiTiNbO_3$ waveguide of n = 2.234. The deflected beams from switches I and II would not coincide if the refractive index differed from this value. In that case, the geometry of the switching matrix shown in Figure 3-5 would have to be changed, and a new switching matrix would have to be fabricated.

The change from the switching matrix design shown in Figure 3-1 where $\theta_i = \theta_d$, to that shown in Figure 3-5, where $\theta_i \neq \theta_d$, results in a reduction in deflection efficiency. This reduction is caused by a diffraction effect which is introduced by the finite width w of the diffraction grating of the switches. The reduction in deflection intensity, when $\theta_i = \theta_d$ is given by

$$I = I_o \frac{\sin^2 \left( \frac{\pi w \sin \Theta_{ia}}{\lambda_o} \left( \Theta_d - \Theta_i \right)_a \right)}{\left( \frac{\pi w \sin \Theta_{ia}}{\lambda_o} \left( \Theta_d - \Theta_i \right)_a \right)^2} \qquad (3\text{-}2)$$

where all values in Eq. 3-2 are those measured in air. For $\Theta_d - \Theta_i = 0.2111°$, $(\Theta_d - \Theta_i)_{air} = 0.47°$ and w = 0.55 mm,

$$I \approx 0.76\ I_o,$$

That is, the deflection efficiency is decreased to 0.76 of its value for $\Theta_i = \Theta_d$.

Though the mask shown in Figure 3-3 had to be used to fabricate the switching matrix, which resulted in the omission of the fourth switch and in a reduction in deflection efficiency, the program was not really jeopardized. The feasibility of the switching matrix design, using electro-optic Bragg diffraction switches in planar optical waveguide, could be demonstrated.

## 3.2 EXPERIMENTAL RESULTS

The switching matrix in Figure 3-5 has been fabricated at Microwave Associates on a $LiNbO_3$ substrate of 2" x 1". Figures 3-6a, b, and c show photographs of the periodic electrodes of the three switches, and Figure 3-7 shows a photograph of the switching matrix. The uniformity of the periodic electrodes is equal to that of the single switch which had been tested previously (Section 4).

The switching matrix was tested in DCC's laboratory. In the test set-up shown in Figure 3-8, the input and output couplers to the switching matrix are rutile prisms. For proper alignment, the prisms and the matrix are rotated together in the x-y plane until the incident HeNe laser beam arrives at the input prism at the synchronous angle of the fundamental mode of the $LiTiNbO_3$ waveguide.

The incident HeNe laser beam is focused by a diffraction limited lens of 15 cm focal length. The switching matrix is placed at the beamwaist of the focusing lens. The beam radius of the HeNe laser beam is approximately 0.4 mm; the laser is 37 cm from the lens. The transformation from the beamwaist of the HeNe laser $2w_1$ through the lens with the focal length f to the second beamwaist $2w_0$, is given by

$$\frac{1}{w_0^2} = \frac{1}{w_1^2}\left(1 - \frac{d_1}{f}\right)^2 + \frac{1}{f^2}\left(\frac{\pi w_1}{\lambda_0}\right)^2 \qquad (3\text{-}3)$$

where $d_1$ is the distance from the beamwaist $2w_2$ to the lens. The distance of the second beamwaist from the lens, $d_0$ is

$$d_0 - f = \left(d_1 - f\right)\frac{f^2}{\left(d_1 - f\right)^2 + \left(\frac{\pi w_1^2}{\lambda_0}\right)^2} \qquad (3\text{-}4)$$

For $w_1 = 0.04$ cm, $d_1 = 37$ cm, $f = 15$ cm, $w_0 = 73$ microns, and $d_0 = 15.73$ cm.

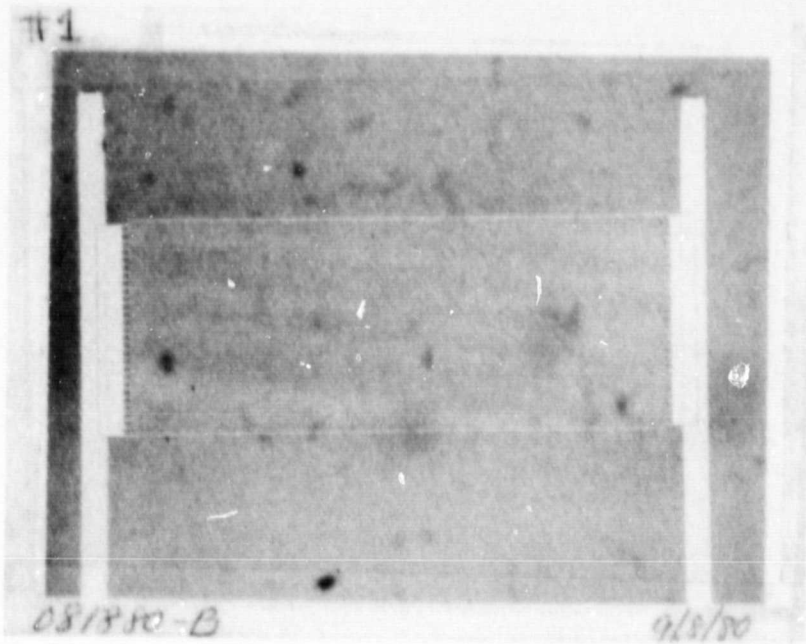


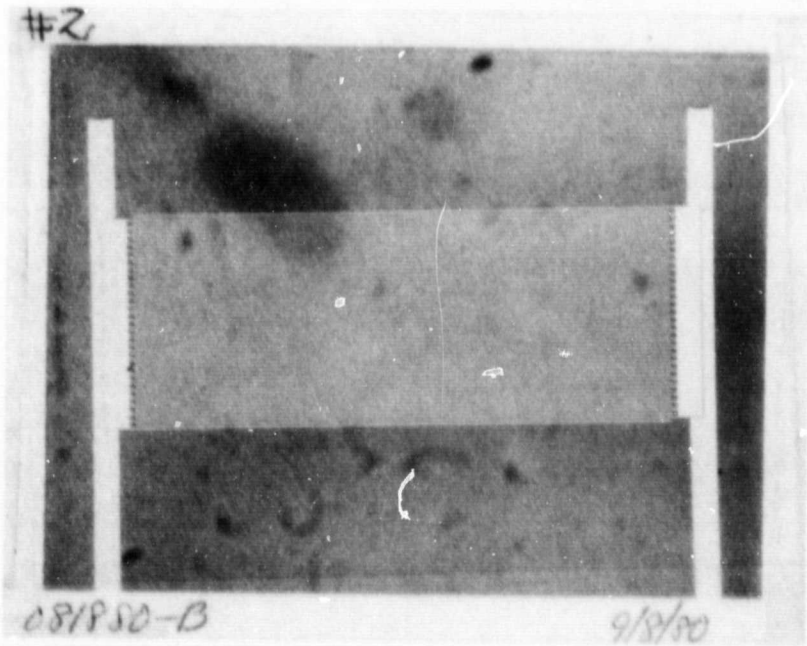


2359
8/81

Figures 3-6a and b. Photographs of Magnified Periodic Electrodes of Switches I and II

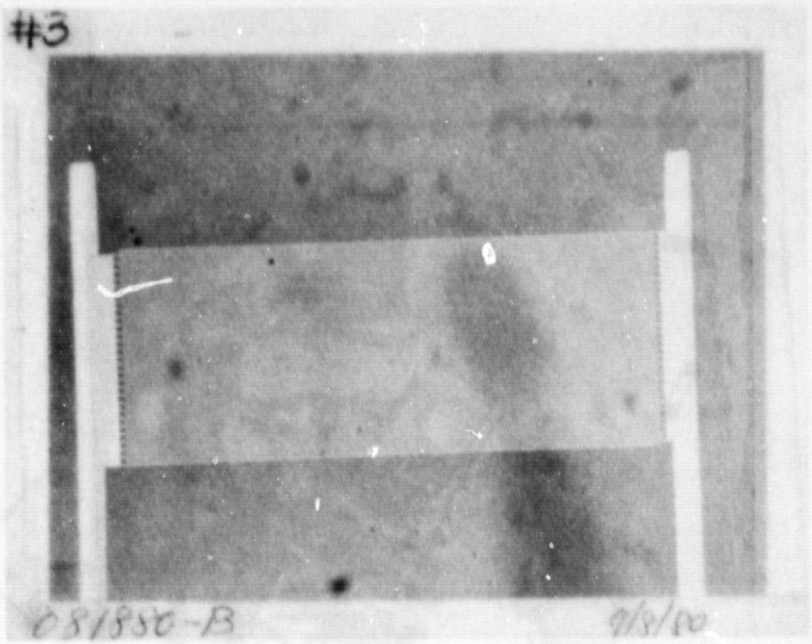


2356
8/81

Figure 3-6c. Photograph of magnified Periodic Electrodes of Switch III

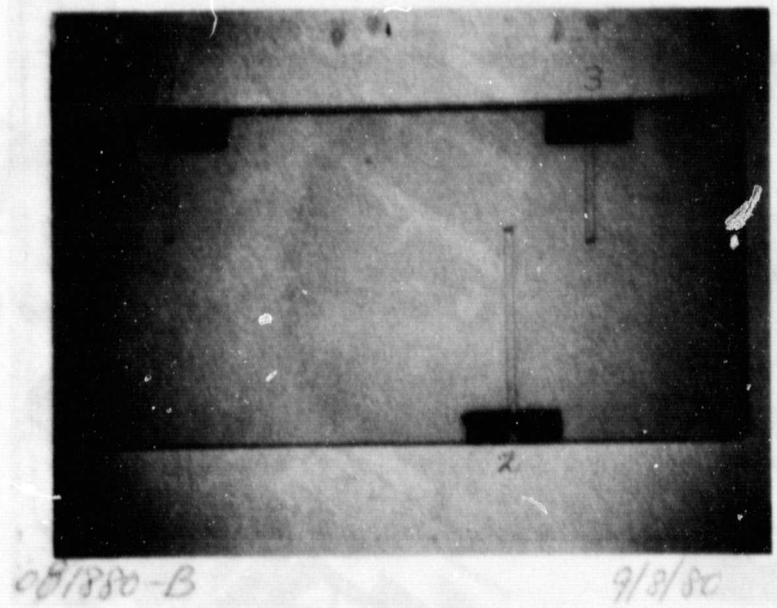


2357
8/81

Figure 3-7. Photograph of the Switching Matrix Shown in Figure 3-5a

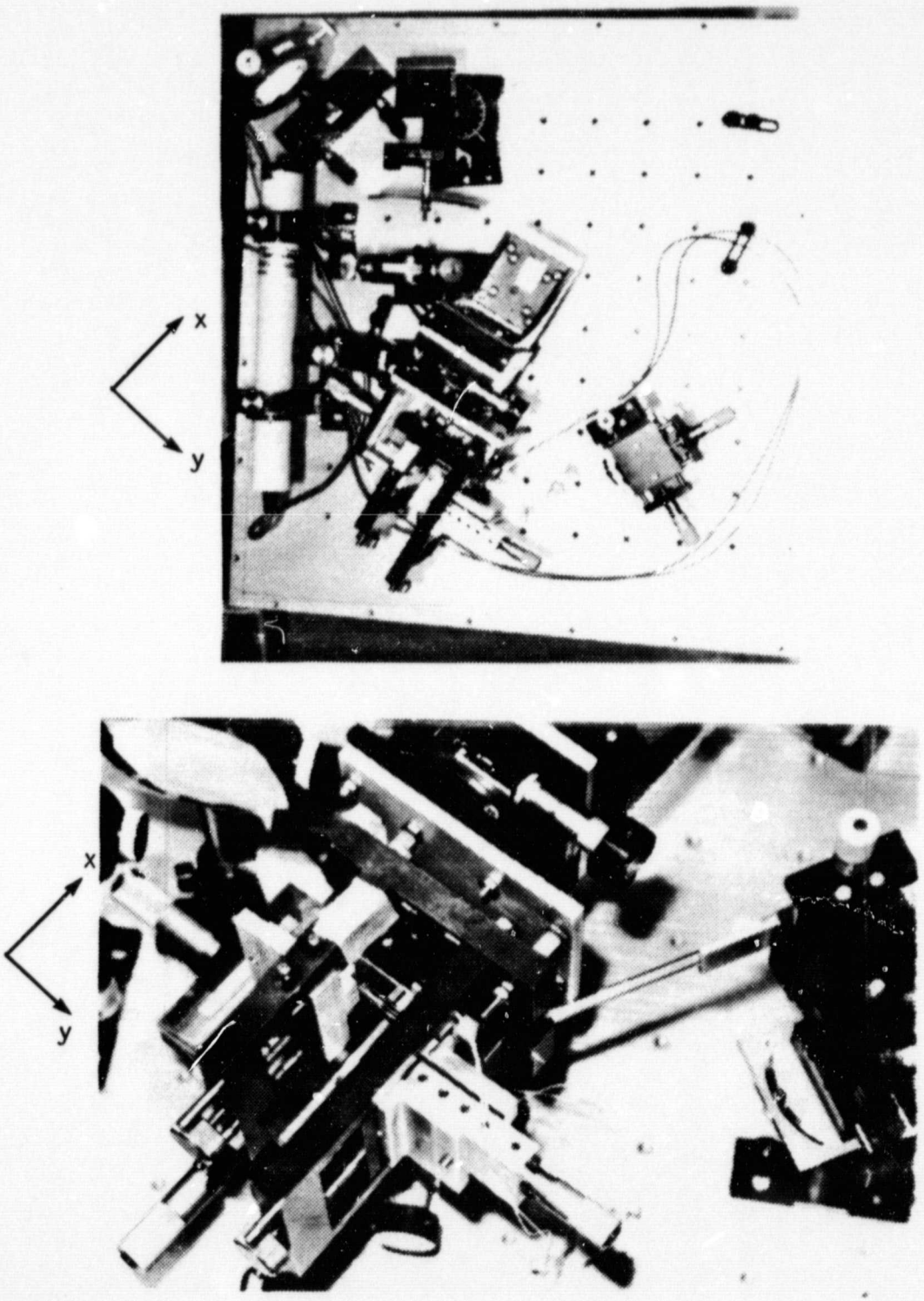


2358
8/81

Figure 3-8. Test Set-Up

The laser beam is focused into the $LiTiNbO_3$ waveguide with a refractive index of n = 2.234. The radius of the beamwaist in the dielectric is the same as that in air (Section 9, Eq. 9-6), $w_o$ = 73 microns. However, the position of the beamwaist is affected by the dielectric; it is moved further into the dielectric. Then the distance between lens and coupling prism $d_c$ becomes

$$d_c = d_o - \frac{y_1}{n_1} - \frac{y_2}{n_2} \quad ,$$

where $y_1$ corresponds to the pathlength through the prism $y_1 \approx 1$ cm and $n_1 = 2.86$; $y_2$ is the distance to the center of the $LiTiNbO_3$ waveguide, $y_2 \approx 2.5$ cm and $n_2 = 2.234$.

The laser beam expands from the beamwaist. The distance over which the beam expands by no more than a factor 1.1 (Section 9, E2. 9-9) is 5.4 cm. Thus, over the entire length of the switching matrix the beam expands by no more than a factor 1.1.

The angle of incidence on the Bragg diffraction switches shown in Figure 3-5 is $\Theta_i = 0.909°$. This angle had to be adjusted very precisely in the y-z plane to attain the beam transformation shown in Figure 3-5. To do so, a precision rotational stage was added to the mounting platform, as shown in Figure 3-8. The switching matrix, together with the coupling prisms, is mounted on this rotational stage. For proper rotation the center of rotation of this stage has to coincide with the refracting surface of the input coupling prism. Because of the refraction at the prism surface, a rotation of $\Theta$ degrees of the rotational stage corresponds to a rotation of the incident laser beam in relation the switches of matrix of $\frac{n-1}{n}$ $\Theta$degrees, where n = 2.86.

To test the switching matrix, the focused laser beam enters the switching matrix at the height of input port 1. The deflection of the input beam by switch I to output port 4 and by switch III to output port 3 is monitored. The laser beam is then moved to the height of input port 2, and

the deflection of the input beam by switch II to output port 4 is monitored. The matrix is well aligned when these switching actions can be performed with good deflection efficiency.

First, the switching action was observed visually. To do so, at a distance of 1.5 cm from the output prism, the two output ports were marked. They were spaced at a distance of 1.1 mm from each other, corresponding to the spacing of the deflected beams shown in Figure 3-5. The markings were mounted on the same holder as the switching matrix, and remained in a fixed position in relation to the switching matrix.

The two input beams, which were deflected by the Bragg diffraction switches, illuminated the proper markings. When the incident laser beam from port 1 illuminated switches I and III, the deflected beams were directed to output ports 4 and 3 respectively. The deflected beam from switch II, when illuminated by the incident beam from port 2, was also directed to output port 4.

To ascertain the accuracy of the visual observation, the markings were replaced by a pin hole of approximately 300 microns in diameter which was attached to a radiameter. The diameter of the pinhole was close to the Gaussian width of the deflected laser beams at a distance of 1.5 cm from the output prism. The measured distance of the deflected beams from switches I and III is 1.06 mm; the deflected beams from switches I and II coincide within 2 microns. This, not only proves the correctness of the design, but also of the assumed refractive index of the $LiTiNbO_3$ waveguide. The alignment of the switching matrix is comparatively simple; it does not require tuning of the individual switches, but simply a rotation of the entire switching matrix. The good result proves that the design principle is correct and can be extended to larger switching matrices.

Crosstalk reduction between the output beams at port 3 and port 4, which is described in Section 6, could not be implemented because no time was left to do so. The optical design to accomplish crosstalk reduction, which is described in Section 6, is shown in Figure 3-9. Under the present contract,

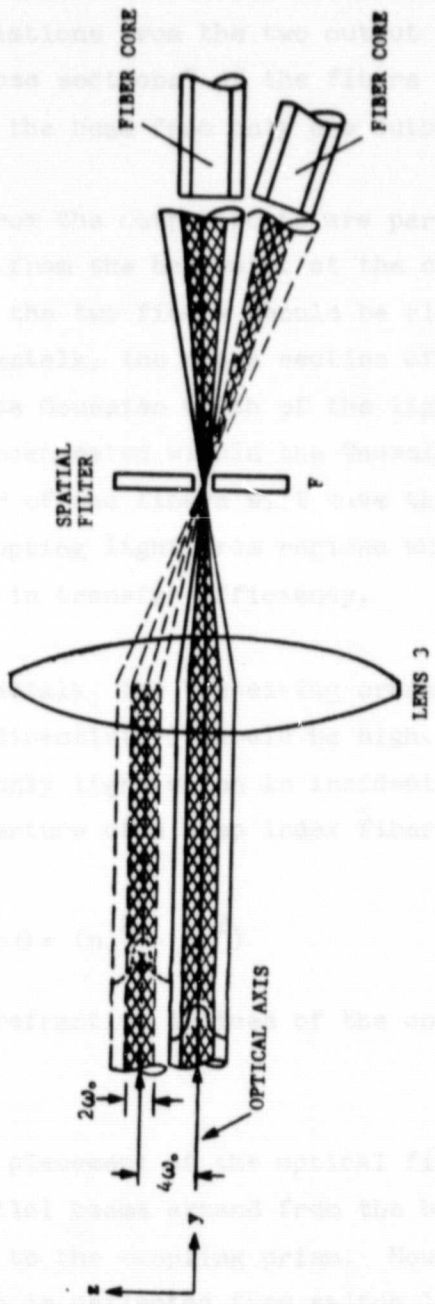


Figure 3-9. Optical Design of Crosstalk Reduction

the lens and the spatial filter shown in Figure 3-9 were omitted. Thus, no protection against crosstalk by incoherent interaction, like scattering, can be provided. To provide protection against coherent interaction, two optical fibers intercept the radiations from the two output ports, as shown in Figure 3-10. The "receiving cross sections" of the fibers are such that each fiber intercepts predominantly the beam from only one output port.

The two beams from the output ports are parallel and spaced 1.06 mm apart. The beams expand from the beamwaist at the center of the switching matrix. For this reason the two fibers should be close to the coupling prisms. To minimize crosstalk, the cross section of the two fibers should not exceed the diameter of the Gaussian width of the light beams. Since most of the optical energy is concentrated within the Gaussian width of the laser beams, the small diameter of the fibers will have the effect of reducing crosstalk (by not intercepting light from regions where the beams overlap) without substantial loss in transfer efficiency.

To minimize crosstalk, the "receiving cross section" of the optical fibers, (that is, their directivity) should be high. This requires that the optical fibers transfer only light which is incident over a small angle range. The numerical aperture of a step index fiber is

$$NA = \sin\Theta = (n_1^2 - n_2^2)$$

where $n_1$ and $n_2$ are the refractive indices of the core and the cladding, respectively.

For the correct placement of the optical fibers, two effects have to be considered. The parallel beams expand from the beamwaist, requiring that the fibers be very close to the coupling prism. However, when the fiber is too close, the beam which is deflected from switch III is not sufficiently separated from the undeflected beam from input port 2.

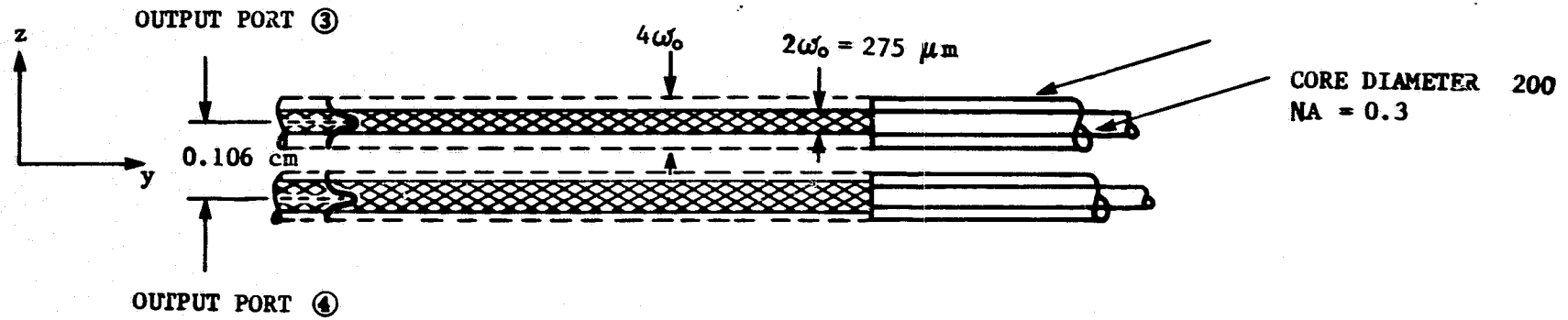


2308
8/81

Figure 3-10. Coupling of Radiation From the Two Output Ports to Two Optical Fibers

The radius w of the expanding laser beam is

$$w^2 = w_o^2 \left(1 + \left(\frac{\lambda_o y}{\pi w_o^2}\right)^2\right) \qquad (3\text{-}5)$$

where $w_o$ is the radius of the beamwaist at the center of the switching matrix, $\lambda_o$ is the wavelength in air and

$$y = \frac{y_1}{n_1} + \frac{y_2}{n_2} + y_3$$

where $y_1$ is half the length of the $LiTiNbO_3$ waveguide, $n_1 = 2.234$, $y_2$ is the length of the optical path through the prism, $n_2 = 2.86$ and $y_3$ is the distance from the prism to the fiber. For $y_1 = 2.5$ cm, $y_2 = 1$ cm, $y_3 = 1.5$ cm and $w_0 = 73$ microns, $w = 110$ microns. For the deflected beam where the beamwidth is increased by a factor 1.25 (Section 5), $w = 138$ microns.

The laser beams from the switching matrix are transferred to the prism by traveling wave interaction, where no refraction occurs. They are refracted at the interface between the prism and air. For the present alignment of the switching matrix and the prisms, the undeflected beams propagate through the prism perpendicular to the interface, and are not refracted. The deflected beam is incident on the interface under an angle of $2.03°$ ( $\Theta_i + \Theta_d$), and refracted to an angle of $5.8°$ for $n = 2.86$.

At a distance of 1.5 cm, the centers of the undeflected beam from input port 2 and the deflected beam from switch III are separated by 1.2 mm, which should provide sufficient isolation between the beams.

Crosstalk between the light beams in the switching matrix was measured by using a small pin hole of approximately 300 microns in diameter and a radiameter. The pinhole was placed about 1.5 cm from the output prism. The pinhole diameter subtends an area close to the Gaussian width of the laser beams.

To measure the crosstalk to output port 4, the pinhole was placed at output port 4. The voltages of switches I and II were then turned off to measure the feed-through from the input lines. Subsequently, switch III was energized to measure the crosstalk from the beam which is deflected to output port 3. Crosstalk between all ports was more than 30 dB below the intensity of the beam deflected to that port. The crosstalk might have been even lower, but could not be measured with our present set-up. Crosstalk can be further reduced by using a lens and a spatial filter in the Fourier plane, as shown in Figure 6-5, Section 6. Low crosstalk can be attained only when optical damage is avoided.

In measuring the crosstalk, we observed that the optical power in a deflected beam could not be turned off completely, though the voltage had been turned off and both terminals were grounded. The remaining power decayed slowly. It seems that a weak electric field (which slowly decays) remains inside the $LiTiNbO_3$ waveguide. Further investigations are required to introduce faster decay of the remaining electric field.

## SECTION 4
## ELECTRO-OPTIC BRAGG DIFFRACTION SWITCH

**Evaluation of width of diffraction grating to yield a diffraction beam similar in width to incoming beam.**

### 4.1 WIDTH OF DIFFRACTION GRATING

A typical thin-film electro-optic Bragg diffraction switch is shown in Figure 4-1. The switch is based on the linear electro-optic effect, where as external electric field can change the refractive index of a ferroelectric material such as $LiNbO_3$. The optical switch is built into a planar waveguide which is formed by in-diffusion of metal into the ferroelectric substrate. An interdigital electrode structure is formed on top of the optical waveguide.

In the electro-optic Bragg diffraction switch, a phase grating is induced by a spatially periodic electric field. In the switching matrix using Bragg diffraction switches, the optical waves are guided by the planar waveguide in the x-direction while in the z-direction; the beam shape is determined by the external optics. A voltage applied to the periodic electrodes on top of the planar waveguide sets up the periodic electric field. The electric field vector, which gives rise to the periodic refractive index variation, is parallel to the z-direction. The shape of the periodic phase grating is outlined by the shape of the periodic electrodes. The minimum width of ($w_{min}$) of the phase grating is determined by the requirement that the laser beam incident on the periodic phase grating diffracted in a single beam (Bragg domain), rather than in a multitude of grating lobes (Raman and Nath domain). The minimum width for Bragg diffraction is

$$w_{min} = \frac{Qn\Lambda^2}{2\pi\lambda_o} \qquad (4\text{-}1)$$

where $\lambda_o$ is the optical wavelength in air, n is the refractive index of the $LiTiNbO_3$ waveguide, $\Lambda$ is the periodicity of the phase grating and $Q \approx 10$.

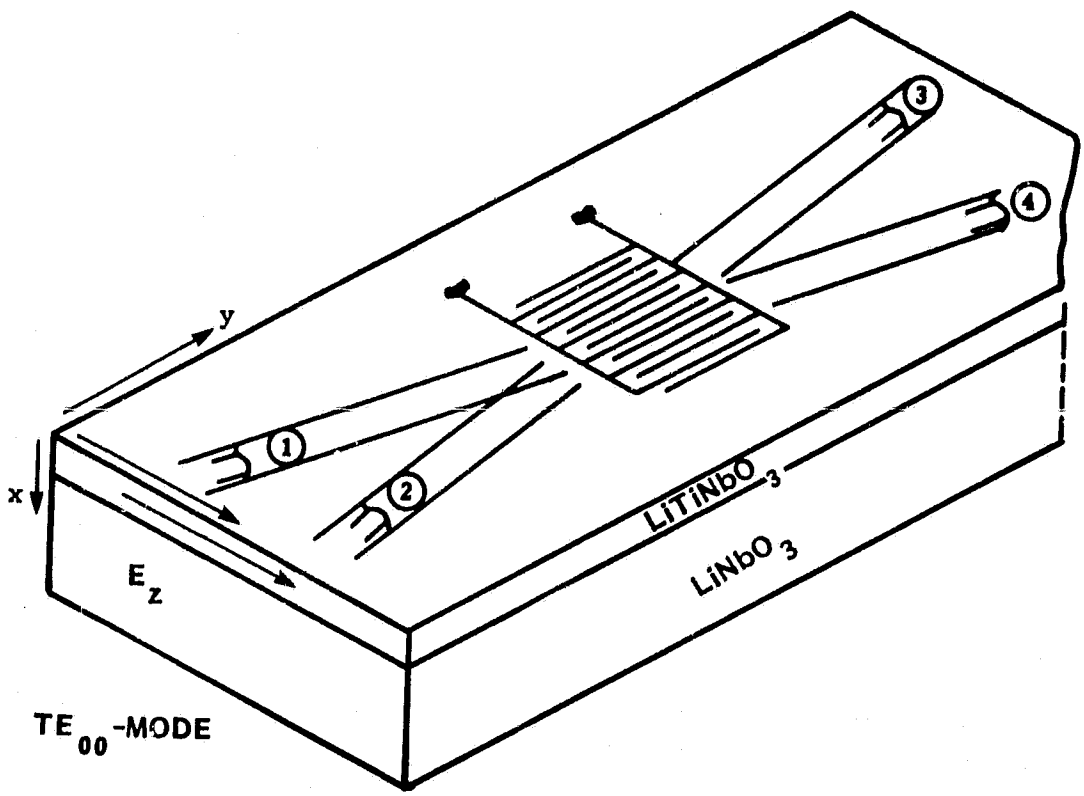


Figure 4-1. Electro-Optic Bragg Diffraction Switch in $LiTiNbO_3$ Waveguide

From Equation 4-1, $w_{min}$ for Q = 10 and n = 2.234 is

| | $\Lambda = 4\mu$ | | $\Lambda = 8\mu$ | |
|---|---|---|---|---|
| | $\lambda_o = 0.6328$ | $\lambda_o = 0.83$ | $\lambda_o = 0.6326$ | $\lambda_o = 0.83$ |
| $w_{min}$ = | 0.090 mm | 0.068 mm | 0.360 mm | 0.274 mm |

The analysis of the beam deflection in the Bragg domain uses ray optics. Each crest of the phase grating is considered a reflecting plane. However, the reflectivity of the reflecting plane is small because the change in refractive index $\Delta n$, introduced by the electro-optic effect, is small. Thus, all the incident rays are reflected at many of these reflecting planes as shown in Figure 4-2. The multiple periodic reflections will add in phase, when

$$\sin \theta_i + \sin \theta_d = \frac{\lambda_o}{n \Lambda} \tag{4-2}$$

where $\theta_i$ and $\theta_d$ are the angles of the incident and the deflected rays inside the optical waveguide,

$$\sin \theta_i = \sin \theta_d = \frac{\lambda_o}{2n\Lambda} \tag{4-3}$$

$$\text{for } \theta_i = \theta_d$$

From Equation 4-2, the Bragg angle $\theta_i$ can be computed for $\theta_i = \theta_d$, it is

| | $\Lambda = 4\mu$ | | $\Lambda = 8\mu$ | |
|---|---|---|---|---|
| | $\lambda_o = 0.6328$ | $\lambda_o = 0.83$ | $\lambda_o = 0.6328$ | $\lambda_o = 0.83$ |
| $\theta_i$ = | 2.03° | 2.66° | 1.014° | 1.33° |

Because of the multiple reflections of the rays when traveling through the phase grating, the amplitude of the incident wave decays and the amplitude of the diffracted wave increases. Since these waves are coupled by

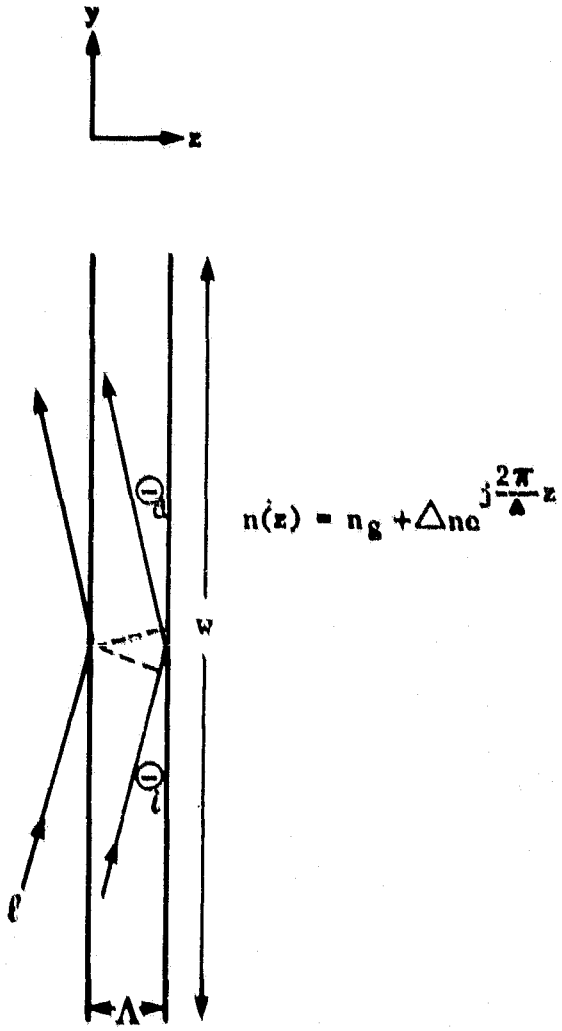


2310 8/81

$$\sin\Theta_i + \sin\Theta_d = \frac{\lambda_0}{w\Lambda}$$

Figure 4-2. Phase Relation in Bragg Diffraction Domain

the periodic spatial phase variations of the diffraction grating, their decay and build-up can be expressed by coupled wave equations. To express these equations in terms of the coordinate system shown in Figrue 4-2, the direction of the wavenormal $\ell$ must be transformed to the y-axis. It is

$$\ell = \frac{y}{\cos\theta_i} \tag{4-4}$$

The coupled wave equations which relate the normalized amplitude of the incident wave $E_i$ to the normalized amplitude of the diffracted wave $E_d$ are

$$\frac{dE_i}{dy} = jk \frac{\Delta n}{2} \frac{E_d}{\cos\theta_i}$$

$$\frac{dE_d}{dy} = jk \frac{\Delta n}{2} \frac{E_i}{\cos\theta_i} \tag{4-5}$$

where $k = \frac{2\pi}{\lambda_o}$, $\lambda_o$ is the optical wavelength in air, and

$$\Delta n(z) = \overline{\Delta n} \quad \exp j \frac{2\pi}{\Lambda} z$$

$$\overline{\Delta n} = -n_e^3 r_{33} \frac{E_{e,z}}{2} \tag{4-6}$$

where $n_e$ is the extraordinary refractive index of the $LiTiNbO_3$ waveguide ($n_e = 2.234$), $r_{33}$ is the appropriate dielectric tensor component ($r_{33} = 30 \times 10^{-10}$ cm/V) and $E_{z,e}$ is the external electrical field.

The solutions of the coupled wave equations, (Equations 4-5) using the boundary conditions that $E_i = 1$ for $y = 0$ and $E_d = 0$ for $y = 0$, are

$$E_i(y) = \cos\left(k \frac{\Delta n}{2} \frac{y}{\cos\theta_i}\right)$$

$$E_d(y) = \sin\left(k \frac{\Delta n}{2} \frac{y}{\cos\theta_i}\right) \tag{4-7}$$

The progressive build-up of the diffracted wave reaches its maximum when

$$k \frac{\overline{\Delta n}}{2} \frac{w}{\cos\theta_i} = \frac{\pi}{2} \tag{4-8}$$

where w is the width of the phase grating. It follows that the length of the propagation path of the waves through the grating, for highest diffraction efficiency, from Equations 4-6 and 4-8 is

$$\frac{w}{\cos\theta_i} = \frac{\lambda_o}{n_e^3 \, r_{33} \, E_{z,e}} \tag{4-9}$$

For the electro-optic Bragg diffraction switch in the optical waveguide, neither the external electrical field $E_{z,e}$ nor the optical fields $E_i$ and $E_d$, are constant over the depth of the waveguide (x-direction). Because of this transverse dependence, the argument of the cosine and sine functions in Equations 4-7 must be multiplied with the overlap integral F. Equations 4-8 and 4-9 then become

$$k \frac{\overline{\Delta n}}{2} \frac{w}{\cos\theta_i} F = \frac{\pi}{2} \tag{4-8a}$$

$$\frac{w}{\cos\theta_i} = \frac{\lambda_o}{n_e^3 \, r_{33} \, F E_{z,e}} \tag{4-9a}$$

## 4.2 OVERLAP INTEGRAL

The overlap integral is given by

$$F = \frac{\int v(x) \left| U(x) \right|^2 dx}{\int \left| U(x) \right|^2 dx} \tag{4-10}$$

where v(x) and U(x) are the transverse variations of the electrical field $E_{z,e}$ and of the optical field in the $LiTiNbO_3$ waveguide. The overlap integral can vary from 0 to 1; it is strongly dependent on v(x), since it becomes 1 for v(x) = 1.

## 4.3 ELECTRICAL FIELD DISTRIBUTION

For the periodic interdigital electrode structure of the Bragg diffraction switch shown in Figure 3-4, the fundamental Fourier component of the tangential electrical field (in-plane component)[1], is

$$E_{z,e} = a_1(b)\,\frac{V}{S}\exp\left(\frac{\pi x}{S}\right)\cos\left(\frac{\pi z}{S}\right) \qquad (4\text{-}11)$$

where V is the voltage applied to the electrodes, S is the center-to-center spacing between electrodes, $S = \frac{\Lambda}{2}$, bS is the width of one electrode and $a_1(b)$ is the amplitude of the fundamental space harmonic of the tangential electric field. The tangential electrical field in Equation 4-11 is directly proportional to the applied voltage and inversely proportional to the electrode spacing. The tangential electric field is given by a cosine function with its maximum centered between electrodes. The tangential electric field decays exponentially from the electrodes into the waveguide and the substrate, with a decay constant $\frac{\pi}{S}$.

Typical values for the field decay are

| x | $\Lambda = 4\,\mu$ $e^{\frac{\pi}{S}x}$ | $\Lambda = 8\,\mu$ $e^{\frac{\pi}{S}x}$ |
|---|---|---|
| 0.1 μ | 0.85 | 0.92 |
| 0.25 μ | 0.67 | 0.82 |
| 0.5 μ | 0.456 | 0.67 |
| 0.58 μ | 0.405 | 0.64 |
| 0.75 μ | 0.31 | 0.55 |
| 1.0 μ | 0.21 | 0.46 |
| 1.25 μ | 0.145 | 0.37 |
| 1.5 μ | 0.095 | 0.31 |
| 1.75 μ | 0.064 | 0.25 |
| 2.0 μ | 0.044 | 0.21 |

The amplitudes $a_{2n+1}(b)$ of the five lowest order space harmonics of the tangential electrical field are shown in Figure 4-3 as a function of b, which is the ratio of the electrode width to the electrode spacing. The amplitude of the fundamental space harmonic $a_1(b)$ increases slowly as the electrodes become wider. Equal dimensions of the electrode width and the interelectrode gap, where b = 0.5, should yield good performance. The amplitude $a_1(b)$ shown in Figure 4-3, for b = 0.5 is $a_1(b) \approx 1.7$ and close to its largest value $\left[a_1(b)_{max} = 2\right]$; the amplitudes of the third and seventh space harmonics are zero.

## 4.4 OPTICAL FIELD DISTRIBUTION

In the $LiTiNbO_3$ waveguide, the width of the optical mode is determined by the refractive index profile introduced by the diffusion of titanium into the $LiNbO_3$ substrate. The titanium diffusion produces a composition gradient, where the Ti to Nb count ratio decreases towards the interior of the $LiNbO_3$ substrate. The concentration profile versus the depth below the substrate surface where x = 0, approaches a Gaussian function for a diffusion time which is long compared to the time required for the titanium to completely enter the $LiNbO_3$ crystal. The diffusion shape f(x,D) is given by

$$f(x,D)_g = \exp - \frac{x^2}{D^2} \qquad (4\text{-}12)$$

where D is the diffusion depth. For short diffusion times, when the titanium is not completely diffused into the $LiNbO_3$ substrate, the diffusion shape follows a complementary error function

$$f(x,D)_e = \operatorname{erfc}\left(\frac{x}{D}\right) \qquad (4\text{-}13)$$

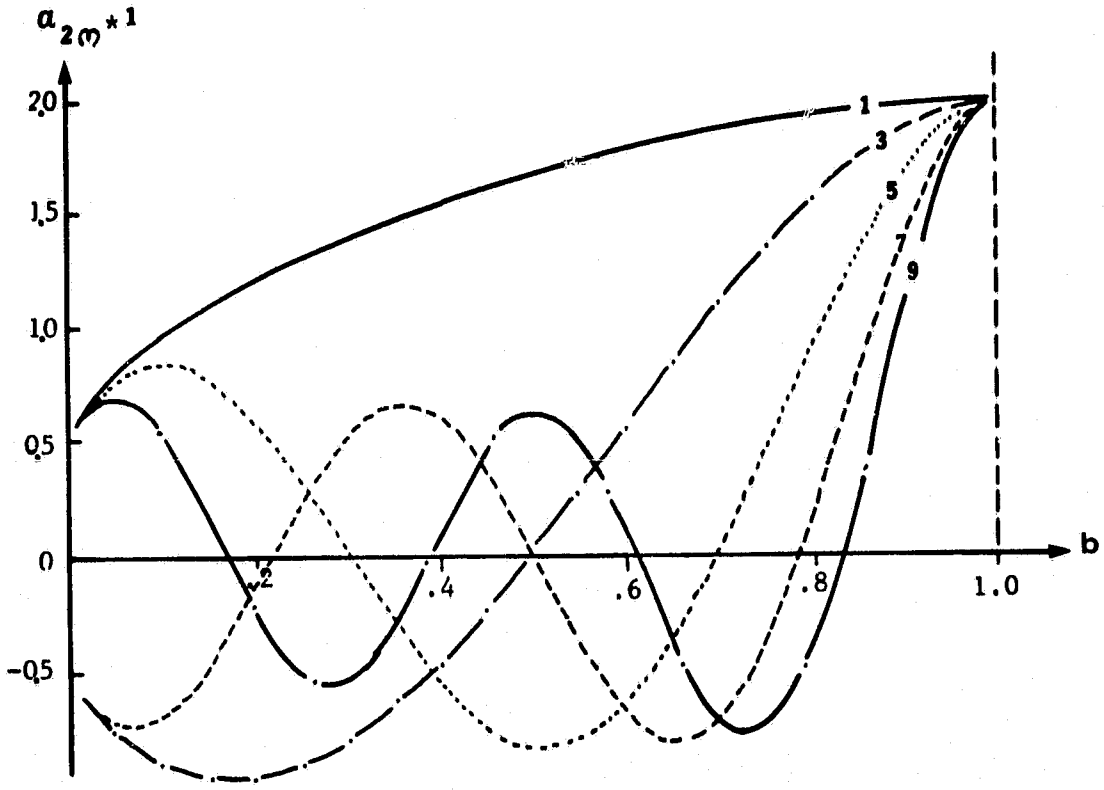


2311
8/81

Figure 4-3. Amplitudes of the Five Lowest Space Harmonics as Functions of b

The transverse variation of the refractive index in the optical waveguide, formed by titanium diffusion into $LiNbO_3$, is given by

$$n(x) = n_b + \Delta n\, f(x,D) \qquad (4\text{-}14)$$

where $n_b$ is the refractive index of the $LiNbO_3$ substrate, and $\Delta n$ is the index change due to the titanium diffusion at the waveguide surface, where $x = 0$.

W. K. Burns and G. B. Hocker [2] have computed the amplitude distribution of the fundamental mode in a planar diffused waveguide as a function of the normalized diffusion depth $\frac{x}{D}$. The computed amplitude distribution is shown in Figure 4-4 for V = 3.55, where

$$V = \frac{2\pi}{\lambda_0} (n_s^2 - n_b^2)^{1/2} D, \qquad (4\text{-}15)$$

$n_s$ is the refractive index at the waveguide surface; it is

$$n_s = n_b + \Delta n.$$

Also displayed in Figure 4-4, is the approximation of the computed amplitude distribution by a Gaussian function.

From the computed values in Figure 4-4, we can calculate the width of the fundamental mode, and the transverse variation of the optical field U(x) in Equation 4-10 for a typical $LiTiNbO_3$ waveguide, where $n_b = 2.203$ and $n = 0.04$ (Section 7). For these values, we compute the diffusion depth D from Equation 4-15 to D = 0.85 micron and the Gaussian fullwidth of the fundamental waveguide mode to 1.15 microns. The Gaussian fullwidth ($2w_x$) was also derived for the other two values in the insert. It is

| V | D | $2w_x$ |
|---|---|---|
| 3.00 | 0.72 micron | 1.15 microns |
| 3.55 | 0.85 micron | 1.15 microns |
| 4.3 | 1.03 microns | 1.17 microns |

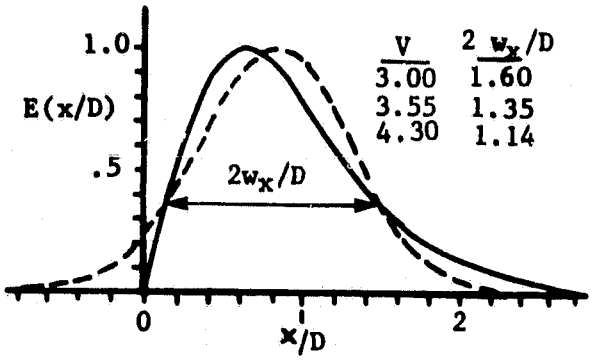


2312
8/81

Figure 4-4. The Field Amplitude in Depth for a Planar Diffused Waveguide with V = 3.55 is Shown as a Function of the Normalized Diffusion Depth x/D

Though V in Equation 4-15 and the diffusion depth are different, the Gaussian width $(2w_x)$ seems to remain fairly constant.

The overlap integral in Equation 4-10 cannot be solved in closed form. We can observe from Figure 4-5 and from Section 4.3 that at the peak of the optical waveguide mode at $x \approx 0.5$ micron, the relative amplitude of the applied electric field has decreased to 0.45 for $\Lambda = 4$ microns, and to 0.67 for $\Lambda = 8$ microns. For the overlap integral, estimate would yield $F = 0.5$ for $\Lambda = 4$ microns and $F = 0.7$ for $\Lambda = 8$ microns. Then, from Equations 4-9a and 4-11, the relation between the width of the phase grating w and the applied voltage V is

$$w = \cos\theta_i \frac{\lambda_o S}{n_e^3 r_{33} \overline{Fa_1(b)} V}$$

$$w = \frac{B}{V} \qquad (4\text{-}16)$$

From Equation 4-16, we compute the width of the diffraction grating as a function of external voltage for maximum efficiency; it is

| | $\Lambda = 4\mu$ | | $\Lambda = 8\mu$ | |
|---|---|---|---|---|
| | $\lambda_0 = 0.6328\mu$ | $\lambda = 0.83\mu$ | $\lambda = 0.6328\mu$ | $\lambda = 0.83\mu$ |
| B | 0.454cmV | 0.595cmV | 0.648cmV | 0.85cmV |
| w for 5 volt | 0.908mm | 1.19mm | 1.3mm | 1.7mm |
| w for 10 volt | 0.45mm | 0.595mm | 0.648mm | 0.85mm |

2313
8/81

Figure 4-5. Relation Between the Beamwidth of the Incident Beam, the Width of the Phase Grating and the Beamwidth (in the near-field) of the Diffracted Beam. Also Shown is the Near-field Amplitude Distribution.

## 4.5 WIDTH OF DIFFRACTED BEAM

The width of the phase grating also affects the beamwidth and the amplitude distribution of the diffracted beam. As the incident beam propagates through the phase grating, the number of periodic reflections which build up the diffracted beam varies over its cross section. This is because fewer reflections contribute to the outer rays of the diffracted beam than to its center, as shown schematically in Figure 4-5.

As the outer ray $\theta_i$ propagates through the phase grating and is periodically reflected, progressively more reflected rays are added in phase to the reflection from ray $\theta_i$. These reflections form part of the diffracted beam with linearly increasing amplitude and a spatial dimension of $2w\sin\theta$, (assuming that the amplitude of the incident beam is uniform over its cross-section $BW_i$).

Over the center part of the diffracted beam from $2w\sin$ to $BW_i$, the number of periodic reflections remains constant. Thus, the amplitude of the diffracted beam is constant over a width of $BW_i = 2w\sin\theta$.

The amplitude of the diffracted beam finally decreases linearly over the symmetrical cross-section $2w\sin\theta$. As the outer ray ($R_i$) propagates through the phase grating and is periodically reflected, progressively less reflected rays are added in phase to the reflections from ray $R_i$. The reflections form part of the diffracted beam with linearly decreasing amplitude and a cross-section $2w\sin\theta$.

Figure 4-5 shows schematically the formation of the diffracted beam together with its near-field amplitude distribution. We observe that a laser beam with uniform amplitude distribution, when propagating through a phase grating, is diffracted into a beam with symmetrical and partially tapered amplitude distribution. Also, the width of the diffracted beam, $BW_d$, in the near-field, is increased over that of the incident beam $BW_i$.

$$BW_d = BW_i + 2w\sin\theta_i \qquad (4\text{-}17)$$

Generally, the increase in width of the diffracted beam (in the near-field), which is introduced by the finite width of the phase grating, is small. This is because the Bragg angle $\theta_i$ in Equation 4-17 is a very small angle. Also, the tapered amplitude distribution should result in reduced coupling between adjacent diffracted laser beams; and, in the far-field, the sidelobes of a beam with tapered near-field distribution are lower than the sidelobes of a beam with uniform near-field distribution.

The beam transformation through the 2 X 2 switching matrix is in the near-field, since the laser beam is focused into the planar waveguide of the switching matrix by a long-focal-length lens. (Section 9). Thus, Equation 4-17 is valid and the requirement that the width of the diffracted beam in the near-field should be similar to the width of the incident beam, limits the width w of the phase grating.

Consideration must be given that the incident laser beam has Gaussian rather than uniform amplitude distribution. The Gaussian distribution can be synthesized by multiplying the uniform spatial distribution of the incident wave with a Gaussian spatial distribution. Because of the similarity of the diffracted beam in the near-field, for $2w\sin\theta_i \ll BW_i$, to the incident beam, we can assume that the spatial near-field distribution of the diffracted beam, shown in Figure 4-5 can also be multiplied with a Gaussian spatial distribution. For a Gaussian incident beam, the increase and decrease in amplitude over the outer sections ($2w\sin\theta_i$) of the diffracted beam will change from a linear slope to a slope which can be approximated by the product of a linear and a Gaussian function. Because of the gradual build-up and decay of a Gaussian function, we can conclude that the increase in the near-field width of the diffracted beam in Equation 4-17 becomes less effective when weighted with a Gaussian spatial distribution.

## 4.6 PERIODIC ELECTRODES

In the switching array, using Bragg diffraction switches, the minimum width of the periodic electrodes is determined by the requirement to diffract the incident wave into a single beam (Equation 4-1). An upper limit to the

width is set by the requirement that the diffracted beam should not be appreciably wider than the incident beam. (The relation between the beamwidth of the diffracted beam and the width of the periodic electrodes is given in Equation 4-17). To meet both requirements, the width of the periodic electrodes will be made w = 0.55 mm. For a periodicity of the induced phase grating of $\Lambda$ = 8 microns, and an optical wavelength of 0.6238 micron, the Bragg diffraction switch with a width of 0.55 mm will reach its maximum efficiency at an external voltage of 12 volts (Equation 4-9). The Gaussian full-width of the diffracted beam will be approximately 0.120 mm, when the Gaussian fullwidth of the incident beam is 0.100 mm. For an optical wavelength of 0.83 micron, the maximum efficiency will be reached at 15 volts, and the Gaussian beamwidth of the diffracted beam will be approximately 0.125 mm.

The periodicity of induced phase grating in the first model of the integrated switching matrix to be built will be 8 microns, rather than 4 microns in an optimized larger switching matrix. The larger periodicity will facilitate the effort at the initial stage of the development program. The width of the electrodes and of the interelectrode gaps are both 2 microns.

In the Bragg diffraction switches, the periodicity $\Lambda$ of the induced phase grating is determined by the center-to-center spacing of the interdigital electrodes. It can be anticipated that this dimension, which is determined primarily by the precision in fabricating the photomask, can be held with great accuracy. Thus, the Bragg diffraction angle which is inversely proportional to the periodicity $\Lambda$ (Equation 4-2) should hardly fluctuate. However, the width of the electrodes can be subjected to statistical variations, since the width of the electrodes is not only determined by the photomask, but also by the photolithographical process. A variation in the width of the electrodes will affect the amplitude of the electric field, which is a slowly varying function of the width of the electrodes (Figure 4-3). A statistical variation of the electrode width can result in a statistical amplitude modulation, which should not seriously affect the digital information on the optical wave.

The number of electrodes in the periodic structure must be sufficiently large to intercept the incident laser beam to a fullwidth of $4\omega_o$ ($w_o$ is the Gaussian halfwidth of the laser beam) where the beam intensity has decayed to about 0.0003 the intensity at the beam center. The periodic electrodes should not be larger, because that would adversely affect the propagation of the optical beams in the adjacent communication channels. To subtend the incident laser beam with a Gaussian fullwidth of $2w_o$ = 100 microns, the interdigital electrode structure must have at least 26 electrode pairs. This electrode structure will not affect the propagation of the laser beams in the adjacent channels. However, great precision in aligning the incident laser beam with the Bragg diffraction switch will be necessary. To somewhat ease the precision alignment requirement, the first model of the Bragg diffraction switch will be designed and fabricated with 28 electrode pairs to yield an induced phase grating with a length of approximately 220 microns. The design of the periodic electrodes is shown in Figure 3-4.

## 4.7 WAVELENGTH DEPENDENCE

The switching matrix with the Bragg diffraction switches is a narrowband device. A change in the optical wavelength (from the design wavelength) will result in a change of the direction of the diffracted beam; also, the finite linewidth of the laser radiation can cause a widening of the diffracted beam. The wavelength dependence of the Bragg diffraction switches follows from Equation 4-2. Since the Bragg angle is small, its change is directly proportional to the change in optical wavelength.

In the HeNe laser, the radiative transition takes place between sharply defined energy levels, resulting in narrow resonance linewidth. A typical value of the atomic linewidth is 0.01Å. Within this linewidth, up to five longitudinal modes with much narrower linewidths can build up. Because of the transition between sharply defined energy levels, the wavelength in the HeNe laser is stable and the atomic linewidth is too narrow to widen the diffracted laser beam. The HeNe laser is well suited as the laser source for the switching matrix using Bragg diffraction switches.

In the semiconductor laser, the radiative recombination emission occurs between broad energy bands; these are the conduction and the valence band. In the AlGaAs laser, because the energy bands are broad, the atomic linewidth is several Angstrom wide. The channeled-substrate-planar structure laser[3] which radiates in a single transverse mode, also has only a single longitudinal mode. This longitudinal mode at high injection current is only $10^{-3}$ Å wide. Though this mode is very narrow, its center wavelength is not locked to a definite wavelength within the much wider atomic linewidth of the laser. The wavelength range taken up by the atomic linewidth is strongly dependent on the Al content in the active region of the AlGaAs laser. Also, the atomic linewidth shifts with temperature to longer wavelengths.

No information is available at the present time on the wavelength stability of the AlGaAs lasers radiating in a single longitudinal mode. Also, no information is available at the present time on the reproducibility of the center wavelength of the single longitudinal mode of different AlGaAs lasers, even when they are cleaved from the same wafer. However, we will obtain these spectral properties at an early date from the manufacturers of the single longitudinal mode AlGaAs lasers.

In the switching matrix, the diffracted beam will not be widened as long as an AlGaAs laser is used with a single longitudinal mode which is only $10^{-3}$ Å wide. However, an AlGaAs laser which radiates in a multitude of longitudinal modes will widen the diffracted beam and increase the crosstalk. This is because the spacings between longitudinal modes in semiconductor laser with the Fabry-Perot cavity of approximately 350 microns length, is up to 3Å.

## REFERENCES
## TO SECTION 4


1. H. Egan, "Excitation of Elastic Surface Waves by Spatial Harmonics of Interdigital Transducers", IEEE Transactions Electron Devices, Vol. ED-16, No. 12, Dec. 1969, pp. 1014-1017.

2. W. K. Burns and G. B. Hocker, "Endfire Coupling between Optical Fibers and Diffused Channel Waveguides", Appl. Optics, Bol. 16, No. 8, August, 1977.

3. K. Aiki, et al. "Transverse Mode Stabilized $Al_xGa_{1-x}As$ Injection Lasers with Channeled-Substrate-Planar-Structure", IEEE J. Quantum Electronics, Vol. QE-14, No. 2, Feb. 1978, pp. 89-94.

# SECTION 5
# ELECTRO-OPTIC BRAGG DIFFRACTION SWITCH

## 5.1 IMPLEMENTATION AND TEST RESULTS

An electro-optic Bragg diffraction switch on a Ti diffused $LiNbO_3$ waveguide has been fabricated at Microwave Associates. The design of the periodic electrodes of the switch is shown in Figure 3-4. The periodicity of the electrodes is $\Lambda = 8$ microns; the width of fingers and the spacings in-between are 2 microns. Figure 5-1 shows a corrected photograph of the magnified electrodes; it demonstrates the high precision of the photolithographic process which was used to form the electrodes.

The electro-optic Bragg diffraction switch has been tested. The test results are summarized in the following: maximum switching efficiency was obtained at an applied voltage of 11.8 volts. This compares well with the computed voltage of 12 volts (Section 4.6). The maximum switching efficiency is 75 percent.

The measured intensity distribution of the deflected light beam is shown in Figure 5-2 together with the computed Gaussian intensity distribution (which is given by $\exp\left[-2\left(\frac{x}{w}\right)^2\right]$) for w = 1.35 mm. It can be seen that the deflected light beam has Gaussian intensity distribution. For comparison, measurements were made of the intensity distribution of the laser beam which had propagated through the $LiTiNbO_3$ waveguide. The measured intensity distribution for propagation through two different areas of the waveguide is shown in Figures 5-3 and 5-4. The intensity distribution is Gaussian with Gaussian widths of 1.05 mm and 1.10 mm. Furthermore, the intensity distribution of the laser beam, which has propagated below the switch, was measured. The intensity distribution is shown in Figure 5-5. The distribution is Gaussian. The Gaussian width is 1.0 mm. From this result we can conclude that the laser beam in the planar waveguide is not affected by the periodic electrodes (no voltage applied). This is an important result since it alleviates the requirement of a $SiO_2$ buffer layer on top of the $LiTiNbO_3$ waveguide.

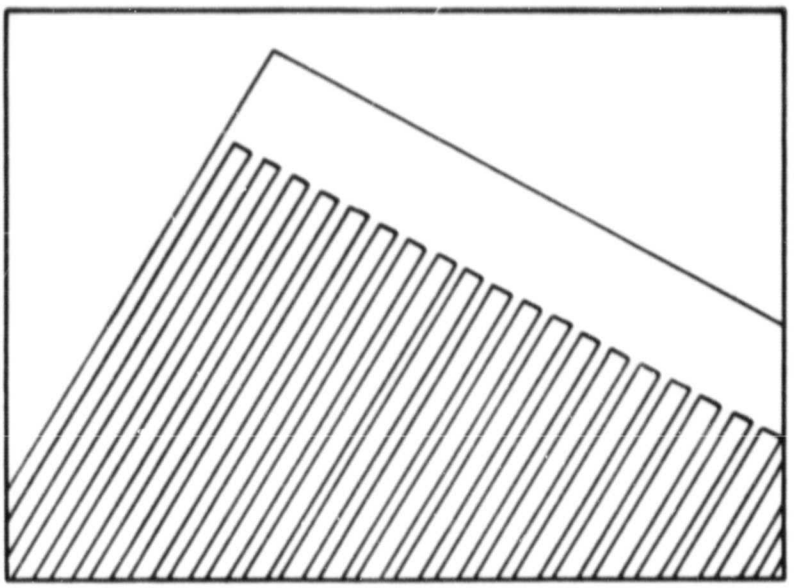

DIMENSIONS

| | |
|---|---|
| CENTER TO CENTER | 8 MICRONS |
| ELECTRODE WIDTH | 2 MICRONS |
| ELECTRODE SPACING | 4 MICRONS |

2355
8/81

Figure 5-1. Periodic Electrode Structure

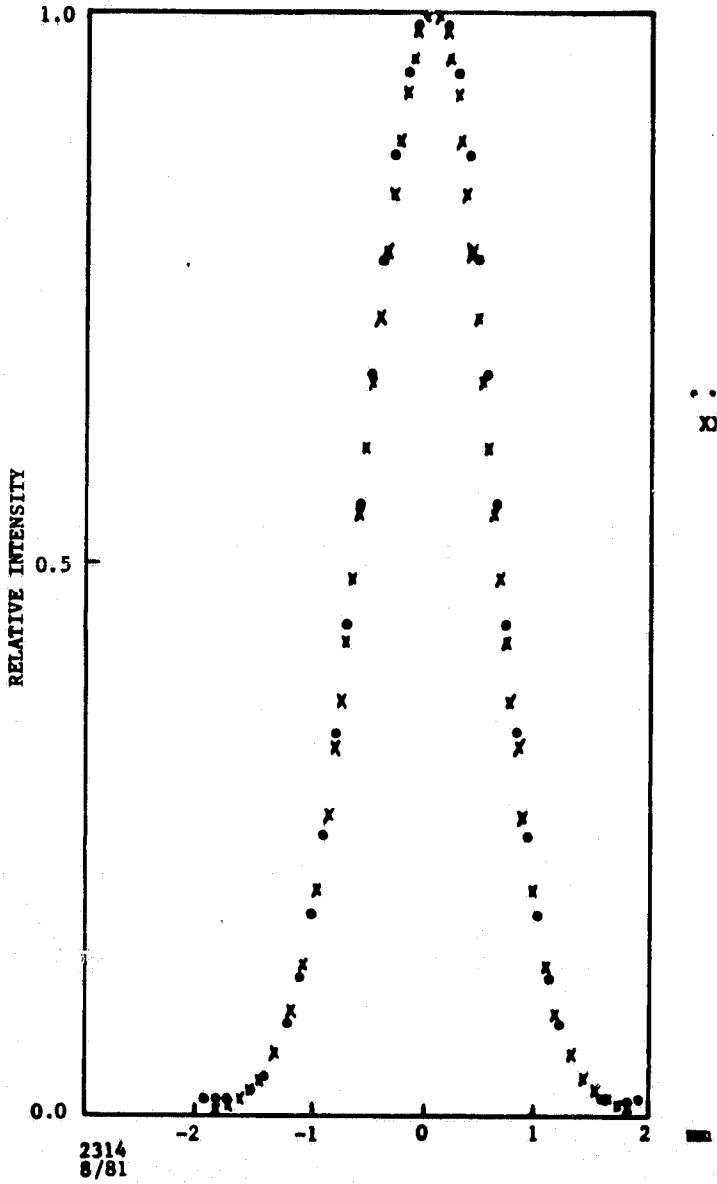


Intensity distribution of laser beam deflected by Bragg Diffraction Switch.

... Measured values at a distance Y = 52cm

XXX Computed distribution $e^{-2(\frac{x}{w})^2}$

for w = 1.35mm

Figure 5-2. Intensity Distribution of Laser Beam Deflected by Bragg Diffraction Switch

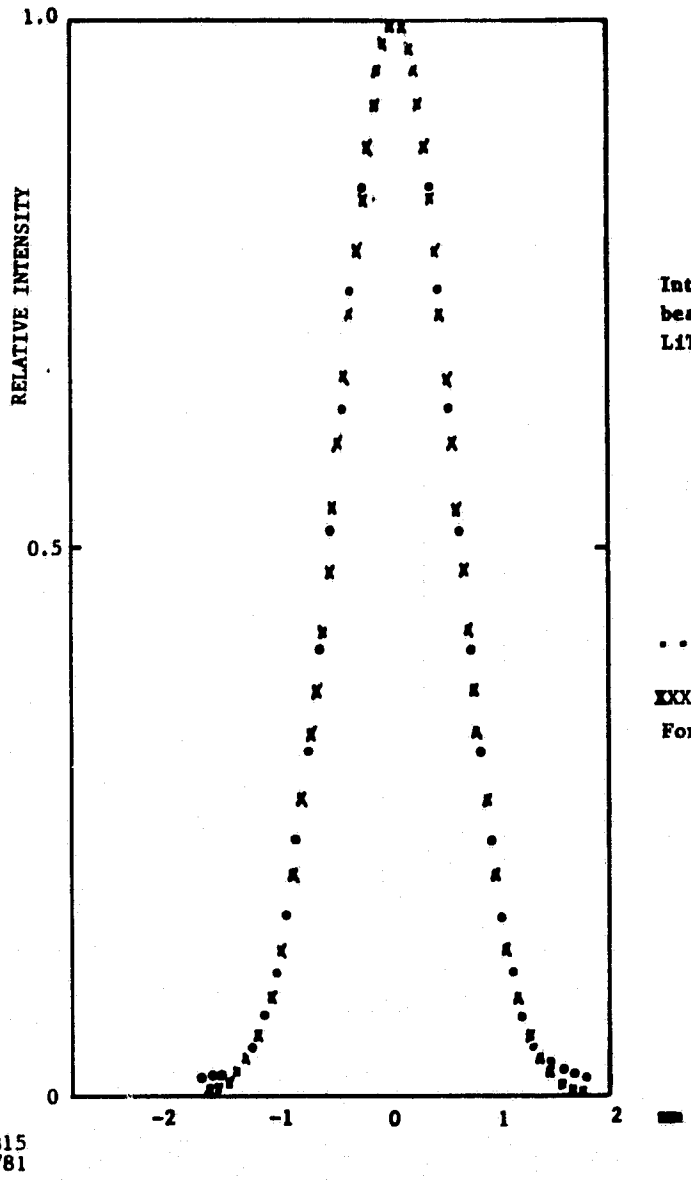


Intensity distribution of laser beam propagating through $LiTiNbO_3$ waveguide.

. . . Measured values at a distance Y = 52cm

XXX computed distribution $e^{-2(\frac{x}{w})^2}$
For w = 1.05mm

Figure 5-3. Intensity Distribution of Laser Beam Propagating Through $LiTiNbO_3$ Waveguide

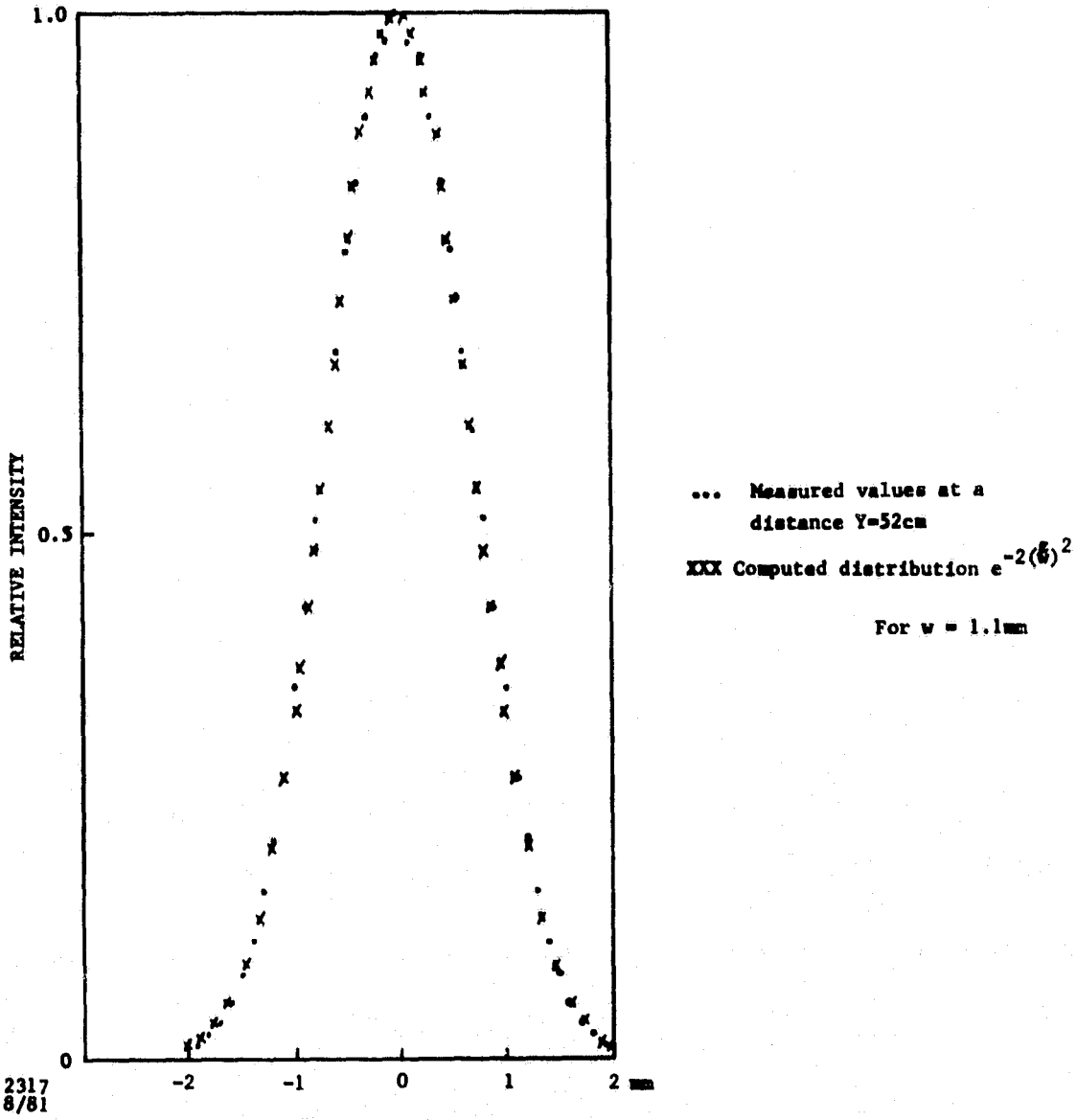


Figure 5-4. Intensity Distribution of Laser Beam Propagating Through $LiTiNbO_3$ Waveguide

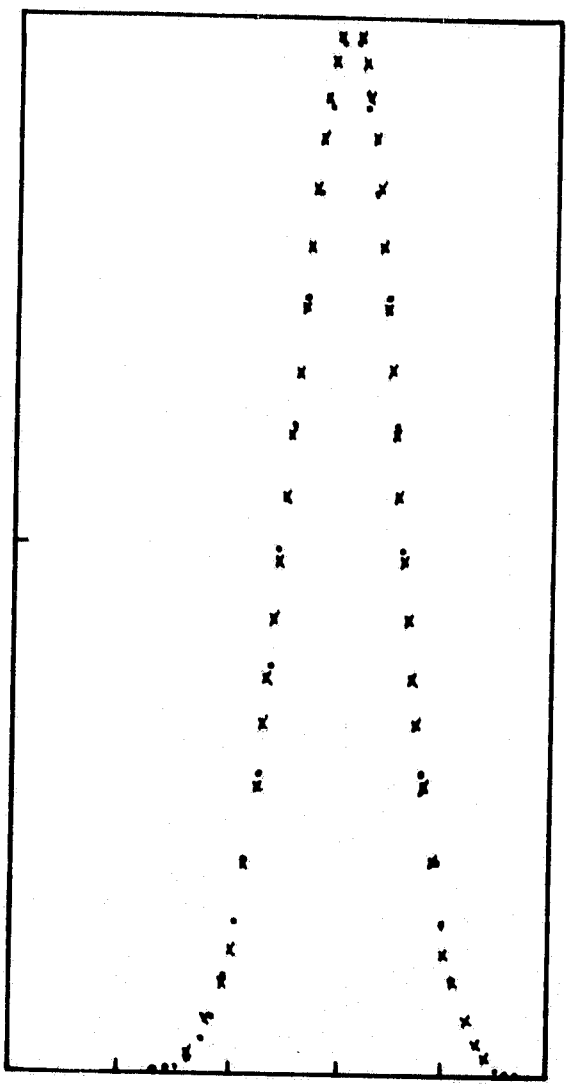

Intensity distribution of laser beam propagating below Bragg Diffraction Switch.

... Measured values at a distance Y = 52cm

XXX computed distribution $e^{-2(\frac{x}{w})^2}$

For w = 1.0 mm

2316
8/81

Figure 5-5. Intensity Distrigution of Laser Beam Propagating Below Bragg Diffraction Switch

Finally, the decrease in deflected laser beam intensity was measured when the incident laser beam propagated off the center of the electro-optic Bragg diffraction switch. The result is shown in Figure 5-6. The intensity of the deflected laser beam decreases to about half its value when the center of the incident laser beam is displaced by 0.09 mm along the z-axis from the center of the periodic electrode structure. (The electrode structure shown in Figure 4-3, is 0.22 mm wide along the z-axis). The intensity distribution of the deflected light beam, when the center of the incident light beam is displaced along the z-axis from the center of the periodic electrode structure, is shown in Figure 5-7. The deflected laser beam has become considerably wider resulting from truncation by the off-center propagation.

A comparison of the intensity distribution is shown in Figure 5-2 with those in Figures 5-3, 5-4, and 5-5 shows that the deflected beam has become wider by a factor of close to 1.25. This widening of the deflected beam finds its explanation in the theory of Bragg diffraction. Only where the incident laser beam is a plane wave, and the periodic electrode structure is infinitely wide along the y-axis, can the Bragg diffraction condition, derived for acoustic waves, be exactly fulfilled (Figure 5-8a). This condition requires that the sum of the wave vectors of the optical wave $\vec{k}$ and the acoustic wave vector $\vec{K}$ is equal to the wave vector of the deflected wave $\vec{k}_s$. It is

$$\vec{k} + \vec{K} = \vec{k}_s \qquad (5\text{-}1)$$

Eq. 5-1 is equally valid for the electro-optic Bragg diffraction switch. When the Bragg diffraction switch is of finite width in the y direction, the direction of $\vec{K}$ is no longer perfectly defined. The width of the diffracted beam then becomes determined by the relation between the diffraction angle $\delta\phi$ of the optical beam, and the width of the periodic electric field along the y-axis.

Figure 5-8b illustrates the case when $\delta\theta \gg \delta\Phi$ , where $2\delta\theta = \frac{\Lambda}{w}$ and $\delta\phi = \frac{\lambda}{\pi w_o}$ , $\Lambda$ is the periodicity of the electrodes, w is the width of the electrodes, w is the width of the electrode structure along the y-axis, $\lambda$ is

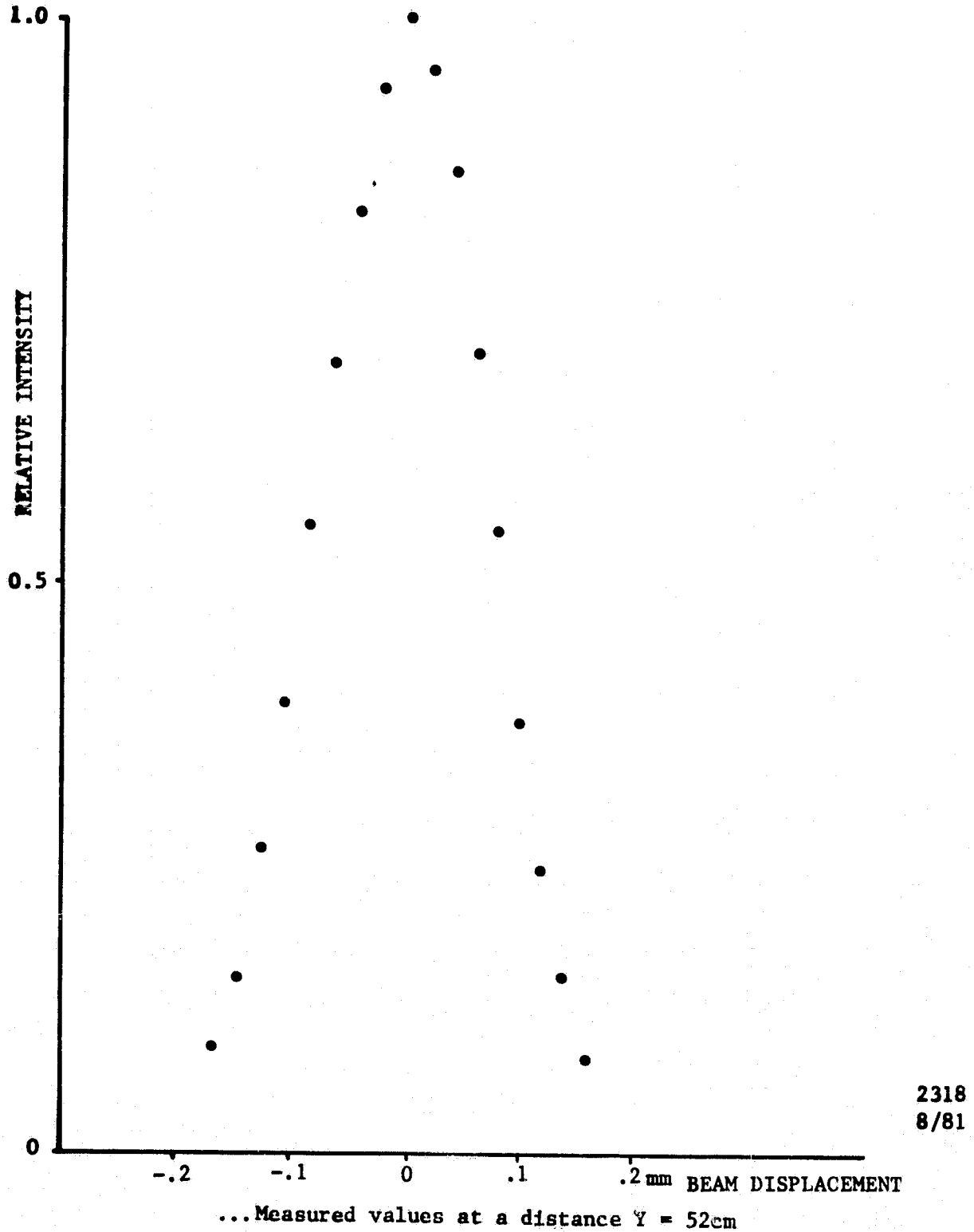


Figure 5-6. Decrease in Intensity of Deflected Beam Displaced From Center of Switch

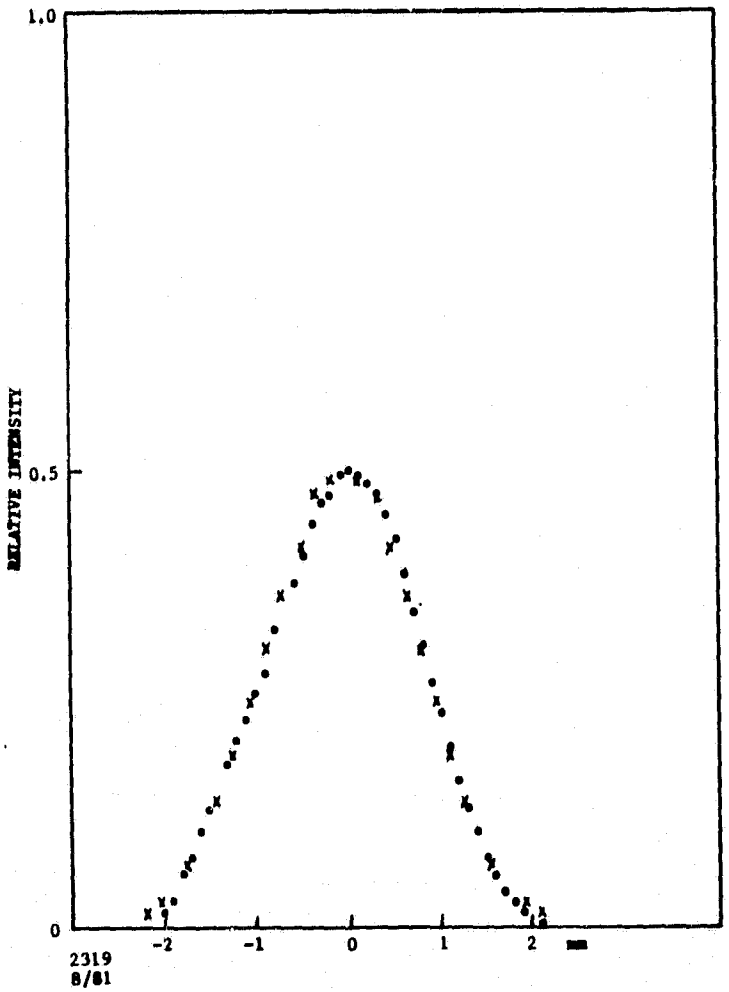


Intensity distribution of laser beam deflected by Bragg Diffraction Switch by 0.09mm along z-axis.

••• Measured values at a distance Y + 52cm Y = 52cm
XXX computed distribution $e^{-2(\frac{z}{w})^2}$

For w = 1.65 mm

Figure 5-7. Intensity Distribution of Laser Beam Deflected by Bragg Diffraction Switch Beam Displaced from Center of Switch by 0.09 mm Along Z-Axis

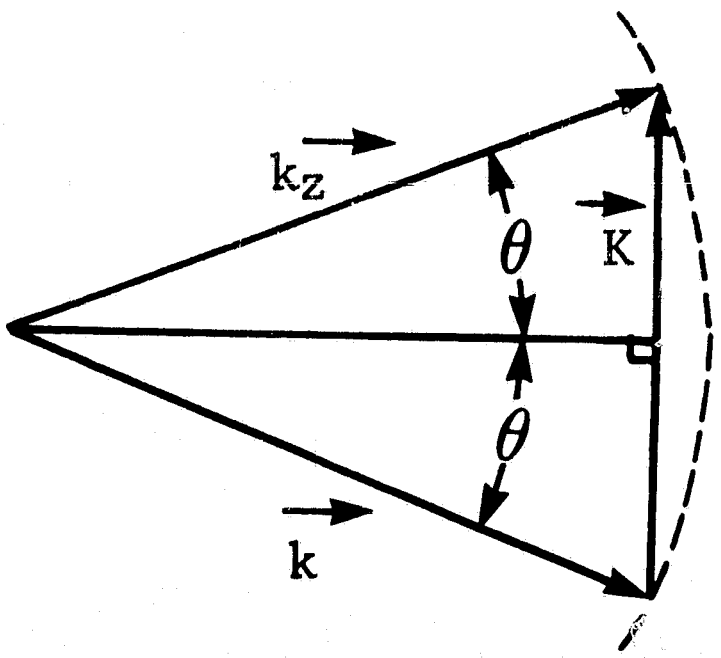


2320
8/81

Figure 5-8a. Momentum scattering for plane, monochromatic optical and acoustic waves. If the direction of $\kappa$ or $K$ is changed, thereby changing the angle of incidence denoted $\theta$, the vector sum $\kappa + K$ no longer falls on the circle and no scattering can occur.

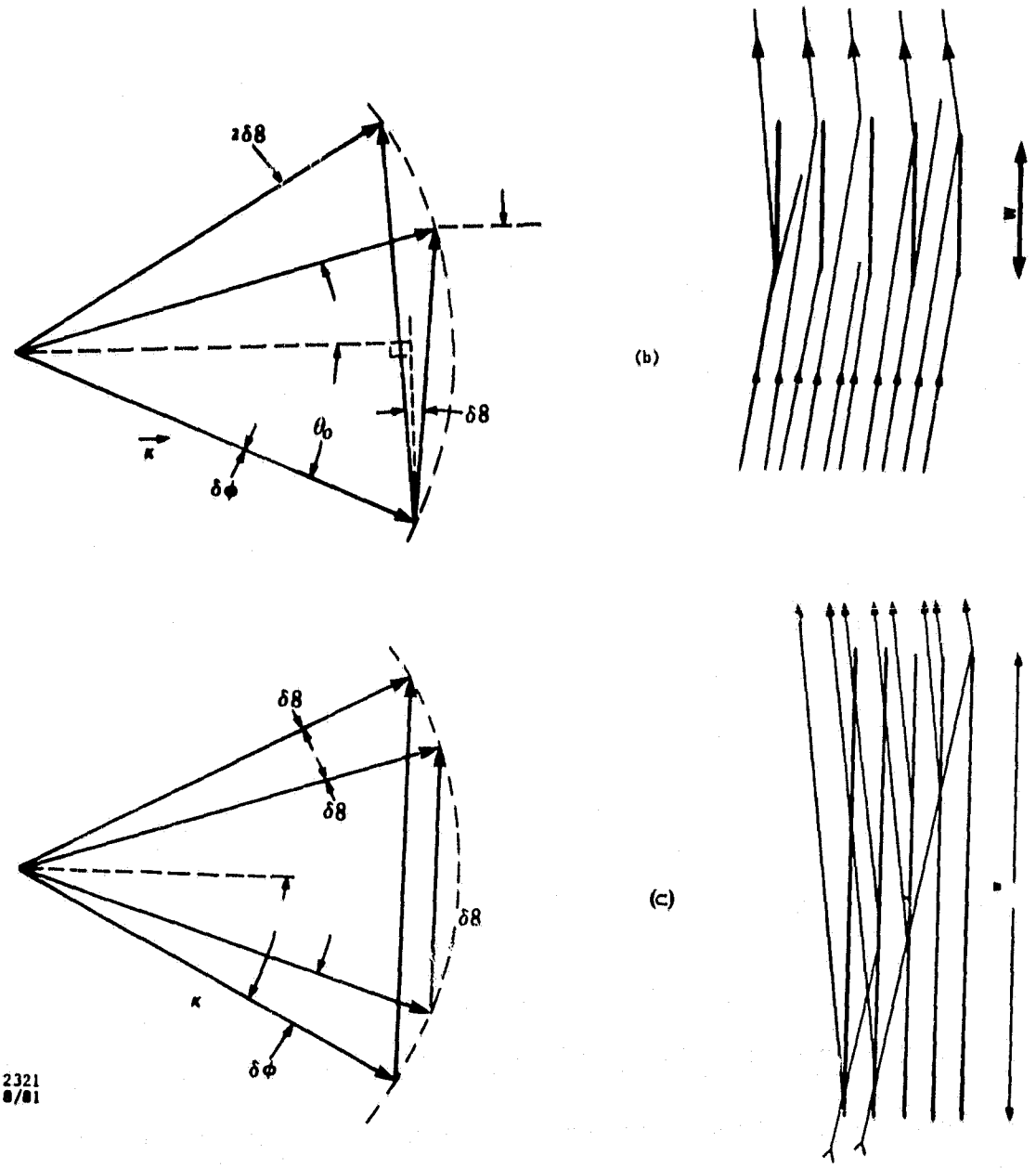


Figure 59b and 59c
Scattering with Phase Grating and Light Beams of Finite Width. The Diffraction Angle of the Light is $\delta\phi$ and that of the Phase Grating is $\delta\theta$. There are Two Possible Configuration:

(b) $\delta\theta >> \delta\phi$ or (c) $\delta\phi >> \delta\theta$

For (a) the Scattered Light Beam had a Diffraction Angle $\delta\phi$, for (b) the Diffraction Angle is $\delta\theta$.

the optical wavelength, and $2w_o$ is the Gaussian width of the incident optical beam at the beamwaist. For $\delta\theta \gg \delta\phi$ shown in Figure 5-8b, the diffraction angle of the deflected beam is the same as the diffraction angle of the incident beam. For $\delta\phi \gg \delta\theta$, shown in Figure 5-8c, the diffraction angle of the deflected beam is equal to $\delta\theta$.

For the electro-optic Bragg diffraction switch shown in Figure 3-4, $\Lambda$ = 8 microns, w = 0.55 mm, $\lambda$ = 0.6328 micron and $w_o$ = 105 microns, then $\delta\theta = 0.7 \times 10^{-2}$ radian and $\delta\phi = 0.2 \times 10^{-2}$ radian. Thus, the diffraction angles of the incident laser beam and of the periodic electric field are of the same magnitude. An explanation for the measured increase in diffraction angle of the deflected beam to $0.25 \times 10^{-2}$ radian can be found in the interaction between the incident laser beam and the periodic electric field of finite width.

# SECTION 6

# EVALUATION OF MINIMUM SEPARATION BETWEEN ADJACENT CHANNELS TO REDUCE COUPLING TO LESS THAN 50 dB

The smallest separation between adjacent laser beams forming the input and output lines of the switching matrix shown in Figures 3-1 and 3-5, is restricted by the requirement to minimize coupling between light beams in the planar optical waveguide.

## 6.1 TRAVELING WAVE INTERACTION

To evaluate the minimum separation between laser beams, a study was performed to determine whether traveling wave interaction is possible between the parallel laser beams in the planar optical waveguide of the switching matrix. In this study, the phenomena of traveling wave interaction is described and it is shown that, because of the homogeneity of the planar optical waveguide, traveling wave interaction between the parallel laser beams cannot occur.

Traveling wave interaction can occur between electromagnetic waves. At optical wavelengths, traveling wave interaction has been observed in parallel channel optical waveguides. These channel optical waveguides are similar to the planar optical waveguides of the switching matrix, with the exception that the optical field is not only confined in the x-direction, but also in the z-direction, as shown in Figure 6-1. The confinement is accomplished by the higher refractive index of the channel waveguide, not only in the x-direction, but also in the z-direction. Coupling between parallel channel waveguides requires that they are sufficiently closely spaced so that energy can be transferred from one to another. For traveling wave interaction, the coupling must be cumulative over a substantial length of the waveguide; this requires that the phase velocities of light in the two parallel waveguides be the same. The fraction of the power coupled per unit length is determined by the overlap of the modes in the separate channel waveguides. The directional coupler of the "Cobra" switch (Final Report of NASA contract NAS5-24449,

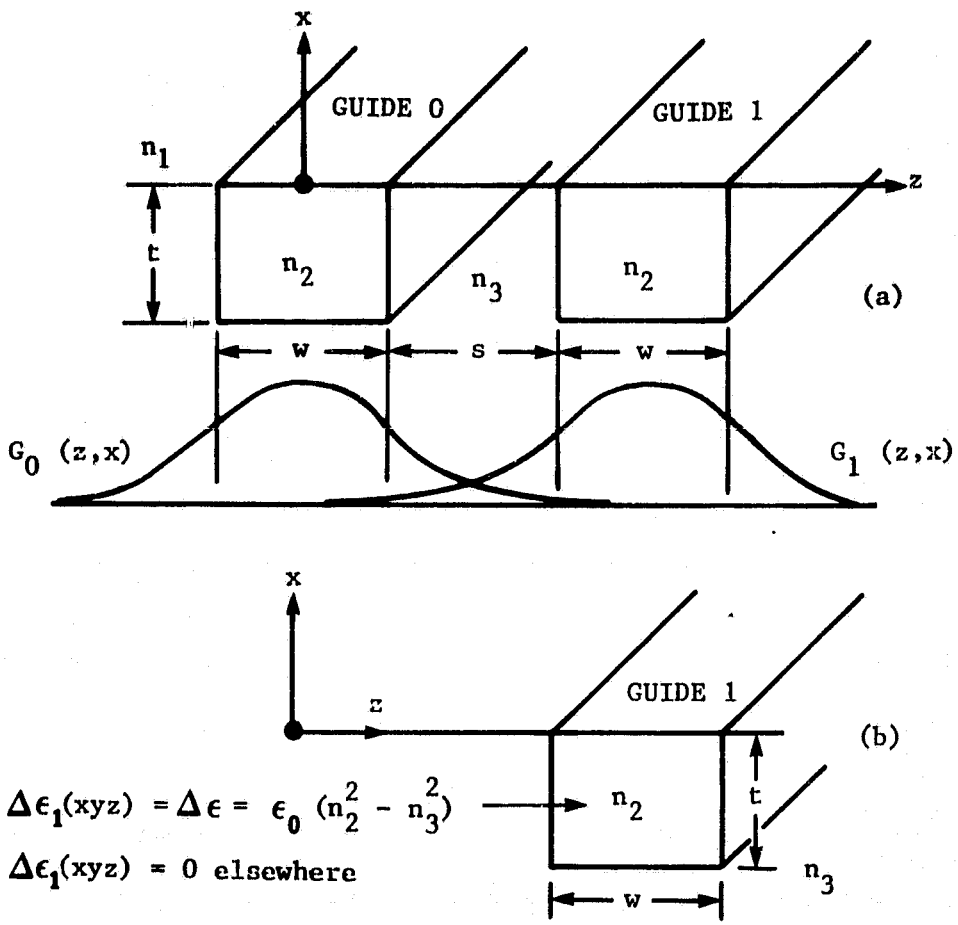


2322
8/81

Figure 6-1: (a) Sketch of two adjacent rectangular waveguides propagating modes.
(b) definition of the dielectric discontinuity $\Delta\epsilon_1(xyz)$.

Appendix A) uses traveling wave interaction between channel optical waveguides.

Traveling wave interaction has also been observed between collimated optical beams in planar optical waveguides. This interaction requires the presence of a distributed perturbation in the form of a periodic refractive index variation, set up by a periodic electric field or sound wave or in form of a surface corrugation. In the electro-optic Bragg diffraction switch in the planar waveguide (Section 4) the incident collimated laser beam couples energy to the diffracted laser beam by traveling wave interaction. The distributed perturbation is introduced by the periodic electric field which changes periodically the refractive index of the electro-optical $LiTiNbO_3$ waveguide.

In the switching matrix in the spaces between the switches, there is neither a periodic electric field, nor a sound wave nor a surface corrugation. Therefore, the laser beams in the switching matrix which propagate from switch to switch can not be coupled by this type of distributed perturbation.

However, the question arises whether the mechanism which sets up traveling wave interaction in channel optical waveguides might not also be effective in coupling the parallel laser beams in the planar waveguide of the switching matrix. It seems necessary, therefore, to investigate the phenomena which is effective in coupling two channel optical waveguides. The geometry of the two parallel optical waveguides is shown schematically in Figure 6-1. Guide 0 in the absence of guide 1 supports the fundamental mode with a transverse field distribution given by $G_0(z,x)$. The field distribution of the fundamental channel waveguide mode $G_0(z,x)$ is shown in Figure 6-2. This mode, in spite of having long tails into the substrate in the z and x directions, suffers no loss, (assuming that the optical waveguide and the substrate are lossless) and propagates with constant power. When guide 1 is introduced, the tail of the mode $G_0(z,x)$ in guide 0 will penetrate into guide 1.

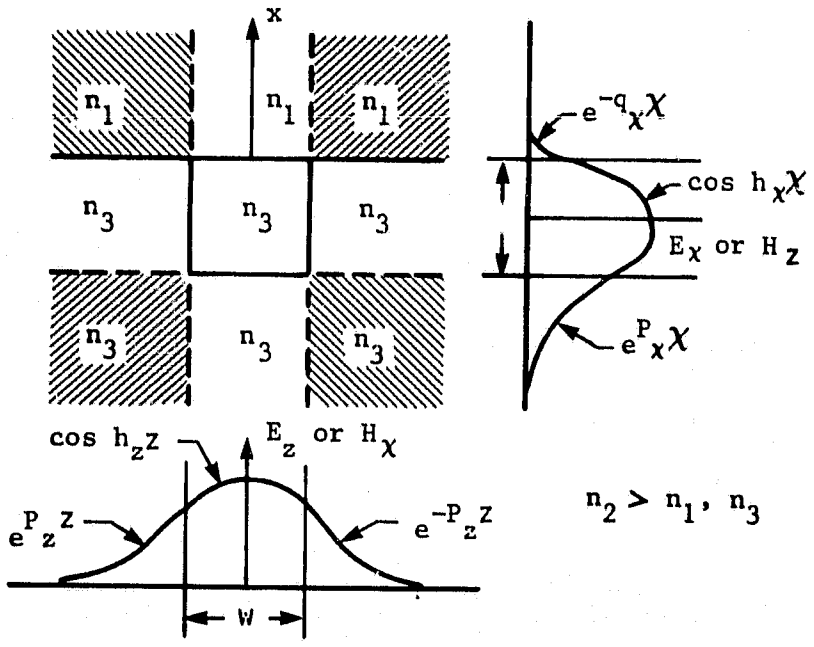


2323

8/81

Figure 6-2. Mode Profile of a Rectangular Channel Guide

Because the refractive index of the guides ($n_2$) is larger than refractive index of the substrate ($n_3$), an additional electric polarization is generated in the mode $G_0(z,x)^{(1)}$. This perturbation in the polarization of the mode $G_0(z,x)$ drives the mode in guide 1.

The macroscopic electric polarization of a dielectric is the sum of the microscopic dipol moments induced by an applied electric field. For sinusoidally varying electromagnetic field quantities, the electric field $\vec{E}(\omega)$ and the electric displacement $\vec{D}(\omega)$ are related by

$$\vec{D}(\omega) = \epsilon_0 \vec{E}(\omega) + \vec{P}(\omega) \tag{6-1}$$

where $\epsilon_0$ is the dielectric constant in free space and $\vec{P}(\omega)$ is the macroscopic electric polarization. In a linear medium, the polarization $\vec{P}(\omega)$ is linearly related to the electric field $E(\omega)$ in the form

$$\vec{P}(\omega) = \chi(\omega)\epsilon_0 \vec{E}(\omega) \tag{6-2}$$

where $\chi(\omega)$ is the electric susceptibility of the linear medium. The relationship between $\vec{D}(\omega)$ and $\vec{E}(\omega)$ then becomes

$$\vec{D}(\omega) = \epsilon_0 \left[1 + \chi(\omega)\right] \vec{E}(\omega) = \epsilon(\omega)\vec{E}(\omega) \tag{6-3}$$

where $\epsilon(\omega)$ is the dielectric constant of the dielectric.

To vary the polarization, power must be spent. The power per unit volume $\frac{P}{V}$ expended by an electric field to vary the electric polarization is

$$\frac{P}{V} = \overline{\vec{E}(\omega) \frac{\partial \vec{P}(\omega)}{\partial t}} \tag{6-4}$$

where the horizontal bar denotes averaging over a time interval long compared to $\frac{2\pi}{\omega}$. Conversely, power per unit volume is generated by a perturbation of the electric polarization. Thus, the perturbation of the polarization of the

mode in guide 0 (introduced by the higher refractive index of guide 1) $\vec{P}_{10}(\omega)$ will generate power in guide 1. That is

$$\frac{dP_1}{dt} = -\vec{E}_1(x,y,z,\omega) \frac{\partial P_{10}(x,y,z,\omega)}{\partial t} \tag{6-5}$$

The perturbation in the electric polarization $\vec{P}_{10}(x,y,z,\ )$ can be approximated by multiplying the electric field of guide 0 by the disturbance of the dielectric constant caused by the introduction of guide 1.

$$\vec{P}_{10}(x,y,z,\omega) = \Delta\varepsilon_1(x,y,z,\omega)\ \vec{E}_0(x,y,z,\omega) \tag{6-6}$$

Over the cross section of guide 1, $\Delta\varepsilon(x,y,z,\omega)$ has a constant value,

$$\Delta\varepsilon_1 = \varepsilon_2 - \varepsilon_3 = \varepsilon_0(n_2^2 - n_3^2) \tag{6-7}$$

and is zero everywhere else, as shown in Figure 6-1. The electric field in the guides is given by

$$\vec{E}(x,y,z,\omega) = A(y)\vec{G}(z,y)e^{j\omega t} \tag{6-8}$$

where A(y) is the complex amplitude of the propagating mode which includes the phase term $e^{j\beta y}$. From Equations 6-5, 6-6, and 6-8, the growth of the optical power carried by the mode in guide 1 becomes

$$\frac{dP_1}{dV} = -A_1(y)G_1(z,x)e^{j\omega t}\Delta\varepsilon_1 j\omega A_0(y)G_o(z,x)e^{j\omega t} \tag{6-9}$$

The growth of the optical power in guide 1 in Equation 6-9 is proportional to the additional polarization introduced by the disturbance of the mode in guide 0. This disturbance is introduced by the extension of the mode $G_0(z,x)$ in guide 0 into the region of higher refractive index of guide 1. This phenomena which causes the traveling wave interaction in channel optical waveguides cannot occur in the planar waveguide of the switching matrix. This is because the refractive index of the $LiTiNbO_3$ waveguide is uniform over the cross section of the planar waveguide (in the y-z plane). The important result of

this investigation is that traveling wave interaction cannot occur between the parallel laser beams in the spaces between the switches in the switching matrix shown in Figures 3-1 and 3-5.

## 6.2 EFFECT OF OPTICAL COMPONENTS AT THE OUTPUT PORTS ON CROSSTALK

Since traveling wave interaction does not take place between the parallel laser beams in the planar waveguide of the switching matrix, coupling between light beams is determined by the optical components at the output ports of the switching matrix, shown in Figure 6-3. Specifically, the coupling is determined by the beam transformation through lens 3, by the cross talk reduction in the spatial filter and by the "receiving cross-section" of the optical fiber.

The beam transformation of a laser beam through an ideal lens leaves the transverse field distribution of the laser beam unchanged; an incoming fundamental Gaussian beam will emerge from the lens as a fundamental beam. The lens changes only the radius of the phasefront curvature R and the beam radius w.

The transformation of a laser beam through an ideal lens with the focal length f, to a distance d behind the lens can be derived from the ray transfer matrix. It is

$$\begin{pmatrix} z_2 \\ z_2' \end{pmatrix} = \begin{pmatrix} 1 - \frac{d}{f} & d \\ -\frac{1}{f} & 1 \end{pmatrix} \begin{pmatrix} z_1 \\ z_1' \end{pmatrix} \qquad (6\text{-}10)$$

where $z_1$ and $z_2$ are the distances of a paraxial ray from the optical axis and $z_1'$ and $z_2'$ are the slopes of the paraxial rays with respect to the optical axis. For a light beam incident along the optical axis of the lens $z = z_1' = 0$ and from Equation 6-10, $z_2 = z_2' = 0$. For a light beam which propagates parallel to the optical axis of the lens but offset by the distance s, $z_1 = s$ and $z_1' = 0$. For the transformed beam from Equation 6-10. $z_2 = (1 - \frac{d}{f})$ and $z_2' = -\frac{s}{f}$. Furthermore, when $d = f$, $z_2 = 0$

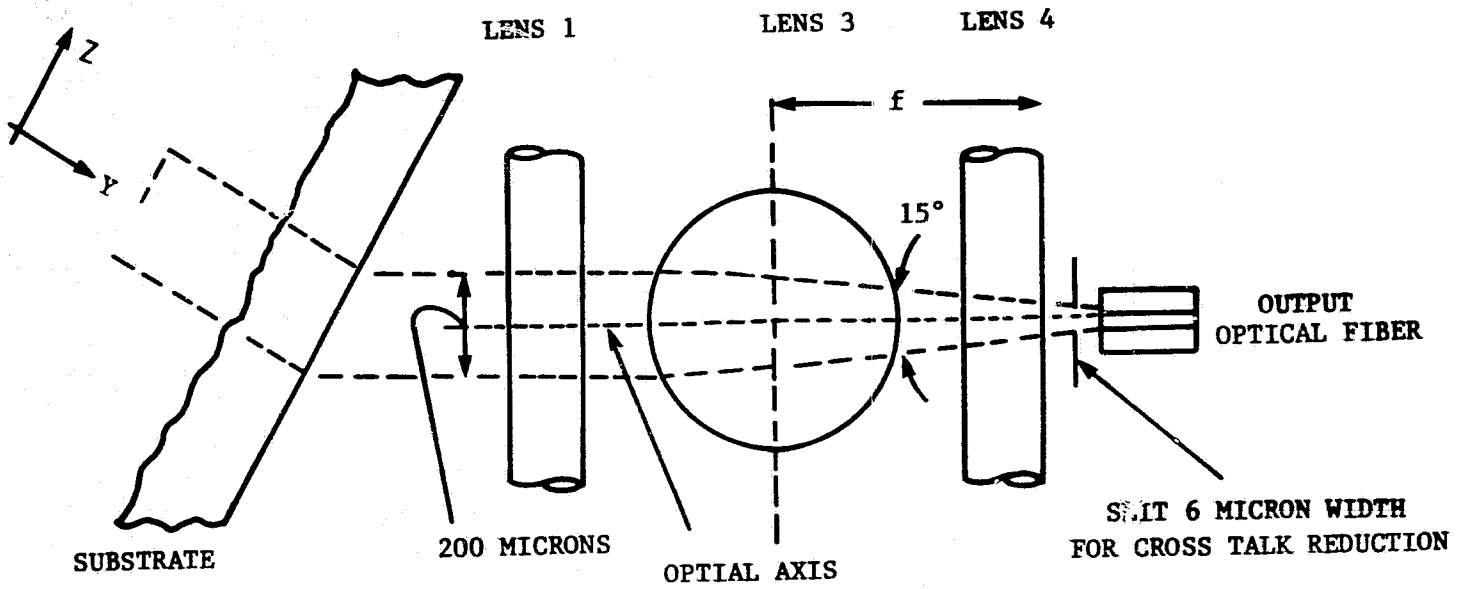


2324
8/81

Figure 6-3. Crosstalk Reduction

and $z_2' = \frac{s}{f}$. The transformed beam which had been parallel to but offset from the optical axis, crosses the optical axis of the lens in the focal plane, where d = f. Its slope is $z_2' = \frac{s}{f}$. At a distance d>f, the beam is displaced from the optical axis by $-(1 - \frac{d}{f})$, its slope remains $z_2' = -\frac{s}{f}$, as shown in Figure 6-4.

The transformation of two adjacent light beams from the switching matrix through an ideal lens can be evaluated using the ray transfer matrix in Equation 6-10. In Figure 6-5, the transformation of the two collimated fundamental Gaussian beams through an ideal lens is shown. One beam propagates along the optical axis of the lens; the center of the second beam which is parallel to the first, is at a distance of four times the Gaussian beam radius. The shaded sections correspond to the Gaussian beam diameter of the light beams, where most of the optical energy is concentrated. The transformed beams are focused in the focal plane of the lens, where the two beams interfer. From the focal plane, the two beams separate and expand.

The optical fibers at the output ports of the switching matrix intercept the expanding light beams. To minimize crosstalk, the cross sections of the fibers should not exceed the diameter of the Gaussian width of the light beams. Since most of the optical energy is concentrated within the Gaussian width of the light beams, the small diameter of the fibers should have the effect of reducing crosstalk (by not intercepting light from the regions where the beams overlap) without substantial loss in transfer efficiency.

To minimize crosstalk, the "receiving cross section" of the optical fibers, that is their directivity, should be high. This requires that the optical fibers only transfer light which is incident over a small angle range. The numerical aperture (NA) of fiber defines this angle range. The numerical aperture of a step index fiber is

$$NA = \sin\Theta = (n_1^2 - n_2^2)^{1/2} \qquad (6\text{-}11)$$

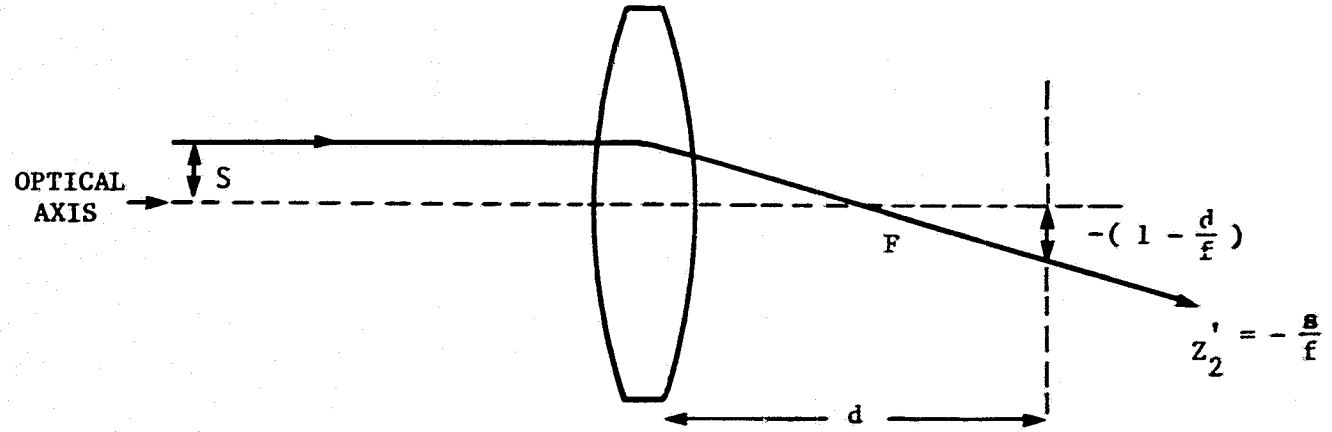


2325
8/81

Figure 6-4. Transformation Through a Lens

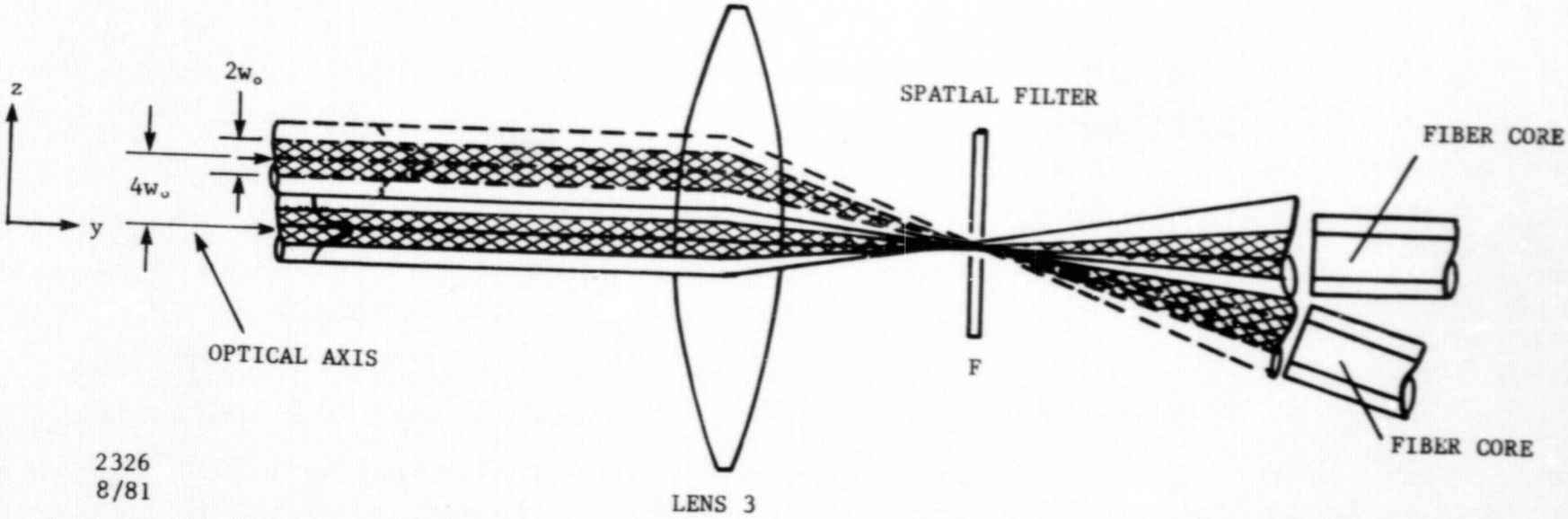


Figure 6-5. Transformation of Two Light Beams Through Lens 3

where $n_1$ and $n_2$ are the refractive indices of the core and the cladding, respectively. The smallest numerical aperture for a single mode fiber was reported to NA = 0.067, or $\Theta = 4°$. For a single mode fiber, the core diameter 2a is related to the NA by

$$2.4 \leqq \frac{2\pi}{\lambda} a \, NA; \tag{6-12}$$

for $\lambda = 0.6328$ micron, $2a \leqq 7$ microns.

Optical step-index fibers with 7 microns diameter, however, cannot be used at the output ports of the switching matrix. This is because the Gaussian beam diameter of the laser beams in the focal plane of the lens is 6 microns (Figure 6-3). Since the optical fibers must be placed outside the focal plane where the beams have separated and expanded, the core diameter of the optical fiber must be larger than 7 microns. The optical fibers at the output ports of the switching matrix, therefore, can only be multi-mode fibers with small NA or graded-index fibers. It follows that a correct design and alignment of the optical fibers at the output ports of the switching matrix will reduce the coherent interaction between adjacent laser beams.

The spatial filter in the focal plane of the lens 3 (Figure 6-5) does not reduce the coherent interaction. The spatial filter discriminates against scattered radiation set up by statistically distributed inhomogeneities in the planar waveguide, as outlined.

In summary, crosstalk between adjacent channels cannot occur by traveling wave interaction. Crosstalk be coherent interaction is reduced by the optical fibers at the output ports; cross talk by incoherent interaction is reduced by the spatial filters. The spacing of four times the Gaussian beam radius between the parallel light beams in the switching matrix seems conservative to accomplish a crosstalk reduction of 50 db. This design approach, however, must be confirmed by actual measurements of scattering in the planar waveguide. It also requires an examination of the transform properties of lens 3, since the crosstalk reduction outlined above requires that lens 3 be diffraction limited.

# SECTION 7
# COUPLING PRISM AND SUBSTRATE

## 7.1 DESIGN OF PRISM COUPLER

The function of the prism coupler is to transfer the collimated laser beam, propagating in free space, to a dielectric waveguide mode in the planar optical waveguide, formed by Ti-diffusion in a $LiNbO_3$ substrate. The prism coupler can also perform the reciprocal operation. Figure 7-1 shows schematically the transfer of the laser beam from air through the prism to the optical waveguide, in the direction where the wave is guided by the planar dielectric waveguide. In reference to the orientation of the electro-optic Bragg diffraction switches on the $LiNbO_3$ substrate, the beam transformation in Figure 7-1 is in the x-y plane. The coupling prism should not affect the beam shape in the z-direction.

The principle of the prism coupler is based on traveling wave coupling through the evanescent field from the prism to the optical waveguide. In the coupler, the prism is placed above the optical waveguide and is separated by a small gap of air, which is of the magnitude of a half-wavelength. The incident laser beam is totally reflected at the base of the prism, and the waves in the prism and in the waveguide are coupled through the evanescent field. For traveling wave interaction over the entire width of the laser beam at the base of the prism, the components of the wave vectors parallel to the gap must be equal for the wave in the prism and the wave in the optical waveguide. This requires that

$$k_3 \sin\theta_3 = k_1$$

$$\text{where } k_3 = \frac{\omega}{c} n_3 = \frac{2\pi}{\lambda_o} n_3$$

$$k_1 = \beta = \frac{2\pi}{\lambda_o} n_g \qquad (7\text{-}1)$$

$\lambda_o$ is the free space wavelength, $n_3$ is the refractive index of the coupling prism, $\beta$ is the propagation constant of the optical waveguide mode and $n_g = \frac{\beta\lambda_o}{2\pi}$. The refractive index $n_g$ in the optical waveguide is between

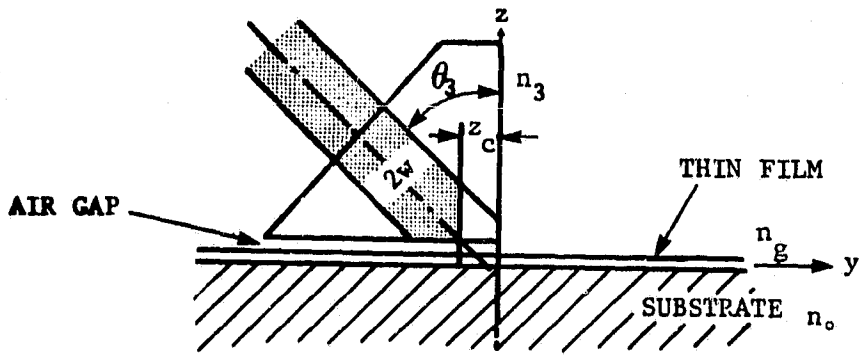


Figure 7-1. Traveling Wave Coupling from Prism to Optical Waveguide

that of $LiNbO_3$ substrate and that for the $LiTiNbO_3$ waveguide. It is

$$n_{LiNbO_3} < n_g < n_{LiTiNbO_3} \qquad (7\text{-}2)$$

For a given diffusion depth of the Titanium in the $LiNbO_3$ substrate, the refractive index $n_g$ is different for different mode numbers in the x-direction. The refractive index $n_g$ is largest for the fundamental mode. For Equation 7-1 it follows that the refractive index of the prism $n_3$ must always be larger than the refractive index of the waveguide mode $n_g$.

The angle $\theta_3$, shown in Figure 7-1, specifies the orientation of the prism in relation to the laser beam. By proper adjustment of the angle $\theta_3$, the prism coupler will excite only the fundamental mode in the optical waveguide.

Coupling prisms are generally made of titanium dioxyd (rutile) or strontium titanate; both meet the requirement that $n_3 > n_g$. $TiO_2$ is a uniaxial crystal, $SrTiO_3$ is a cubic crystal. The refractive indices of both crystals at different wavelength are summarized in Table 7-1.

The polarization of the laser beam which is incident on the Bragg diffraction switch in the $LiTiNbO_3$ waveguide is in the $TE_{oo}$-mode, where the electric field vector is parallel to the optical axis. For this polarization, the light in the optical waveguide formed by titanium diffusion into the uniaxial $LiNbO_3$ crystal, propagates as the extraordinary ray. The refractive index of $LiNbO_3$ for the extraordinary ray is 2.203 at the HeNe wavelength of 6328A.

Titanium diffusion into the $LiNbO_3$ substrate increases the refractive index by an increment of up to $\Delta n_e = 0.04$. From the relation 7-2 for the effective refractive index of the waveguide mode $n_g$, we obtain $2.203 < n_g < 2.243$. For the evaluation of the orientation of the coupling prism in relation to the laser beam, we will assume that the effective refractive index in the $LiTiNbO_3$ optical waveguide of 1 to 1.5 microns diffusion depth and for the fundamental mode is $n_g \approx 2.234$.

TABLE 7-1

REFRACTIVE INDICES OF $TiO_2$ and $SrTiO_3$

| | $TiO_2$ | |
|---|---|---|
| WAVELENGTH | $n_o$ | $n_e$ |
| 5700Å | 2.621 | 2.919 |
| 6900Å | 2.555 | 2.836 |
| 10100Å | 2.484 | 2.747 |

| | $SrTiO_3$ |
|---|---|
| WAVELENGTH | n |
| 6400Å | 2.3837 |
| 8500Å | 2.3337 |
| 8900Å | 2.3276 |

The orientation of the coupling prism is shown in Figures 7-2 and 7-3. The optical axis of the rutile prism, when mounted on the $LiNbO_3$ waveguide, is parallel to the optical axis in the $LiNbO_3$ crystal. Thus, the incident laser beam, which is polarized to set up the $TE_{00}$-mode in the optical waveguide with the electric field vector parallel to the optical axis, will propagate as the extraordinary ray through the prism. The refractive of the extraordinary ray in rutile from Table 7-1 at $\lambda_0 = 6328\text{Å}$, is $n_{3e} = 2.86$.

From these values for the refractive indices and from Equation 7-1 we can compute the angle $\Theta_3$. It is

$$\sin\Theta_3 = \frac{n_{g,e}}{n_{3,e}} = \frac{2.22}{2.86}$$

$$\Theta_3 = 51° \qquad (7\text{-}3)$$

In Figure 7-2 an optimized design of the coupling prism is shown. The right angle has been increased to 95° for greater mechanical stability, the edge at the 30° angle is truncated for mounting purposes and the laser beam incident on the hypotenuse is close to 90°. This design had been sent to Atomergic in New York for bid. The charge was $850.00 per prism; delivery was 8 to 10 weeks.

The design of the prism which had been ordered from Valtec in Massachusetts, is shown in Figure 7-3. The design was modified to conform with the standard product of Valtec where the angle at the coupling edge is 60°. This required a change of the angle of incidence to 26.5°. The price is $500.00 per prism; the delivery time is 8 weeks.

## 7.2 INVESTIGATION OF AVAILABILITY OF SINGLE CRYSTAL $LiNbO_3$ SUBSTRATE AS A FUNCTION OF SIZE, SURFACE FINISH AND COST

Lithium Niobate is manufactured in the United States by Crystal Technology (CT) in Palo Alto, and by Union Carbide (UC) in San Diego. Both

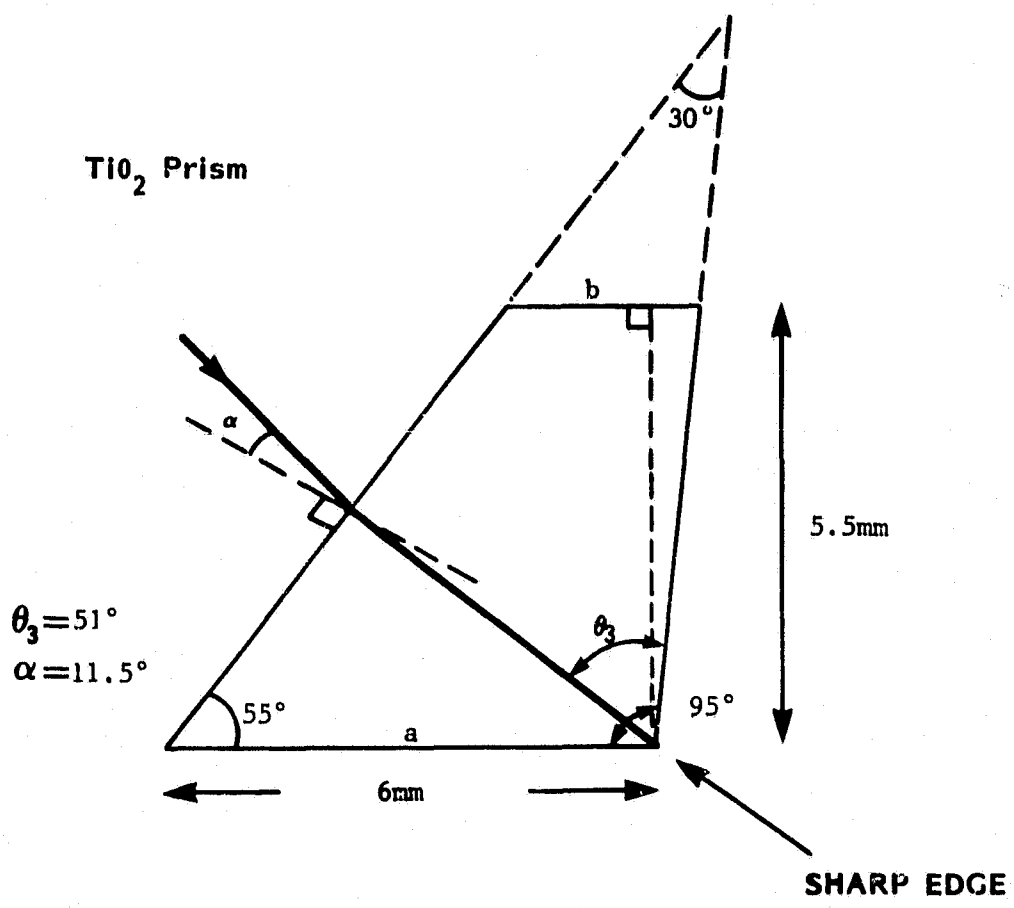


b parallel to a
optical axis parallel to edge of 55° angle
prism depth 10mm
surfaces should have good optical polish
flat to better than $\frac{\lambda_0}{2}$
$\lambda_0$=6328 Å

2328
8/81

two prisms required

Figure 7-2. Truncated Coupling Prism

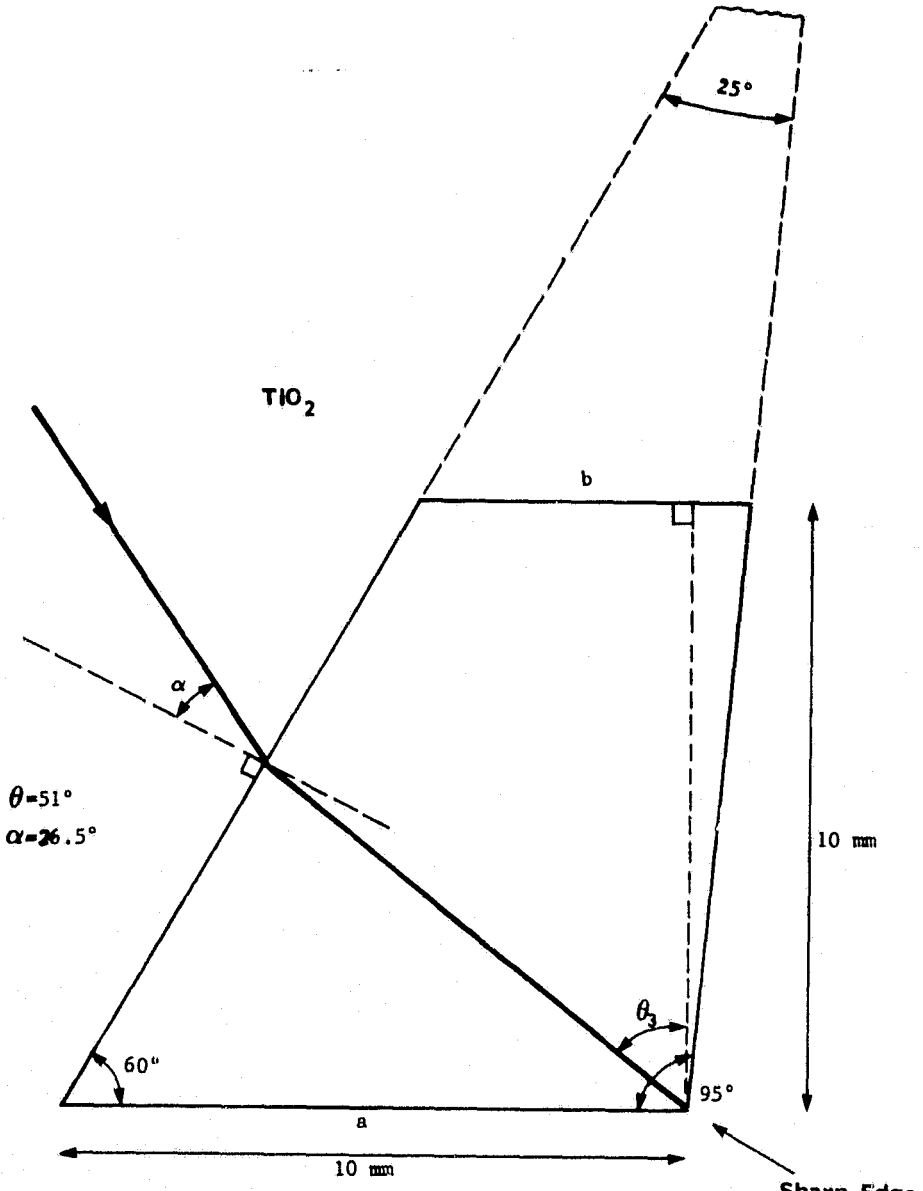


Optical axis parralled to edge of 60° angle

b parralled to a

Surfaces should have good optical polish

flat to better than $\frac{\lambda^\circ}{2}$ ($\lambda_\circ$ = 6328Å)

prism depth 10mm

two prisms required

2329
8/81

Figure 7-3. Truncated Coupling Prism.

companies grow their crystals from the "congruent" melt which ensures that the crystal is uniform in composition, and therefore index of refraction, down its entire length. The use of the "congruent" melt and careful control of growth conditions minimizes striations and precipitates in the material. Therefore, material is selected and graded according to the extinction between cross polarizers. UC uses the terms "acoustic grade" and "electro-optic grade"; CT uses the terms "selected acoustic grade" and "electro-optic grade". In the case of UC, "acoustic grade" sometimes contains discoloration and stria, while with CT "selected acoustic grade" contains no stria. UC grows the two grades under different growth conditions and uses minimal inspection, while CT grows using one set of growth conditions and sets the grade by the measured properties under more severe inspection.

Both companies utilize a chem-mechanical polish to produce a damage-free and scatter-free surface. CT claims to deliver a flatness of 0.5 to 1 fringe per inch, while UC claims flatness of 1 to 2 fringes per inch. UC can improve on this by having the material polished by their specialty group (at a higher price). The prices and delivery for X-cut pieces, 1 mm thick, are as follows:

| | UC (Acoustic Grade) | CT (Select Acoustic Grade) |
|---|---|---|
| SIZE | 1.5" X 2.1" | 1.5" X 1.5" |
| PRICE | $67 each | $88 each |
| DELIVERY | 3 - 4 weeks | 8 - 10 weeks |

The price* for electro-optic grade has not been given yet.

It was pointed out that the extinction measurements are actually only valid on short samples, such as those used in optical modulators and the like. Therefore, no prediction could be made concerning the actual deviation of optical path there might be over a one or two inch long piece. This is particularly true when one considers the variations in index of refraction which will result from the titanium diffusion.

---

* Provide in final document

At the present time, UC grows only Z-axis crystals. This restricts the dimensions of X cut wafers to 2" in the Y-axis. CT can grow crystals of 5 to 6" in the Y-axis. They believe that Y-axis crystals could be grown up to 15" long, but they have no plans to do so at the present time.

# SECTION 8
# $LiTiNbO_3$ WAVEGUIDE

## WAVEGUIDES

Six planar $LiTiNbO_3$ waveguides have been formed by titanium diffusion into $LiNbO_3$ at MA. The six waveguides have different parameters. The objective was to determine the optimum planar waveguide parameters for use for the switching matrix. To do so, three waveguides were formed on $LiNbO_3$ substrates purchased from Crystal Technology and three on substrates purchased from Union Carbide. Also, the thickness of the titanium before diffusion was different and the corresponding diffusion times were varied.

Coupling from free space radiation to guided modes in the waveguides could be accomplished in all waveguides. To evaluate the properties of each $LiTiNbO_3$ waveguide, the synchronous angles for coupling from a $TiO_2$ prism into the fundamental mode (m = 0), and the first order mode (m = 1) of the waveguide for the extraordinary ray (y-direction of propagation) was compared to the synchronous angle for coupling into the fundamental substrate mode of the $LiNbO_3$ wafer. Though the absolute value of the synchronous angles can not be evaluated precisely, their differences can be measured with great precision using the scale on the rotational mount which supports the prism holder.

The range of the synchronous angle was measured over which energy could be coupled from the prism into the planar waveguide. This measurement was performed at different sections of the substrate. The result is shown in Figures 8-1 and 8-2. The half-width in both cases is 0.11°, indicating that the waveguide mode seems to be the same at different sections of the substrate.

The highest coupling efficiency which was obtained was 25 percent.

The absolute value of the synchronous angle of the fundamental $LiNbO_3$ substrate mode was computed from Equations 7-1, 7-2, 7-3, and 7-4 in

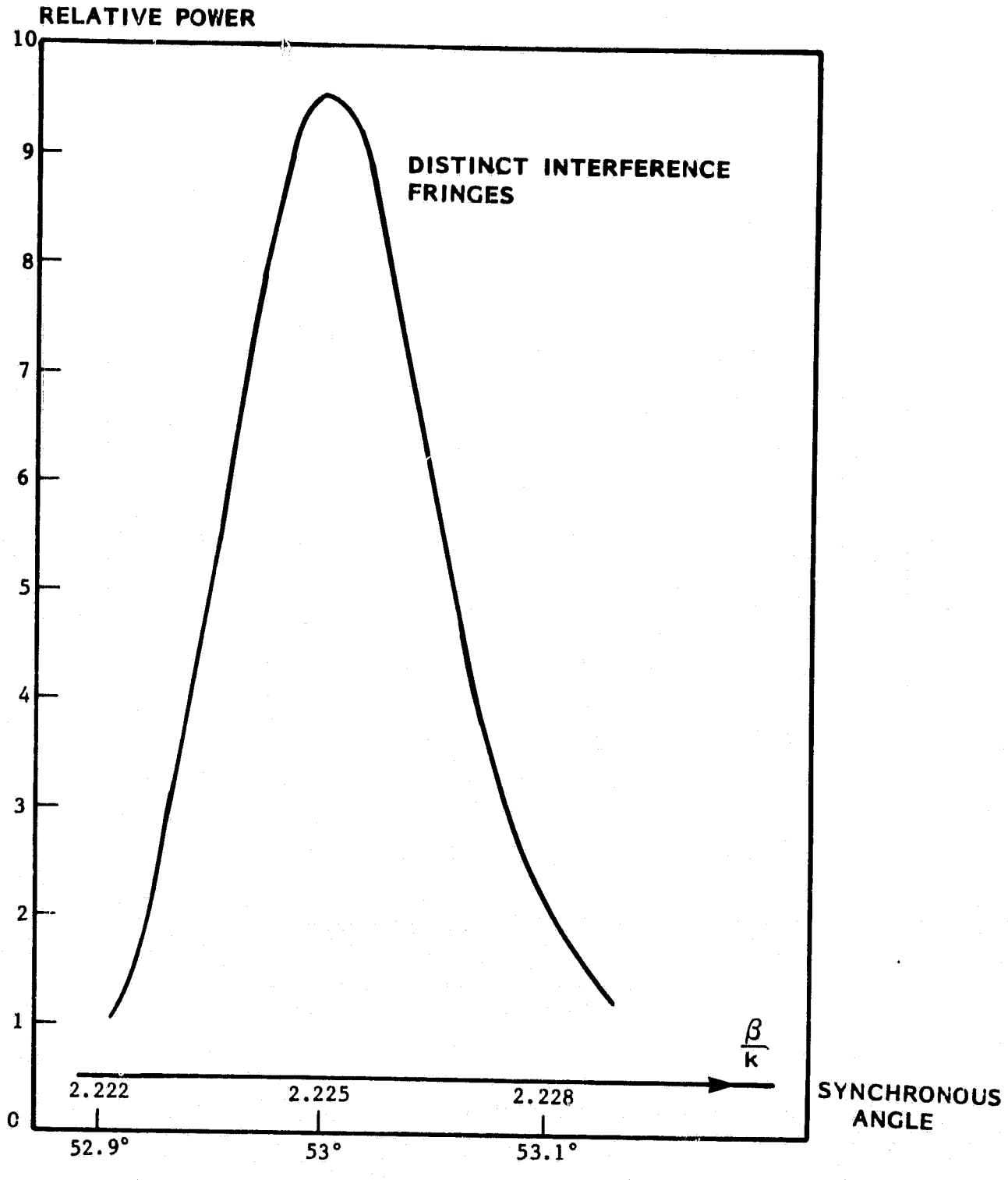


2330
8/81

Figure 8-1. Relative Optical Power Coupled into Planar Optical Waveguide as a Function of Synchronous Angle and of Relative Propagation Constant $\frac{\beta}{k}$ of Zero-order mode.

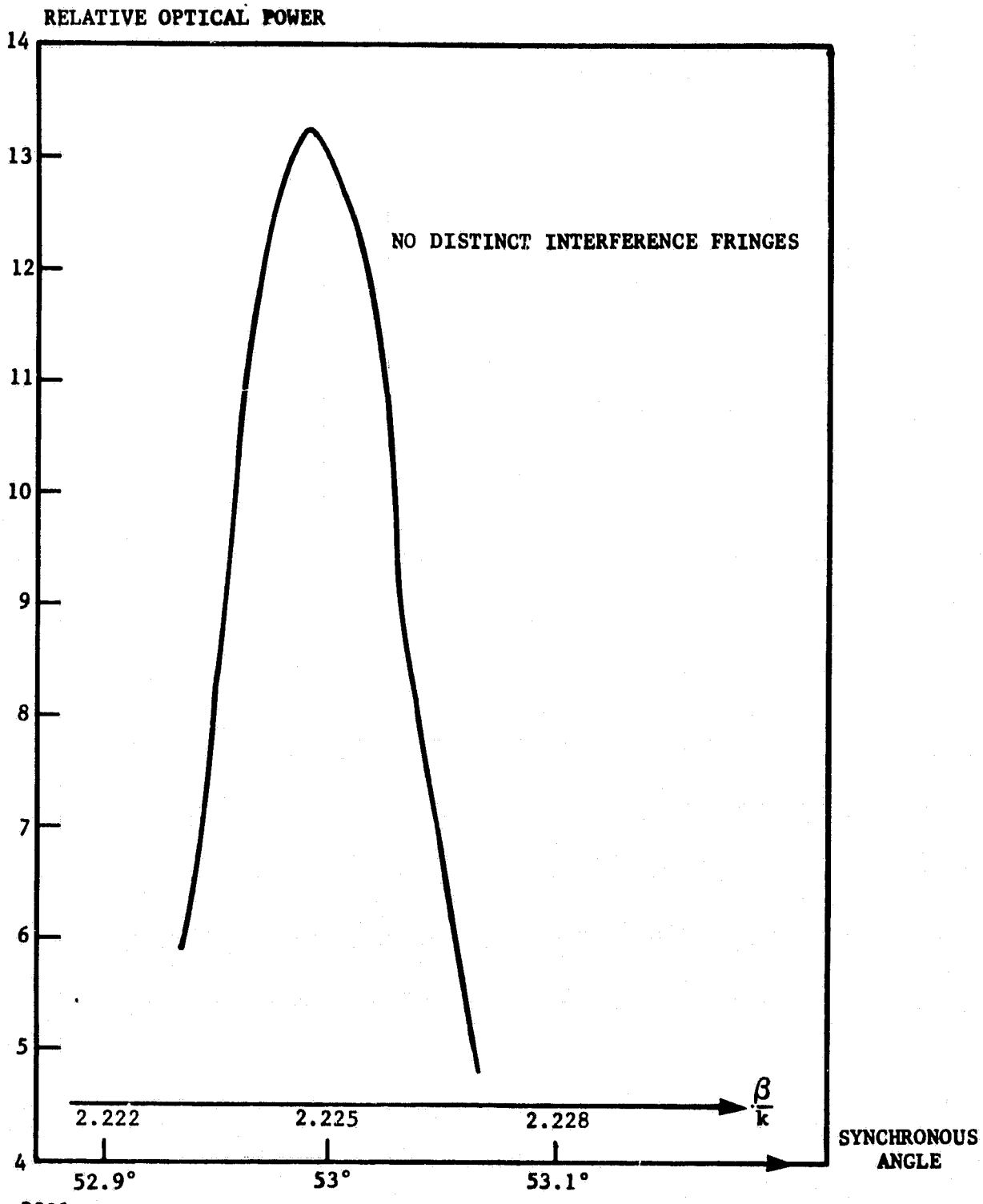


Figure 8-2. Relative Optical Power Coupled into Planar Optical Waveguide as a Function of Synchronous Angle and of Relative Propagation Constant $\frac{\beta}{k}$ of Zero-order Mode

Section 7 to $\theta_{0,s}$ = 50.38° for the refractive index of the extraordinary ray in $LiNbO_3$ of $n_1$ = 2.203, for a thickness of the $LiNbO_3$ substrate of 1 mm and for the refractive index of the extraordinary ray in the $TiO_2$ prism of $n_e$ = 2.86. The normalized propagation constant $\frac{\beta_{m=0}}{k}$ = 2.203.

To simplify the computation of the refractive index ($n_1$) and the depth of the $LiTiNbO_3$ waveguides (w), the normalized relations shown in Figure 8-3 were used, rather than Equations 7-3 and 7-4 in Section 7. In Table 8-1 the properties of the three waveguides which have been computed so far, are summarized.

Table 8-1

Waveguide Properties

| | $\theta_{m=0}$ | $\theta_{m=1}$ | $\frac{\beta_{m=0}}{k}$ | $\frac{\beta_{m=1}}{k}$ | $n_1$ | w |
|---|---|---|---|---|---|---|
| UC320Å, t = 4.5 hrs. | 51.17° | 50.43° | 2.22979 | 2.2046 | 2.2395 | 1.12 μ |
| UC350Å, t = 5.0 hrs. | 51.22° | 50.445° | 2.2295 | 2.205 | 2.2399 | 1.23 μ |
| UT320Å, t = 5.5 hrs. | 51.17° | 50.6° | 2.22797 | 2.21 | 2.235 | 1.55 μ |

Though the diffusion with the layer of 320 Å of Titanium into the Union Carbide and into the Crystal Technology substrates were done simultaneously in the same apparatus, their properties seem to be quite different. So far as the efficiency of the electro-optic Bragg diffraction switch is concerned, the shallower waveguide in the UC material would be advantageous. However, the waveguides in the UC show diffraction spreading, which later on was identified as optical damage.

The $LiNbO_3$ substrates from Union Carbide have a square shape, so that the properties of the $LiTiNbO_3$ waveguide could also be evaluated along the optical axis, that is for the ordinary ray. The refractive index of $LiNbO_3$ for the ordinary ray in $n_1$ = 2.295. The synchronous angle of the fundamental substrate mode for the ordinary ray in $LiNbO_3$ is $\theta_{0,s}$ = 53.365. The synchronous angle for the fundamental mode in the $LiTiNbO_3$

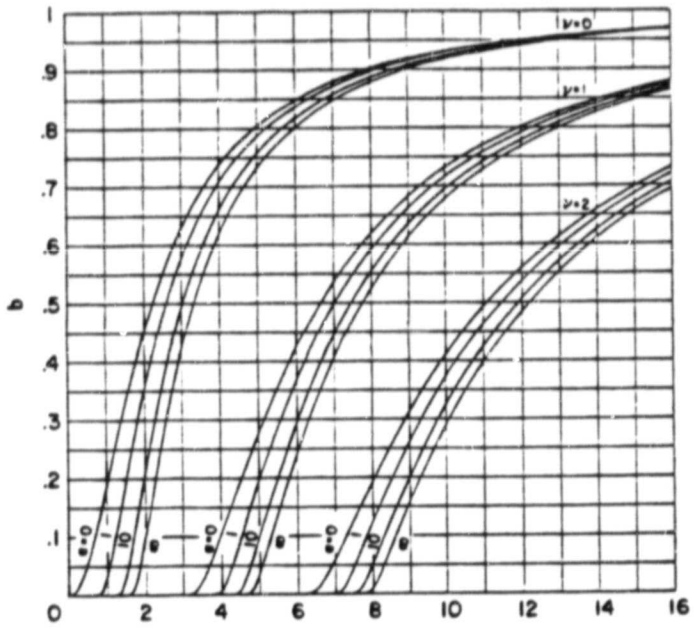


$$V = kw(n_1^2 - n_o^2)^{\frac{1}{2}}$$

$$b = (\beta^2 - n_o^2)/(n_1^2 - n_o^2)$$

$$a = (n_o^2 - 1)/(n_1^2 - n_o^2)$$

2332
8/81

Figure 8-3. Normalized $\omega - \beta$ Diagram of a Planar Slab Waveguide Showing the Guide Index b as a Function of the Normalized Thickness $V$ of Asymmetry

waveguide on the substrate UC320° A is $\Theta_{m=0} = 53.765°$, and the normalized propagation constant in the waveguide is $\frac{\beta_{m=0}}{k} = 2.3069$. No higher order mode can build up in the direction of the ordinary ray (z-direction).

Because of the single mode in the waveguide, the refractive index and the waveguide thickness can not be computed separately. There are sets of refractive indices and waveguide thicknesses for the normalized propagation constant of the fundamental mode in the $LiTiNbO_3$ waveguide of $\frac{\beta_{m=0}}{k} = 2.3069$. The functional relation between the refractive index and the depth of $LiTiNbO_3$ waveguide for $\frac{\beta_{m=0}}{k} = 2.3069$ is given in Figure 8-4.

In testing the newly diffused $LiTiNbO_3$ waveguides, great difficulties were experienced which finally could be resolved. It was found that the $LiTiNbO_3$ waveguide where coupling to the fundamental mode had been previously observed was not oriented correctly. The long dimension of the substrate was along the optical axis (z-direction) and not along the y-axis, as specified. The ray which propagates along the optical axis is the ordinary ray and its refractive index in $LiNbO_3$ is $n_0 = 2.295$.

The orientation of the newly diffused substrates of Crystal Technology is correct, the long dimension is along the y-axis. The correct orientation of the newly diffused substrate of Union Carbide can be adjusted, since the substrate is of square shape.

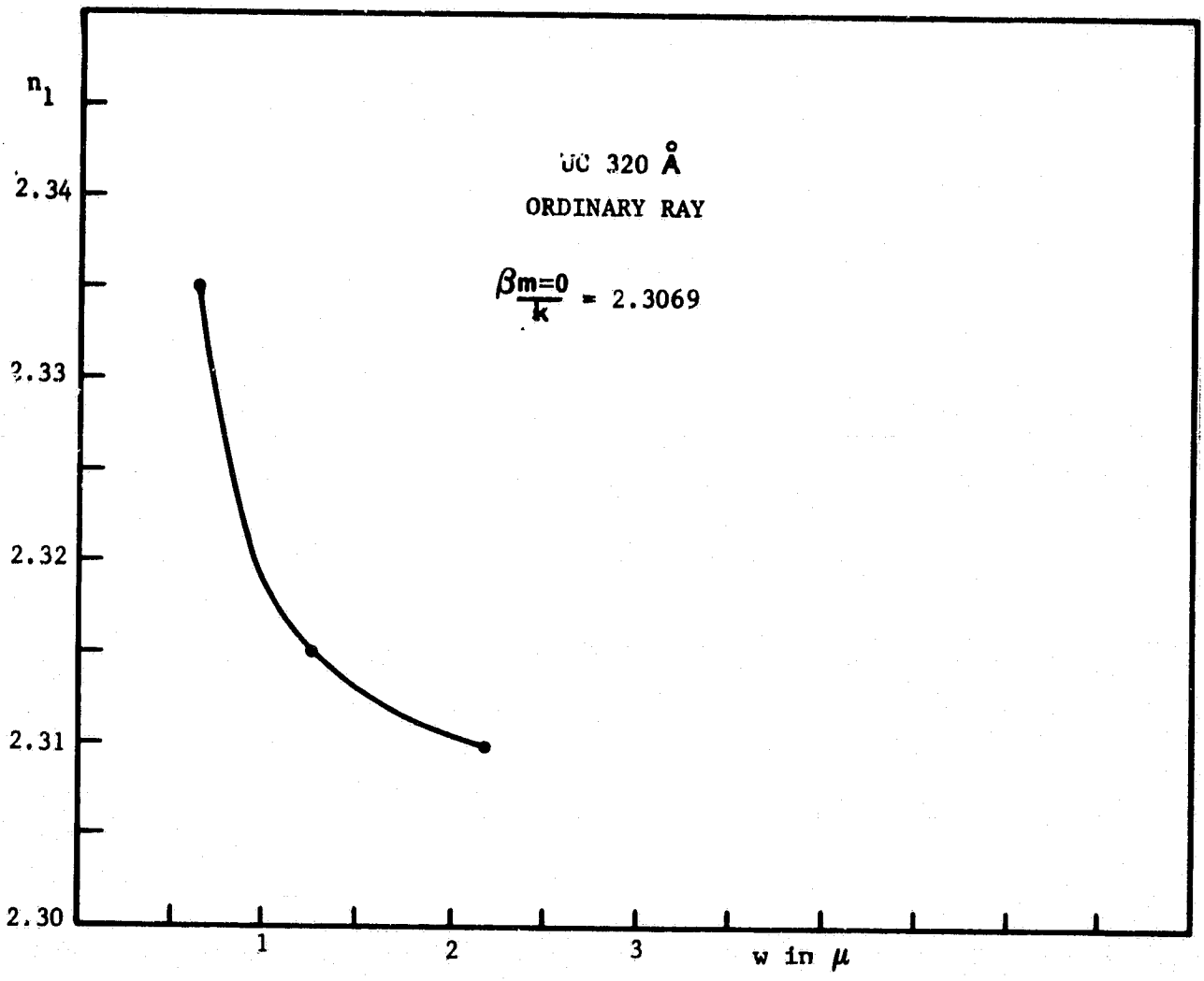


2333
8/81

Figure 8-4. The Functional Relation Between the Refractive Index and the Depth of $LiTiNbO_3$ Waveguide for $\frac{\beta_{m=0}}{k}$ = 2.3069



C-2

## REFERENCES
## TO SECTION 8

1. H. Kogelnik "Integrated Optics" Springer Verlag, 1975, p. 24.

## SECTION 9

## COMPUTATION OF EXTERNAL OPTICS TO YIELD A COLLIMATED LASER BEAM INSIDE THE OPTICAL WAVEGUIDE OVER THE LENGTH OF THE SWITCHING MATRIX (IN THE Y-DIRECTION)

In the switching matrix to be developed under this contract, the transmission of the coherent light beams between switches is in planar optical waveguide where the waves are guided in only one dimension (x-direction) along the diffusion depth of the waveguide. In the orthogonal dimension (z-direction), the waveform of the laser beams is determined by the external optics. The function of the external optics is to transform the diameter of the input laser beam to the proper diameter, required for an optimized switching matrix design. Conceptually, the beam transformation can be performed by either a single long focal length lens or by an inverted telescope. In both designs, the beamwaist of the laser beam which is focused by the lens closest to the switching matrix must be centered on the switching matrix, as shown in Figure 9-1. To minimize the beam spreading, the incident laser beam should be collimated over the entire length of the switching matrix. This requirement determines the numerical aperture $NA = \frac{a}{f}$ of the lens, where f is the focal length of the lens and 2a is the diameter of the laser beam at the lens.

When the laser beam is focused into the $LiTiNbO_3$ waveguide, the rays of the incoming laser beam are refracted at the interface between air and the $LiTiNbO_3$, such that the angles between the asymptotes to the beam contour and the beam axis becomes $\frac{\Theta}{n}$ inside the waveguide, where $\Theta$ is the respective angle in air, shown in Figure 9-1 and 9-2, and n is the refractive index of the $LiTiNbO_3$ waveguide mode. The angle $\Theta$ is the far-field diffraction angle of the fundamental transverse mode. For Gaussian beam, the

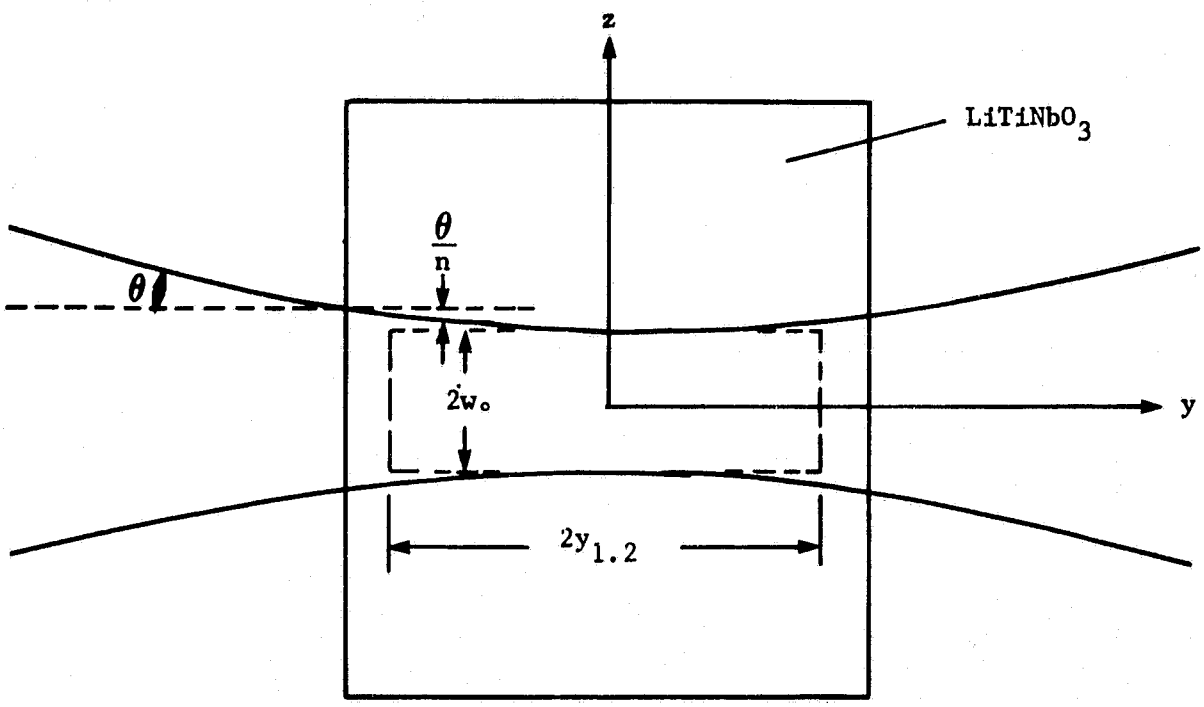


2334
8/81

Figure 9-1. Contour of Gaussian Beam Focused in the Center of the $LiTiNbO_3$ Waveguide

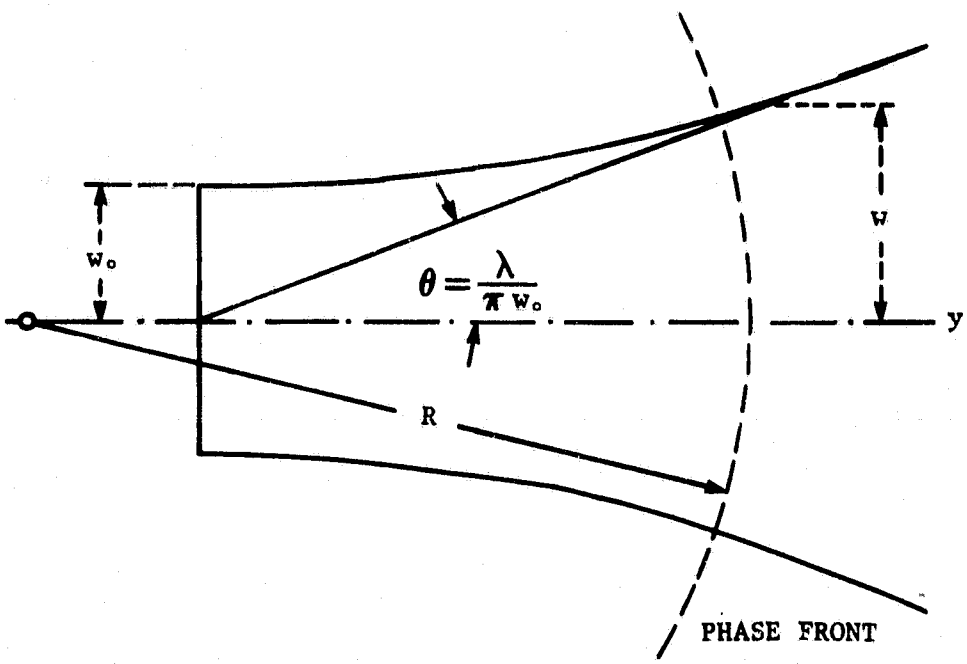


2335
8/81

Figure 9-2. Contour of Gaussian Beam

angle , which is related to the beam parameters, can be derived from the beam expansion equiation. It is

$$w^2(y) = w_o^2(1 + \xi^2)$$

$$\text{where } \xi = \frac{2y}{k_1 w_o} 2$$

$$k_1 = \frac{w}{c} n, \tag{9-1}$$

[n corresponds to $n_g$ in Section 7], y is the direction of wave propagation, $2w(y)$ is the beam diameter, $2w_o$ is the beam diameter at the beamwaist, $\frac{\omega}{c} = \frac{2\pi}{\lambda o}$ and $\lambda_o$ is the optical wavelength in air. (The beam diameter defines the width of a Gaussian beam where the amplitude of the electric field is $\frac{1}{e}$ times that on the axis). In the far-field $\xi^2 << 1$ and the far-field diffraction angle $\Theta$ from Equation 9-1 is

$$\Theta = \tan^{-1} \frac{w(y)}{y} = \tan^{-1} \frac{2}{k_1 w_o} \tag{9-2}$$

The far-field diffraction angle in air is

$$\Theta = \tan^{-1} \frac{\lambda o}{\pi w_o} \approx \frac{\lambda o}{\pi w_o} \tag{9-3}$$

and the far-field diffraction angle in the waveguide is

$$\frac{\Theta}{n} = \tan^{-1} \frac{\lambda o}{n \pi w_o} \approx \frac{\lambda o}{n \pi w_o} \tag{9-4}$$

The sine of the angle $\Theta$ is defined by the numerical aperture of the focusing lens. It is

$$\sin\Theta = \frac{a}{f} \tag{9-5}$$

and for small numerical aperture lenses, $\sin\Theta \approx \Theta$. From equations 9-3, 9-4, and 9-5 we obtain

$$w_o = \frac{\lambda o}{\pi} \frac{f}{a} \tag{9-6}$$

Thus, the beam radius $w_o$ in the focal plane of the focusing lens with the numerical aperture $\frac{a}{f}$ is the same whether the laser beam is focused in air or in the $LiTiNbO_3$ waveguide.

The laser beam expands from the beamwaist, where the beam expansion for a Gaussian beam is given by Equation 9-1. For the design of the optics for the switching matrix, the assumption will be made that the beam width of the laser beams should not expand by more than by a factor 1.2 over the entire length of the switching matrix. Using this restriction, it follows from Equation 9-1 that the total length of the matrix $2y_{1.2}$ is related to the beam radius at the beamwaist $w_o$ by

$$2y_{1.2} = 0.66 \frac{2\pi n}{\lambda_o} w_o^2 \tag{9-7}$$

Using Equation 9-6 the total length of the switching matrix as a function of the numerical aperture of the focusing lens, is

$$2y_{1.2} = 2.64 \frac{\lambda_o}{2\pi} n\left(\frac{f}{a}\right)^2 \tag{9-8}$$

From Equations 9-7 and 9-8, it follows that the laser beam expands slower in the dielectric waveguide with the refractive index n than in air, where n=1, and the range over which the beamwidth increases by a factor 1.2 is longer in

the dielectric waveguide by the refractive index n of the waveguide mode, than in air.

For comparison, we derive the beam parameters, when the laser beams can only expand by a factor 1.1 over the entire length of the switching matrix. Then

$$2y_{1.1} = 0.458 \frac{2\pi n}{\lambda_o} w_o^2 \tag{9-9}$$

$$2y_{1.1} = 1.83 \frac{\lambda_o}{2\pi} n(\frac{f}{a})^2 \tag{9-10}$$

M. Born and E. Wolf in "Principles of Optics", Section 8.8, have derived the beam radius $w_o$ at the beamwaist of a focused laser beam, for an incident laser beam with uniform amplitude distribution over its cross-section. The beam radius $w_o$, where the field is $\frac{1}{e}$ times that on axis, for uniform amplitude distribution of the incident beam is

$$w_o = 2.5 \frac{\lambda_o}{2\pi} \frac{f}{a} \tag{9-11}$$

The range $2y_{1.2}$, where the beam width has expanded to 1.2 times that at the beamwaist and where the power density has decreased to 0.7 that at the beamwaist, for uniform amplitude distribution of the incident beam is

$$2y_{1.2} = 7.54 \frac{\lambda_o n}{2\pi} (\frac{f}{a})^2 \tag{9-12}$$

We observe from Equations 9-7, 9-11 and 9-12, that the beamwaist and the range of beam collimation are both smaller for the Gaussian amplitude distribution of the laser beam than for the uniform amplitude distribution. However, the amplitude distribution of a laser beam perpendicular to the direction of propagation is always Gaussian. Uniform amplitude distribution can be approximated by truncating the laser beam. The uniform amplitude, however, can only be maintained in the near-field of the truncating aperture.

When a single long-focal length lens collimates the laser beam inside the planar optical waveguide, its focal length must be computed from Equations 9-8 or 9-10. Should the same function be performed by an inverted telescope, these equations must be modified. In any case, the lenses must be spherical when a coupling prism is used to convert the laser beam to a guided mode.

The telescope is built of two lenses, where the spacing between the lenses is the sum of the focal lengths of the two lenses. The transformation of the laser beam with the beam radius a from the first lens $F_1$ with the focal length $f_1$ to its second focal plane, from Equation 9-5 is

$$w_{10} = \frac{\lambda_o}{\pi} \frac{f_1}{a} \tag{9-13}$$

The beam transformation by the second lens $F_2$ with the focal length $f_2$, from its first focal plane to its second focal plane, is

$$w_{20} = \frac{\lambda_o f_2}{\pi w_{10}} \tag{9-14}$$

and from Equations 9-13 and 9-14

$$w_{20} = a \frac{f_2}{f_1} \quad . \tag{9-15}$$

Assuming a switching matrix of 4 cm in length and a beam diameter of the HeNe laser of 1 mm, than from Equation 9-8 a single lens with a focal length of f = 131 mm can collimate the laser beam so that it expands by no more than by a factor of 1.2 over the length of 4 cm, for $\lambda_o = 0.6328 \times 10^{-4}$ cm and n = 2.234. Then the beam radius at the beamwaist from Equation 9-6 is $w_o = 53.2 \times 10^{-4}$ cm. An improved design, where the collimated laser beam only expands by a factor of 1.1 over a length of 4 cm, requires a lens with a focal length of 157 mm (from Equation 9-12) which yields a beam radius at the beamwaist of $w_o = 63.2 \times 10^{-4}$ cm.

Using an inverted telescope would be a less favorable design. It would require for the second lens $F_2$ to have a focal length of at least 5 cm so that the beamwaist at the second focal plane can be centered on the switching matrix of 4 cm length. To obtain a beam radius at the beamwaist of $53.2 \times 10^{-4}$ cm, the focal length of the first lens $F_1$ from Equation 9-17 must be made $f_1 = 470$ mm.

## SECTION 10
## OPTICAL DAMAGES

In the switching matrix, which is being implemented under this contract, the electro-optic Bragg diffraction switches are built in planar integrated-optics waveguide. In the planar waveguides, the waves are confined in one-dimension only (x-axis); in the orthogonal direction (z-axis), the confinement is performed by the high directivity in the focal plane of the focused laser beam. This design approach eliminates any waveguide junctions, also the wave propagation is not adversely affected by the switches when they are in the "off" position. However, the design of the switchings matrix in planar waveguide requires that the propagation properties of the planar waveguide do not noticeably impair the spatial coherency of the focused laser beam along the z-axis.

Difficulties had been encountered and were outlined in Section 8. We had observed that the spatial coherency of the incident laser beam was measurable deteriorating (in the z-direction) when propagating through the integrated-optics planar waveguide. The phenomena which primarily affect the beam propagation in integrated-optics planar waveguides are scattering, which is independent of optical power density, and scattering which becomes more severe with increasing optical power density.

In earlier experiments on planar integrated-optics waveguides which have been published[1] ZnO or ZnS films were used which were deposited on glass. In these waveguides strong scattering was observed. Experimental results on coupling in and out of this type of waveguide, using a double-sided coupling prism, are shown in Figure 10-1[1]. The propagation of the optical waves in Figure 10-1 is in the x-direction. The incoming laser beam (at the left) is incident in synchronous direction of the m-th waveguide mode. (In the synchronous direction, the phase velocity of the wave in the prism projected on the base of the prism ($\beta_{3,m} = \frac{2\pi}{\lambda_o} n_3 \sin \theta_3$), is equal to the phase velocity $\beta_{1,m}$ of the m-th mode in the film. The bright round spot to the right in Figure 10-1 gives the diameter of the laser beam which had been reflected from the base of the prism. The laser beam incident at the

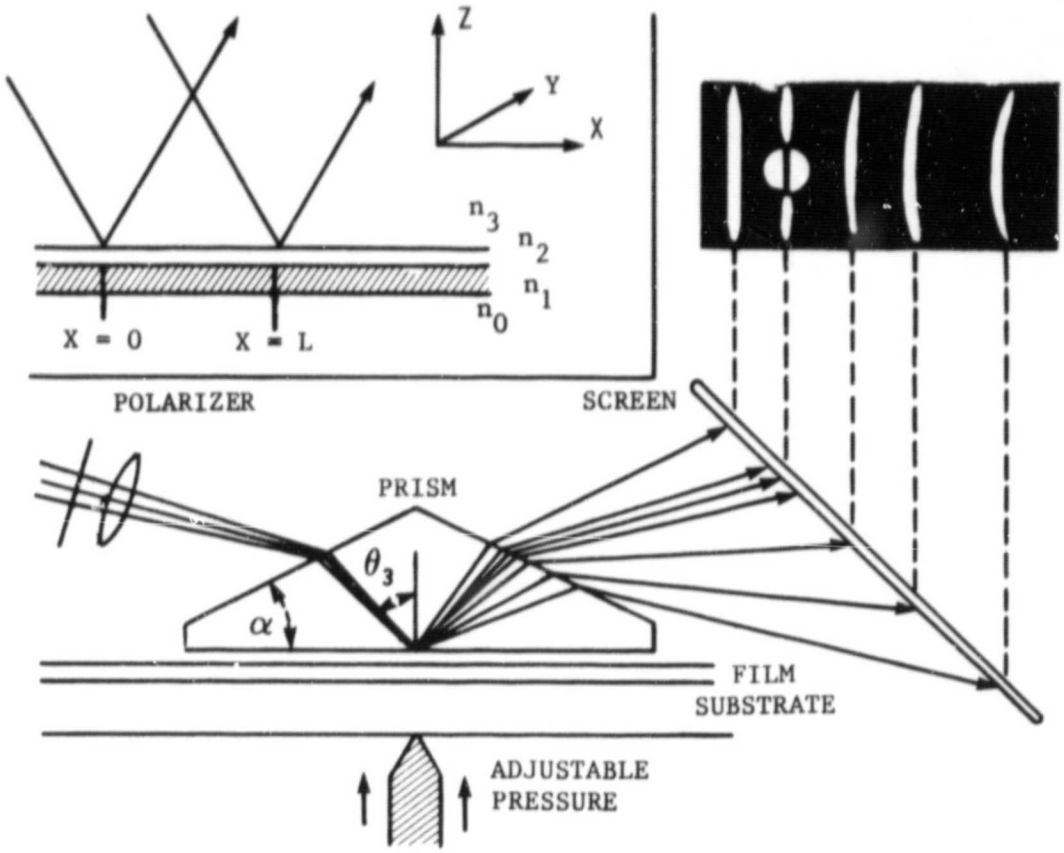


2336
8/81

Figure 10-1. Experimental Arrangement For Observation of Coupling and Intermode Scattering. This Setup was also used for the Determination of the Propagation Constants $\beta$.

synchronous angle of the m-th mode excites in the waveguide this mode. The m-th mode propagates in the x-direction and is coupled out of the waveguide by the second slanted surface of the prism. It forms the bright line that intersects the round laser spot. The extension of this line (in the y-direction) over the diameter of the laser spot is caused by scattering in the planar integrated-optics waveguide. Scattering in the waveguide also produces the additional bright lines in the x-z plane in Figure 10-1. The waveguide, which is formed by ZnO or ZnS disposition on glass, can support many modes along the z-axis; the additional bright lines result from scattering from the m-th mode into waveguide modes of orders different from m.

Scattering, which is independent of optical power density, is considerably smaller in integrated-optics waveguides which are formed by Ti diffusion into $LiNbO_3$[2]. This type of scattering was related to volume imperfections caused by anisotropic refractive index variations in the waveguide rather than by surface roughness. It has been reported that scattering increases in proportion to the amount of Ti used to make the waveguide but is not, within limits, sensitive to the time and temperature of the diffusion process. Polishing of the $LiTiNbO_3$ surface reduces scattering, especially of waveguides formed by thicker layers of Ti. Also, scattering is similar in x-cut and y-cut crystals. A typical in-plane energy distribution as a function of scattering angle, measured in air, is shown in Figure 10-2[2].

Ti diffused $LiNbO_3$ waveguides unfortunately are subject to the type of scattering which becomes more severe with increasing optical power density. This type of scattering in fact results from optical damage. The difficulties described in Section 8 actually were caused by optical damage. Optical damage is an optically-induced inhomogeneity in the refractive index of crystals of $LiNbO_3$ and $LiTaO_3$. The inhomogeneity is not produced instantaneously, but builds up with time. A track of inhomogeneity is produced along the path of the laser beam principally in the extraordinary refractive index, where the beam propagates perpendicular to the optical axis. The beam distorts primarily along the optical axis.

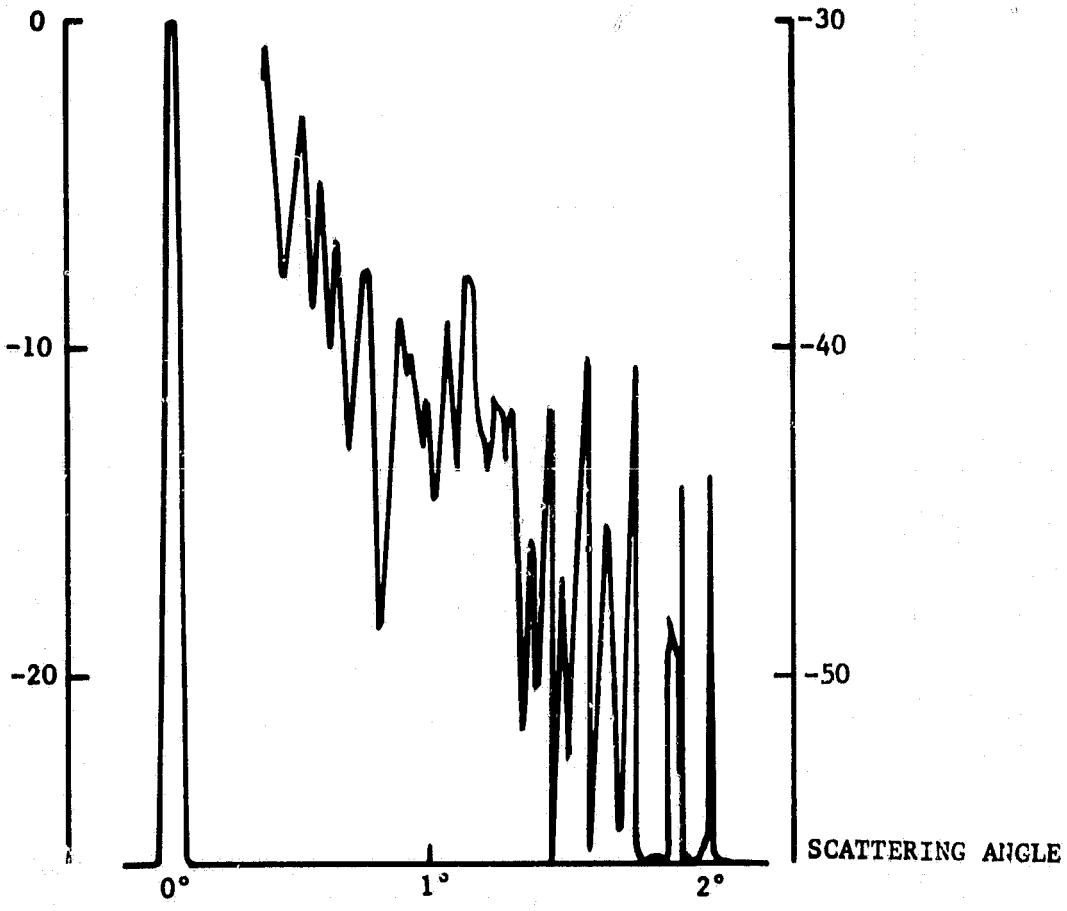


2337
8/81

Figure 10-2. In Plane Scattered-Energy Distribution as a Function Scattering Angle

Similar optical damage has been reported in Ti in-diffused $LiNbO_3$ [3]. However, it also has been reported that integrated-optics waveguides in $LiNbO_3$, formed by crucible out-diffusion do not exhibit any detectable change in the spatial energy distribution even after 12 hours exposure to significantly high power densities of 0.5 kW/cm$^2$ at 4416 Å and 10 kW/cm$^2$ at 4880 Å wavelengths of radiation. In Figure 10-3 [4] the spatial energy distribution as a function of time in a crucible out-diffused $LiNbO_3$ waveguide is compared to those of a vacuum out-diffused $LiNbO_3$ and a Ti in-diffused $LiNbO_3$ waveguide.

The susceptibility to optical damage decreases at longer wavelengths and lower power densities. In our experiments the power density in the Ti in-diffused $LiNbO_3$ waveguide was dropped to approximately 1W/cm$^2$ by the use of a neutral density filter and loose coupling to the waveguide. This power density is considerably below the value where optical damage had been reported in Figure 10-3; also, the wavelength is longer than shown in Figure 10-3c. At this power level, the far-field distribution of the guided wave when transformed through the second coupling prism, has been measured. To do so, the field energy was scanned in the x-direction at a distance of 73 cm, using an iris of approximately 700 microns diameter and a "United Detector Technology" type 11A radiameter. The measured data using a Ti diffused waveguide (400 Å) on a $LiNbO_3$ substrate from Crystal Technology, are shown in Figure 10-4. The energy distribution seems to be Gaussian with a beam radius (where the energy is $e^{-2}$ that at the beam maximum) of w = 2.15 mm. From Equation 9-1 in Section 9 we compute that this corresponds to a beam radius in the planar waveguide in the x-direction of $w_0$ = 60.5 microns.

To investigate whether the energy distribution shown in Figure 10-4 is actually Gaussian, the energy distribution of a Gaussian beam given by exp. $(-2\,(\frac{x}{w})^2)$ was computed for w = 2.15 mm. The computed energy distribution is also shown in Figure 10-4. There is very good agreement between the measured and the computed Gaussian energy profiles.

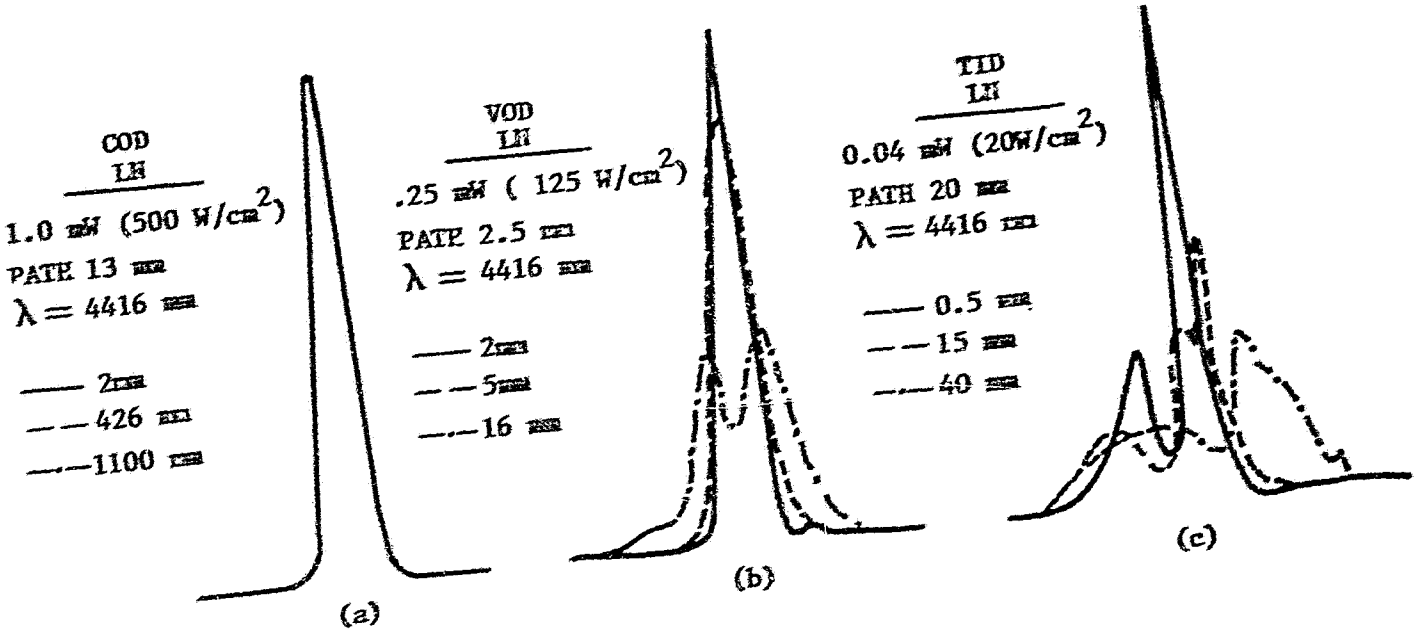


2338
8/81

Figure 10-3: Output intensity profiles of $LiNbO_3$ waveguides along the m line and as a function of time: (a) crucible out-diffused $LiNbO_3$; (b) vacuum out-diffused $LiNbO_3$; and (c) titanium in-diffused $LiNbO_3$.

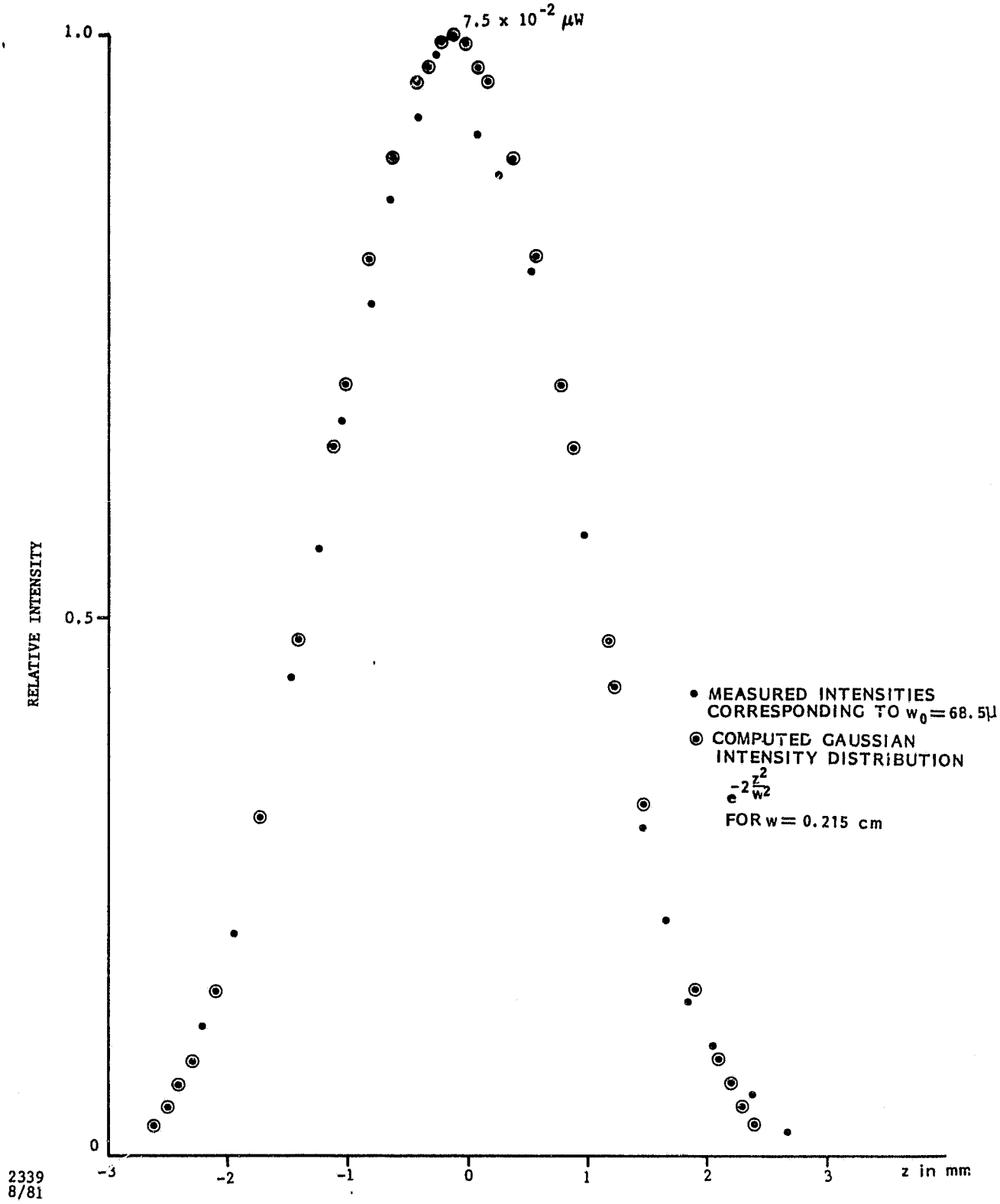


Figure 10-4. Output Intensity Profile of $LiTiNbO_3$, Waveguide Along z-axis

The energy distribution in the planar waveguide in the z-direction is set up by the beamwaist of the HeNe laser radiation, which had been focused by a lens of 15 cm focal length. The Gaussian beam radius of the HeNe laser at a distance of 135 cm was measured to 1.25 mm. From Equation 9-1 in Section 9, this corresponds to a beam radius at the lens of 15 cm focal length at a distance of 37 cm to 0.4 mm, and from Equation 9-6 in Section 9, to a beam radius at the beamwaist of the lens in the planar waveguide of $w_o$ = 74.7 microns. This value is in fair agreement with the beam radius in the planar waveguide $w_o$ = 68.5 microns, which had been derived from the far-field energy distribution shown in Figure 10-4.

The far-field distribution measurements were repeated on the same waveguide at lower power flux densities. The results are shown in Figures 10-5 and 10-6. The energy profiles are similar to those in Figure 10-4, only the far-field distribution in Figure 10-6, measured at the lowest power level, is narrower. The narrower far-field distribution corresponds to a wider beam radius of 87 microns in the planar waveguide. The smaller beam radius of 68.5 microns at the higher power levels might result from self-focusing of the laser beam in the waveguide. Self-focusing can possibly be introduced by the higher temperature of the waveguide at the energy maximum of the Gaussian mode. An increase in temperature due to losses in the waveguide causes an increase of the refractive index in $LiNbO_3$. A temperature gradient from the center of the Gaussian mode can yield a refractive index gradient with the maximum at the center of the mode. This type of gradient effectively has lens-like properties and can decrease the width of the laser beam in the planar waveguide. Obviously, the losses are higher and self-focusing would be stronger at higher optical powers.

The typical Gaussian energy distribution shown in Figure 10-4, remained the same when the laser beam, incident on the waveguide, was displaced in the z-direction. However, there were two small areas on the Crystal Technology substrate where several diffraction lobes became visible in the far-field; also, the main beam became noticeably narrower. This observation indicates optical damage in these areas, resulting in a widening of the laser beam in the planar waveguide and the formation of filaments.

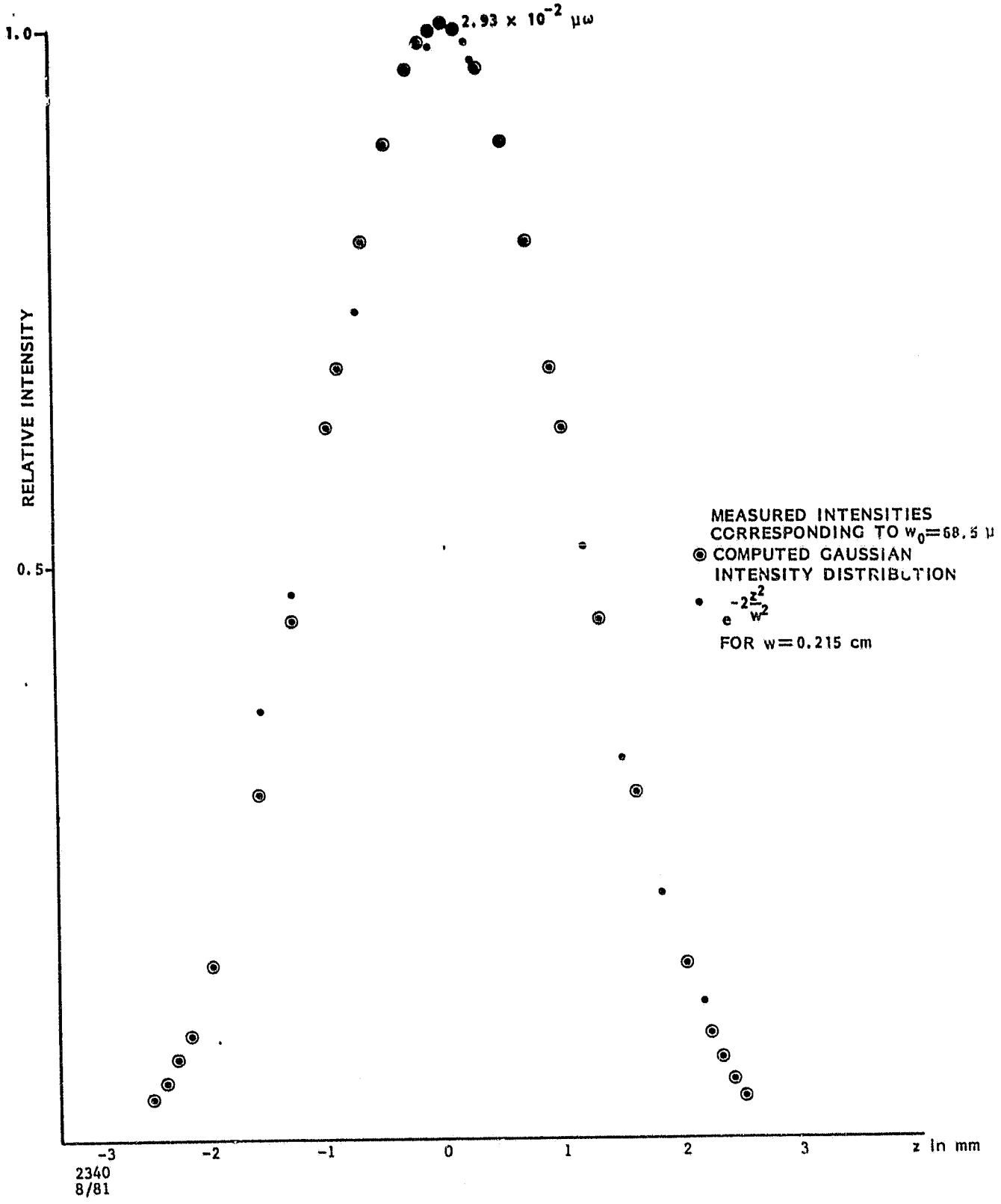


Figure 10-5. Output Intensity Profile of $LiTiNbO_3$, Waveguide Along z-axis

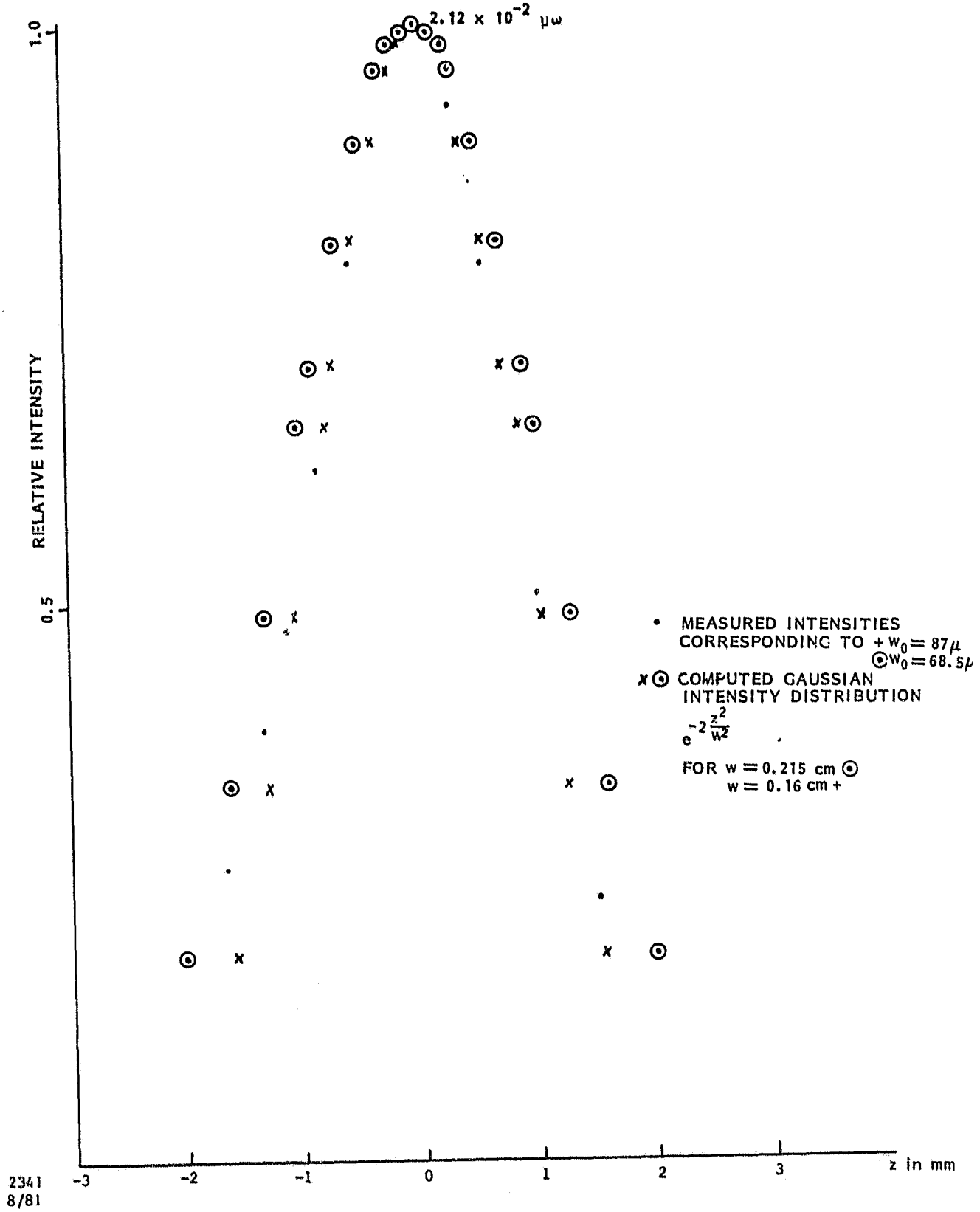


Figure 10-6. Output Intensity Profile of $LiTiNbO_3$ Waveguide Along z-axis

The output energy profile was also investigated of a Ti diffused planar waveguide on a $LiNbO_3$ substrate, purchased from Union Carbide. The measured values and the computed values for a Gaussian energy profile, are shown in Figure 10-7. The far-field is slightly narrower than that shown in Figures 10-4, 10-5, and 10-6, corresponding to a slightly wider beam radius in the planar waveguide of 101 microns.

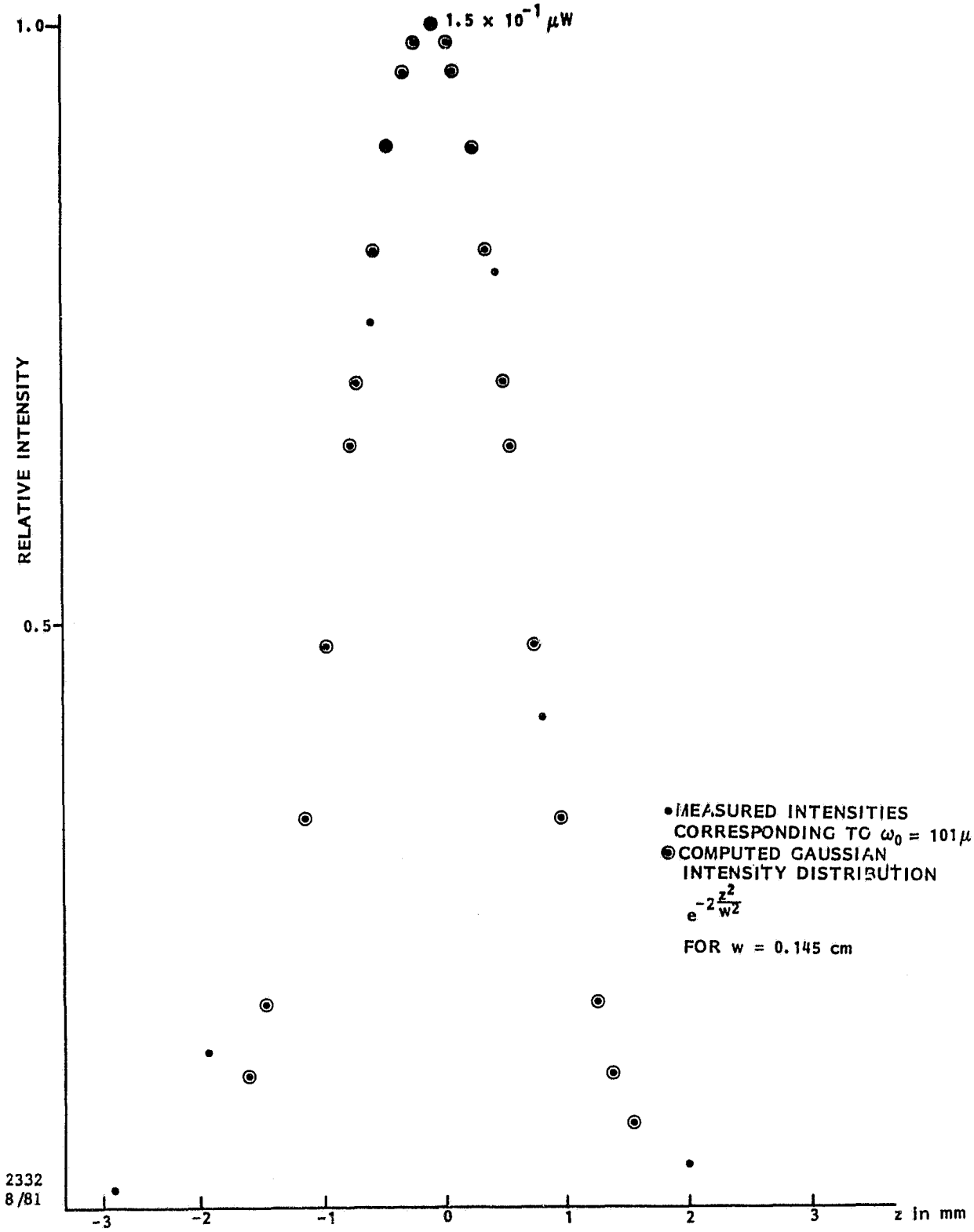


Figure 10-7. Output Intensity Profile of $LiTiNbO_3$, Waveguide Along z-axis

## REFERENCES
## TO SECTION 10


1. R. K. Rien et al. "Appl. Phys. Letters," Vol 14, No 9. May 1, 1969, pp. 291-294.

2. D. W. Vahey et al. "Ferroelectrics," 1980, Vol. 27 pp. 81-84.

3. R. L. Holman et al. "Ferroelectrics," 1980, Vol. 27, pp. 77-80.

4. R. L. Holman et al. "Appl. Phys. Letters," Vol. 32, No 5, March 1, 1978.